

Reef ecosystem recovery following the Middle Permian (Capitanian) mass extinction:

A multi-scale analysis from South China

Kumulative Dissertation

Von

Xia Wang



zur Erlangung des akademischen Grades

"Doctor rerum naturalium"

(Dr. rer. nat.)

in der Wissenschaftsdisziplin

Sedimentologie

eingereicht an der
Mathematisch-Naturwissenschaftlichen Fakultät
Institut für Geowissenschaften
der Universität Potsdam

Potsdam, im September 2020
Datum der Disputation: 08 Dezember 2020

Hauptbetreuerin: Prof. Dr. Maria Mutti
Gutachter*innen: Prof. Dr. Maria Mutti
Prof. Dr. Jitao Chen
Dr. Jens Kallmeyer

Published online on the
Publication Server of the University of Potsdam:
<https://doi.org/10.25932/publishup-48750>
<https://nbn-resolving.org/urn:nbn:de:kobv:517-opus4-487502>

Content

CONTENT	I
LIST OF FIGURES	IV
LIST OF TABLES	VI
ABSTRACT	VII
ZUSAMMENFASSUNG	IX
ACKNOWLEDGEMENTS	XI
CHAPTER 1 INTRODUCTION	1
1.1 CONTEXT AND CHALLENGES.....	3
1.1.1 Reef crisis and mass extinction: History is a guide	3
1.1.2 Permian-Triassic transition and the Middle Permian (Capitanian) mass extinction.....	4
1.1.3 Aims of this study	5
1.2 GENERAL GEOLOGICAL SETTINGS.....	6
1.3 GENERAL METHODOLOGY.....	8
1.4 ORGANIZATION OF THE THESIS	8
CHAPTER 2 PERMIAN (ARTINSKIAN TO WUCHIAPINGIAN) CONODONT BIOSTRATIGRAPHY IN THE TIEQIAO SECTION, LAIBIN AREA, SOUTH CHINA	11
ABSTRACT	13
2.1. INTRODUCTION	13
2.2. GEOLOGICAL SETTING	15
2.3. MATERIALS AND METHODS	17
2.4. STRATIGRAPHY AND CONODONT ZONATION	17
2.4.1. Sakmarian (?).....	17
2.4.2. Artinskian.....	19
2.4.3. Kungurian	20
2.4.4. Roadian	24
2.4.5. Wordian.....	25
2.4.6. Capitanian.....	25
2.4.7. Wuchiapingian	27
2.5. SUBORDINATE ZONES AND REASSESSMENT FOR AGE ASSIGNMENTS OF RARE SPECIES	28
2.6. SYSTEMATIC PALAEONTOLOGY	31
2.6.1. Genus <i>Gullodus</i> Kozur, 1993.....	31
2.6.1.1. <i>Gullodus tieqiaoensis</i> n. sp. Sun and Lai	32
2.6.2. Genus <i>Hindeodus</i> Rexroad & Furnish, 1964.....	33
2.6.2.1. <i>Hindeodus catalanoi</i> Gullo and Kozur, 1992.....	33
2.6.2.2. <i>Hindeodus</i> sp. A	34
2.6.3. Genus <i>Pseudohindeodus</i> Gullo and Kozur, 1992	34

2.6.3.1. <i>Pseudohindeodus elliptica</i> n. sp. Sun and Lai.....	34
2.6.4. Genus <i>Sweetognathus</i> Clark, 1972	35
2.6.4.1. <i>Sweetognathus asymmetrica</i> n. sp. Sun and Lai.....	35
2.6.4.2. <i>Sweetognathus bogoslovskajae</i>	37
2.6.4.3. <i>Sweetognathus hanzhongensis</i> (Wang, 1978).....	37
2.6.4.4. <i>Sweetognathus inornatus</i> Ritter, 1986	38
2.6.4.5. <i>Sweetognathus</i> sp. A	39
2.6.4.6. <i>Sweetognathus toriyamai</i> (Igo, 1981)	39
2.7. CONCLUSIONS.....	40
ACKNOWLEDGEMENTS	41
PLATE CAPTION.....	42
CHAPTER 3 DELAYED RECOVERY OF METAZOAN REEFS ON THE LAIBIN-HESHAN PLATFORM MARGIN FOLLOWING THE MIDDLE PERMIAN (CAPITANIAN) MASS EXTINCTION.....	51
ABSTRACT	53
3.1. INTRODUCTION	53
3.2. GEOLOGICAL AND STRATIGRAPHIC SETTING.....	55
3.3. METHODS.....	57
3.4. RESULTS AND INTERPRETATIONS.....	58
3.4.1. <i>Lithofacies associations and depositional environments</i>	58
3.4.1.1. Slope-basin facies association.....	58
3.4.1.1.1. Lithofacies types.	58
3.4.1.1.2. Interpretation.....	59
3.4.1.2. Initial reef phase facies association.....	59
3.4.1.2.1. Lithofacies types.	59
3.4.1.2.2. Interpretation.....	59
3.4.1.3. Reef core facies association	60
3.4.1.3.1. Lithofacies types.	60
3.4.1.3.2. Interpretation.....	61
3.4.1.4. Reef cap facies association.....	63
3.4.1.4.1. Lithofacies types.	63
3.4.1.4.2. Interpretation.....	63
3.4.1.5. Subtidal outer platform/back reef facies association.....	63
3.4.1.5.1. Lithofacies types.	63
3.4.1.5.2. Interpretation.....	63
3.4.2. <i>Spatial distribution and cyclicity</i>	64
3.4.2.1. 1st transgressive-regressive cycle	65
3.4.2.2. 2nd Transgressive-regressive cycle.....	66
3.4.2.3. 3rd transgressive-regressive cycle.....	67
3.4.2.4. 4th transgressive-regressive cycle.....	67
3.4.2.5. 5th transgressive-regressive cycle.....	68
3.4.2.6. 6th transgressive-regressive cycle.....	72
3.5. DISCUSSION	75
3.5.1. <i>The timing of reef recovery on the Laibin-Heshan platform</i>	75

3.5.2. <i>The Guadalupian-Lopingian evolution of sponge reef ecosystems</i>	76
3.5.3. <i>The role and importance of encrusters in Permian reef-building</i>	77
3.5.4. <i>The recovery pattern for the reef during Wuchiapingian stages comparing with the recovery of reef system after end Permian extinction</i>	79
3.6. CONCLUSION.....	81
ACKNOWLEDGMENTS	81
CHAPTER 4 QUANTIFYING ECOSYSTEM FUNCTIONING IN POST-EXTINCTION REEF COMMUNITIES: A TEST OF ECOLOGICAL RESTRUCTURING AFTER THE MIDDLE PERMIAN MASS EXTINCTION.....	83
ABSTRACT	85
4.1. INTRODUCTION	85
4.2. GEOLOGICAL SETTING	87
4.3. MATERIAL AND METHODS	88
4.3.1. <i>Material and point-counting methods</i>	88
4.3.2. <i>Statistical methods</i>	89
4.4. RESULTS	90
4.4.1. <i>Quantitative analysis of skeletal grains</i>	90
4.4.2. <i>Quantitative analysis of whole rock components</i>	96
4.4.3. <i>Rank correlation of skeletal grains</i>	101
4.5. DISCUSSION	103
4.5.1. <i>Reef-building elements in the Tieqiao reefs</i>	103
4.5.1.1. <i>Microproblematica and sponges</i>	103
4.5.1.2. <i>Additional components</i>	107
4.5.2. <i>Comparison of shallow-water build-ups crossing the G/L transition at the Laibin-Heshan isolated platform</i>	108
4.5.3. <i>Controlling factors of reef evolution during the G/L transition</i>	110
4.6. CONCLUSIONS.....	112
ACKNOWLEDGMENTS	113
CHAPTER 5 SYNTHESIS AND CONCLUSIONS	115
5.1. REVISION OF CONODONT STRATIGRAPHIC ZONATION OF TIEQIAO SECTION AND CONSTRAINING THE AGE OF THE TIEQIAO REEFS	117
5.2. TIMING OF REEF RECOVERY FOLLOWING THE MIDDLE PERMIAN (CAPITANIAN) MASS EXTINCTION	117
5.3. CYCLES OF THE POST-EXTINCTION REEF EVOLUTION AND THE DELAYED RECOVERY OF METAZOAN REEFS AT TIEQIAO SECTION	119
5.4. WUCHIAPINGIAN REEF ECOSYSTEM AND FUNCTIONING OF REEF-BUILDING ORGANISMS	120
5.5. CONCLUSIONS.....	122
5.6. PERSPECTIVE OF FUTURE RESEARCHES	123
REFERENCES	125
APPENDIX.....	141

List of Figures

Figure 1.1. Location map of Tieqiao section in the Laibin-Heshan area.	7
Figure 1.2 Correlation of chronostratigraphic units, lithostratigraphic units and conodont zones.....	7
Figure 2.1: Middle Permian palaeogeographic reconstructions of South China and Permian lithologic units in Laibin area.....	15
Figure 2.2: Field photographs of the studied section.....	16
Figure 2.3: Log of the lower part of Tieqiao section (Asselian to Kungurian) with conodont ranges and zonation.	18
Figure 2.4: Log of the middle part of Tieqiao section (Kungurian to Wordian) with conodont ranges and zonation.	21
Figure 2.5: Log of the upper part of Tieqiao section (Wordian to Wuchiapingian) with conodont ranges and zonation.	24
Figure 2.6: Correlation chart of the Early-Middle Permian with standard conodont zonation (Henderson et al., 2012), Tieqiao (this study) and Nashui (Mei et al., 2002).	28
Plate 1 SEM images of Tieqiao conodonts-genus <i>Sweetognathus</i>	44
Plate 2 SEM images of Tieqiao conodonts—genera <i>Sweetognathus</i> , <i>Pseudosweetognathus</i> , <i>Neostreptognathodus</i> and <i>Hindeodus</i>	45
Plate 3 SEM images of Tieqiao conodonts—genera <i>Sweetognathus</i> and <i>Pseudosweetognathus</i>	46
Plate 4 SEM images of Tieqiao conodonts—genera <i>Sweetognathus</i> , <i>Gullodus</i> , <i>Hindeodus</i> and <i>Pseudohindeodus</i>	47
Plate 5 SEM images of Tieqiao conodonts—genera <i>Mesogondolella</i> and <i>Jinogondolella</i>	48
Plate 6 SEM images of Tieqiao conodonts—genera <i>Jinogondolella</i> and <i>Clarkina</i>	49
Plate 7 SEM images of Tieqiao conodonts—genera <i>Hindeodus</i> , <i>Jinogondolella</i> , <i>Mesogondolella</i> , <i>Pseudohindeodus</i> and <i>Sweetognathus</i>	50
Figure 3.1: Paleogeographic map of the South China Yangtze Platform during the Wuchiapingian.	55
Figure 3.2: Geological map of Laibin-Heshan area, Guangxi, China.	56
Figure 3.3: Stratigraphic succession of the Tieqiao section and relative sea-level curve.	62
Figure 3.4: (A) Aerial drone map marked with the sample locations (orange triangle), stratigraphic profiles (gray line), and locations of acid-etched surfaces (red irregular shape); (B) distribution of lithofacies.	64
Figure 3.5: The grid map showing the abundance of the encruster <i>Archaeolithoporella</i> (A) and sponges (B).	70
Figure 3.6. Thin-section photomicrographs of 1st, 2nd and 5th cycle.	71
Figure 3.7: Thin-section photomicrographs of 3rd to 6th cycles.....	72
Figure 3.8: Close-up photos of acid etched surfaces of the outcrop (A-F, H, I), weathered surfaces of the outcrop (G, J-L) and the outcrop (M, N).....	74
Figure 3.9: Distribution of reefs in South China.	76
Figure 4.1: (a) Location of the South China block during the Late Permian (b) Location of the Tieqiao Section (red star) and the Penglaitan section (black star) (c) Paleogeographic map of the southern part of Yangtze Platform (South China block) during the Wuchiapingian Stage.....	87
Figure 4.2: Cluster analysis with the similarity profile test (SIMPROF) on the skeletal grain data set from the Tieqiao section.....	91

Figure 4.3: Similarity percentages (SIMPER) analysis for the different biocommunity clusters (BCs) identified from the cluster analysis.	92
Figure 4.4: Non-metric multi-dimensional scaling (nMDS) ordination of samples, grouped according to (a) biocommunity cluster (BC), and (b) rock composition cluster (RCC).....	92
Figure 4.5: Thin-section photomicrographs with examples of different biocommunity clusters (BCs) and rock composition clusters (RCCs).....	93
Figure 4.6: Differences in alpha diversity between (a) biocommunity clusters (BC), (b) regressive system tracts, and (c) depositional environments for the Heshan Formation in the Tieqiao section.	94
Figure 4.7: Stratigraphic log with facies associations, transgressive-regressive cycles, biocommunity clusters (BCs), and relative abundance of skeletal grains.	96
Figure 4.8: Cluster analysis with the similarity profile test (SIMPROF) of the whole rock components data set in the samples from the Tieqiao section.	97
Figure 4.9: Similarity percentages (SIMPER) analysis for the different rock composition clusters (RCCs) identified from the cluster analysis.	98
Figure 4.10: Stratigraphic log with facies associations, transgressive-regressive cycles, rock composition clusters (RCCs), and relative abundance of whole rock components.	100
Figure 4.11: Plot of R_s value from Spearman's rank correlation.	102
Figure 4.12: Summary of the spatial distribution and variation in the main components of (a) rock composition clusters (RCCs) and (b) biocommunity clusters (BCs, b); and (c) mean value of components within different environments (facies associations).	104
Figure 4.13: Thin-section photomicrographs of clotted micrite (a, b) and cements (c, d).	107
Figure S1: Trace of the section (dark grey line) and position of samples (red triangle) used for point counting on the Tieqiao section (Chapter 4).	141

List of Tables

Table 4.1: Distribution of biocommunity clusters (BCs) and rock composition clusters (RCCs) within different facies associations and reef cycles..	95
Table 4.2: Positive (a) and Negative (b) correlations which are significant in both Spearman's rank correlation and Partial correlation, and their R_s value.	101
Table S1: Point counting data.....	142
Table S1 continued: Point counting data.....	143
Table S2: Result of Spearman's rank correlation of skeletal grains.....	144

Abstract

To find out the future of nowadays reef ecosystem turnover under the environmental stresses such as global warming and ocean acidification, analogue studies from the geologic past are needed. As a critical time of reef ecosystem innovation, the Permian-Triassic transition witnessed the most severe demise of Phanerozoic reef builders, and the establishment of modern style symbiotic relationships within the reef-building organisms. Being the initial stage of this transition, the Middle Permian (Capitanian) mass extinction coursed a reef eclipse in the early Late Permian, which lead to a gap of understanding in the post-extinction Wuchiapingian reef ecosystem, shortly before the radiation of Changhsingian reefs. Here, this thesis presents detailed biostratigraphic, sedimentological, and palaeoecological studies of the Wuchiapingian reef recovery following the Middle Permian (Capitanian) mass extinction, on the only recorded Wuchiapingian reef setting, outcropping in South China at the Tieqiao section.

Conodont biostratigraphic zonations were revised from the Early Permian Artinskian to the Late Permian Wuchiapingian in the Tieqiao section. Twenty main and seven subordinate conodont zones are determined at Tieqiao section including two conodont zone below and above the Tieqiao reef complex. The age of Tieqiao reef was constrained as early to middle Wuchiapingian.

After constraining the reef age, detailed two-dimensional outcrop mapping combined with lithofacies study were carried out on the Wuchiapingian Tieqiao Section to investigate the reef growth pattern stratigraphically as well as the lateral changes of reef geometry on the outcrop scale. Semi-quantitative studies of the reef-building organisms were used to find out their evolution pattern within the reef recovery. Six reef growth cycles were determined within six transgressive-regressive cycles in the Tieqiao section. The reefs developed within the upper part of each regressive phase and were dominated by different biotas. The timing of initial reef recovery after the Middle Permian (Capitanian) mass extinction was updated to the *Clarkina leveni* conodont zone, which is earlier than previous understanding. Metazoans such as sponges were not the major components of the Wuchiapingian reefs until the 5th and 6th cycles. So, the recovery of metazoan reef ecosystem after the Middle Permian (Capitanian) mass extinction was obviously delayed. In addition, although the importance of metazoan reef builders such as sponges did increase following the recovery process, encrusting organisms such as *Archaeolithoporella* and *Tubiphytes*, combined with microbial carbonate precipitation, still played significant roles to the reef building process and reef recovery after the mass extinction.

Based on the results from outcrop mapping and sedimentological studies, quantitative composition analysis of the Tieqiao reef complex were applied on selected thin sections to further investigate the functioning of reef building components and the reef evolution after the Middle Permian (Capitanian) mass extinction. Data sets of skeletal grains and whole rock components were analyzed. The results show eleven biocommunity clusters/eight rock composition clusters dominated by different skeletal grains/rock components. Sponges, *Archaeolithoporella* and *Tubiphytes* were the most ecologically important components within the Wuchiapingian Tieqiao reef, while the clotted micrites and syndepositional cements are the additional important rock components for reef cores. The sponges were important within the whole reef recovery. Tubiphytes were broadly distributed in different environments and played

a key-role in the initial reef communities. *Archaeolithoporella* concentrated in the shallower part of reef cycles (i.e., the upper part of reef core) and was functionally significant for the enlargement of reef volume.

In general, the reef recovery after the Middle Permian (Capitanian) mass extinction has some similarities with the reef recovery following the end-Permian mass extinction. It shows a delayed recovery of metazoan reefs and a stepwise recovery pattern that was controlled by both ecological and environmental factors. The importance of encrusting organisms and microbial carbonates are also similar to most of the other post-extinction reef ecosystems. These findings can be instructive to extend our understanding of the reef ecosystem evolution under environmental perturbation or stresses.

Zusammenfassung

Um die zukünftige Entwicklung der aktuell sehr dramatischen Änderungen des Ökosystems von Riffen vorherzusagen, welche durch Umweltbelastungen wie die globale Erwärmung und die zunehmende Versauerung der Ozeane verursacht wird, müssen analoge Beispiele aus der geologischen Vergangenheit genauer unter die Lupe genommen werden.

Als eine wichtige Zeit der Neugestaltung von Riffsystemen beinhaltet der Übergang vom Perm in die Trias den wohl einschneidendsten Rückgang von phanerozoischen Riffbildnern, und die dauerhafte Festsetzung von modernen symbiotischen Wechselbeziehungen zwischen den einzelnen riffbildenden Organismen. Zu Beginn dieses Übergangs und nach dem mittelpermischen Massenaussterben im Capitanium fand eine langsame Erholung der Riffe im Wuchiapingium statt, welche sich vor der Radiation der Riffe im Changhsingium bildeten, deren Ursache aber immer noch nicht vollends verstanden wurde.

In dieser Arbeit wird eine detaillierte biostratigraphische, sedimentologische und paläoökologische Untersuchung der Rifferholung im Wuchiapingium nach dem mittelpermischen Massenaussterben vorgestellt. Dies wird an den einzigen jemals in Südchina dokumentierten Riffsedimenten aus dieser Zeit im sogenannten Tieqiao-Riffkomplex durchgeführt.

Biostratigraphische Einteilungen anhand von Konodonten zwischen dem frühpermischen Artinskium bis zum spätpermischen Wuchiapingium im Tieqiao-Riffkomplex wurden überarbeitet. Zwanzig Haupt- und sieben untergeordnete Konodontenzonen wurden definiert, wobei sich zwei Zonen oberhalb und unterhalb des Riffkomplexes befinden. Das Alter des Tieqiao-Riffkomplexes wurde dabei auf das frühe bis mittlere Wuchiapingium festgelegt.

Nachdem das Alter des Tieqiao-Riffes bestimmt wurde, führte die zweidimensionale Kartierung des Aufschlusses sowie die detaillierte Untersuchung der Lithofazies zu einem besseren Verständnis des stratigraphischen Riffwachstums und der lateralen Änderung der Riffmorphologie im Aufschlussmaßstab. Eine semiquantitative Analyse der riffbildenden Organismen wurde angewandt, um deren Entwicklungsmuster während der Erholungsphase des Riffes zu verstehen. Sechs Wachstumszyklen der Riffe innerhalb von sechs regressiven Zyklen der Tieqiao wurden dabei bestimmt. Die Riffe entwickelten sich überwiegend im oberen Teil der regressiven Phase und wurden von unterschiedlichsten Arten dominiert. Der Zeitpunkt der initialen Erholung der Riffe nach dem mittelpermischen Massenaussterben im Capitanium wurde auf die *Clarkina leveni* Konodontenzone aktualisiert, also älter als bisher angenommen. Metazoen wie Schwämme waren bis zum 5. und 6. Zyklus nicht die Hauptbildner des Riffes. Folglich war die Erholung des metazoischen Riff-Ökosystems nach dem mittelpermischen Massenaussterben verzögert. Auch wenn die Wichtigkeit von metazoischen Riffbildnern während des Erholungsprozesses zunahm, spielten enkrustierende Organismen wie

Archaeolithoporella und *Tubiphytes* zusammen mit mikrobiellen Mikriten immer noch eine signifikante Rolle im Prozess der Rifferholung und des -aufbaus.

Anhand der Resultate der Kartierung und der sedimentologischen Untersuchung wurden quantitative Analysen der einzelnen Bestandteile an Dünnschliffen ausgeführt. Dies ermöglichte die weiterführende Untersuchung der riffbildenden Bestandteile und die Entwicklung des Riffes nach dem mittelpermischen Massenaussterben. Dafür wurden Daten der einzelnen fossilen Bestandteile und des gesamten Gesteins analysiert. Dabei wurden elf Fossilvergesellschaftungen identifiziert, welche jede von unterschiedlichen fossilen Bestandteilen dominiert wurde. Schwämme, *Archaeolithoporella* und *Tubiphytes* waren die ökologisch wichtigsten Komponenten im Tieqiao-Riff, während mikrobielle Mikrite und syndepositionale Zemente zusätzliche Bausteine der Riffe darstellen. Schwämme waren dabei besonders wichtig für die Rifferholung. *Tubiphytes* war in den verschiedenen Ablagerungsräumen weit verbreitet und spielte eine Hauptrolle in den ersten Riffzyklen. *Archaeolithoporella* dagegen konzentrierte sich in den flacheren Bereichen des Riffzyklus (d.h. im oberen Teil des Riffes) und war maßgeblich daran beteiligt, das Riffvolumen zu erweitern. Grundsätzlich besitzt die Erholung der Riffe nach dem mittelpermischen Massenaussterben große Ähnlichkeit mit der die dem Massenaussterben an der Perm-Trias Grenze folgte. Typisch dafür ist eine verzögerte Erholung der metazoischen Riffe und ein Muster der schrittweisen Erholung, die ihrerseits durch ökologische und umweltbedingte Faktoren kontrolliert wird. Die Wichtigkeit von enkrustierenden Organismen und mikrobiellen Karbonaten sind ebenfalls vergleichbar zu den meisten anderen Riffsystemen, die sich nach einem Massenaussterben entwickelten. Diese Ergebnisse sind äußerst wichtig um unser Wissen über die Entwicklung von Riffsystemen nach Massenaussterben zu erweitern.

Acknowledgements

First of all, I would like to thank my supervisor Prof. Dr. Maria Mutti for her kindly support and advice, which accompanied me through different stages of my doctoral study (Thank you for sharing the knowledge of wine with me too!). Secondly, thanks to Prof. Jiaxin Yan, who led me into this topic and offered me help selflessly through all my doctoral study. I also appreciate the assistances and friendship from the colleagues of sedimentology group at University of Potsdam that I have met during these years. They are Sara Tomás, Jhosnella Sayago, Yanqiu, Zhang, Xiaoxia Huang, Hannes Nevermann, Max Zitzmann, Michael Krause, Nicolas Christ, Frédéric Amour, Gerd Winterleitner, Gianluca Frijia, Michael Szurlies, Matteo Di Lucia, Ahmed Y. Tawfik, Michele Vallati, Richard Arndt, Sven März, Timothy Tella, Wera Schmidt, Thomas van der Looven and many visiting scholars from all over the world. Special thanks go to William Foster, who kindly shared his knowledge with me, spent a lot of time to help me with my work, and kept me on a happy track of doing research.

In my doctoral project, I received tons of help from the colleagues of China University of Geosciences (Wuhan) (CUG). Prof. Jiaxin Yan and his group, including Aozhu Li, Wuqiang Xue, Xiting Liu, Fei Li, Bo Li, Yajuan Yan, Fayao Chen, and Qi Meng, are gratefully thanked for the assistance with field works in China. Aozhu Li also worked with me for the sample preparation. Yadong Sun, and Prof. Xulong Lai's group from CUG are thanked for their kindly support and fruitful collaborations that contributed to this doctoral project. I also want to thank Shouxian Liu for the thin section preparation.

In addition, other Chinese colleagues including Prof. Daizhao Chen, Prof. Guilian Sheng, Prof. Xindong Hou, Prof. Junxia Yuan, Jianglin He, Liyu Zhang, Lingfeng Song, Yue Hu and Gongjing Zhang are thanked for the discussion, Qian Ding and Jingbin Wang are thanked for the help with field work. Especially Liyu Zhang and Guilian Sheng are thanked for their mental support through all the difficult times.

During my stay in Golm, I would like to thank Tanja Klaka-Tauscher for her generous help, which was so warm for a young stranger who want to fit into a new department quickly. Thanks to Martina Heidemann for all the kindly help through daily issues to project management. Christine Fischer is thanked for the help within the sample preparation. Thanks to Sven März for translating the abstract of this dissertation. Special thanks go to Humaad Ghani who broke the "*kekai*" of our office. Special thanks also go to Weishi Wang, we made it, bro.

I appreciate the China Scholarship Council (CSC) for financially supporting my study in University of Potsdam. Other supports for individual manuscript are mentioned in the acknowledgement sections of Chapter 2 to 4.

Special thanks go to my fellow doctoral students from the CSC Scholarship, whom I shared the same pursuits of knowledge and scientific spirit, which encouraged us to come to a country that is far away from our family and land.

Thanks to all my friends, I cannot put all your names here, but I thank you all for the continuous support and precious friendship. Special thanks go to the 7 Niangniang for your intensive wagering on whether I could finish this PhD or not.

Last but never the least, thanks to my dearest parents and Yang. I could not have achieved this without your full support.

Chapter 1

Introduction

1.1 Context and challenges

1.1.1 Reef crisis and mass extinction: History is a guide

Reefs are the most spectacular natural constructions in the shallow water marine system. As the key habitat of the various organisms, reefs played a significant role in maintaining biodiversity throughout earth history. In the past decades, the rising hazard of reef ecosystem related to global climate change and other threats has caught great attention worldwide (e.g., Hoegh-Guldberg, 1999; Knowlton, 2001; Jackson et al., 2001; Pandolfi et al., 2003). The crisis of the nowadays reef system and the transition of the reef ecosystem under the climatic pressure (e.g., Bellwood et al., 2004; Baker et al., 2008, Pandolfi et al., 2011; Bell et al., 2013), is a critical issue related to the global ecosystem where human is also one of the participants.

To understand the transitions happening now, investigations on the reef evolution and reefs' response to the major crisis within the geological records provide analogs of the modern system (e.g., Copper, 1994, Bell et al., 2013). Traditionally five major mass extinctions (the "Big Five" mass extinctions) have been named in the geologic past (Raup and Sepkoski, 1982). Whether the recent biodiversity loss indicates an ongoing "sixth mass extinction" is still repeatedly under discussion and continuously catching the public attention (e.g., Novacek and Cleland, 2001; Wake and Vredenburg, 2008; Barnosky et al., 2011; Ceballos et al., 2015). Kiessling and Simpson (2011) suggested that three of the "Big Five" mass extinctions are coincident with significant metazoan reef crisis. They also suggested the double strike of ocean acidification and rapid warming turns to be general cause of the reef crises (Kiessling and Simpson, 2011). For the predicted "sixth mass extinction", the ongoing degradation of coral reefs are also closely related with the negative impact of ocean acidification and global warming on carbonate precipitation (Hoegh-Guldberg et al., 2007). Those similarities between the geologic past and the recent changes enhanced the importance of studies on ancient reef crises.

1.1.2 Permian-Triassic transition and the Middle Permian (Capitanian) mass extinction

Among the traditional “Big Five” mass extinctions, the end-Permian mass extinction was evaluated as the most severe one on the reef system (Newell, 1972; Flügel and Kiessling, 2002). This mass extinction severely affected reefs (Kiessling and Simpson, 2011) and led to a metazoan reef eclipse in the Early Triassic with only some microbial-metazoan reef survivors (Zatoń et al., 2018; Heindel et al., 2018; Martindale et al., 2019). The end-Permian mass extinction was followed by a “modernization” of the reef ecosystem, in that the reef communities transformed from late Paleozoic types to Mesozoic types, marked by the emergence of scleractinian coral dominated reefs and the onset of coral-zooxanthellae symbiosis in the Late Triassic (Stanley, 1988; Martindale et al., 2019).

The end-Permian mass extinction was once considered as a two-stage crisis, including a pre-Lopingian/end-Guadalupian event and an end-Changhsingian event (Jin et al., 1994; Stanley and Yang, 1994). The pre-Lopingian/end-Guadalupian event was studied by many workers as the “end-Guadalupian mass extinction”, which happened at the level of the Guadalupian/Lopingian (G/L) boundary (e.g., Kaiho et al., 2005). However, since several studies revealed that some of the marine microfossils actually suffered losses in a much earlier time comparing to the G/L boundary, and the post-extinction fauna occurred in the late Guadalupian interval (e.g., Shen and Shi, 2009; Wignall et al., 2009a, 2009b), this pre-Lopingian event was revised to be the “Capitanian, or late Guadalupian, mass extinction event” (Wignall, 2009b), “Middle Capitanian (Permian) mass extinction” (Bond et al., 2010b), or “Middle Permian (Capitanian) mass extinction” (Bond et al., 2010a). Based on the records of fusulinid and calcareous algae from South China, this extinction was suggested to be within the middle Capitanian *Jinogondolella altudaensis* conodont zone, predating/coincident with a major negative excursion ($\sim 5\%$) of $\delta^{13}\text{C}$, and coinciding with the onset of Emeishan volcanism (Wignall et al., 2009a, Bond et al., 2010b).

Kerithelial-walled fusulinaceans and calcareous algae were the two major victims suffering the most from the Middle Permian (Capitanian) mass extinction, where the large sized,

complex fusulinids (e.g., neoschwagerinids and schwagerinids) fauna in the Middle Permian were replaced by a smaller sized Late Permian assemblage (e.g., *Codonofusiella* and *Reichelina*), and the dominant calcareous algae changed from *Permocalculus* and *Macroporella* to *Gymnocodium*, *Mizza* and *Pseudovermiporella* (e.g., Lai et al., 2008; Wignall et al., 2009a, 2009b). Brachiopods (e.g., Shen and Shi, 2002; Clapham, 2015), corals including tabulate and rugose coral (e.g., Wang and Sugiyama, 2000), and bivalves (e.g., giant alatoconchids) (e.g., Aljinović et al., 2008; Isozaki and Aljinović, 2009; Chen et al., 2018) also suffered species loss during the transition from the Middle Permian to the Late Permian.

Despite the severity of the Middle Permian (Capitanian) mass extinction being continuously debated (Sepkoski, 1996, Bambach et al., 2004, McGhee et al., 2004; Clapham et al., 2009; Stanley, 2016, McGhee et al., 2013, Rampino and Shen, 2019, Fan et al., 2020), the transition of reef ecosystem across the Middle/Late Permian is a pioneer stage of reef demise before the end-Permian mass extinction (Kiessling, 2005). The Middle Permian (Capitanian) mass extinction affected the reef ecosystem by a decline of the reef carbonate production (89%) and reef numbers (47%) (Flügel and Kiessling, 2002), and a 55% loss in reef diversity (Weidlich, 2003) from Middle Permian to Late Permian. In addition, the distribution of reefs in the Wuchiapingian is restricted to the Zechstein Basin, Sicily, Salt range, and south China, within an equatorial belt which is much narrower compared to the Middle Permian (Flügel and Kiessling, 2002, Weidlich, 2002a, 2002b; Weidlich 2003).

1.1.3 Aims of this study

The effect of mass extinction on the reef ecosystem sometimes lingered on well into the post-crisis phases, such as the reef gap in Early Triassic and the stepwise recovery of reefs following the end-Permian mass extinction (Martindale et al., 2019). Similarly, the Wuchiapingian reef recovery also coped with the aftermath of the Middle Permian mass extinction, but it was not well studied because of the eclipse of reefs in the Wuchiapingian (Flügel and Kiessling, 2002, Weidlich, 2002a). However, Wuchiapingian reef recovery is a key scenario to complete the Permian-Triassic transition which is critical for the Phanerozoic reef evolution. The studies of Wuchiapingian reefs are mainly concentrated in the Zechstein Basin,

focused on the spectacular bryozoan and microbial reef complexes (e.g., Hollingworth and Tucker, 1987; Paul, 1980; Peryt et al., 2012, 2020; Fheed et al., 2015; Raczynski et al., 2017). However, the Zechstein reefs are poorly constrained stratigraphically just as most of the Wuchiapingian reef localities. Nevertheless, in South China, the only confirmed Wuchiapingian reef is located in the Tieqiao section, which is the auxiliary section of the Guadalupian/Lopingian Global Stratotype Section and Point (GSSP), where detailed stratigraphic work has been carried out within last decades (Sha et al., 1990; Mei et al., 1998; Jin et al., 2006; Shen et al., 2007). After the initial paleontological and sedimentological studies from last century (Yang, 1987; Sha et al., 1990), the massive limestones from the upper part of the Heshan (Wujiaping) formation at the Tieqiao section were confirmed as a reef recently (Qiu and Wang, 2010; Qiu et al., 2014, Huang et al., 2019a). However, the identification of individual reef bodies, description of reef composition, and understanding of reef growth patterns/cycles, which can significantly affect the determination of timing and patterns of reef recovery, can still be much improved. In addition, the previous studies only focused on the stratigraphic changes of this 150m thick and 100 m wide section, but a study of the lateral reef geometry changes was missing. Thus, here, this thesis presents studies which focus on both the stratigraphic and lateral changes of the Wuchiapingian Tieqiao reef complex, through two-dimensional investigations on both the outcrop and microscopic scale, combined with a detailed biostratigraphic study, to discuss the timing, process, and controlling factors of reef recovery after the Middle Permian (Capitanian) mass extinction, in order to complete the understanding of the reef evolution in the Permian-Triassic transition.

1.2 General geological settings

The Dian-Qian-Gui Basin was located on the southwest margin of the Yangtze Platform (South China block), which was deposited in the equatorial belt from the Middle to Late Permian (Scotese and Langford, 1995; Hou et al., 2020). From the Devonian to the middle Triassic, under the regional background of tectonic extension and subsidence of the basin floor, a couple of isolated carbonate platforms were established in the Dian-Qian-Gui Basin (Wang, 1985, Liu & Xu, 1994, Feng et al., 1996, Ma et al., 2009, Shi et al., 2009). The Laibin-Heshan

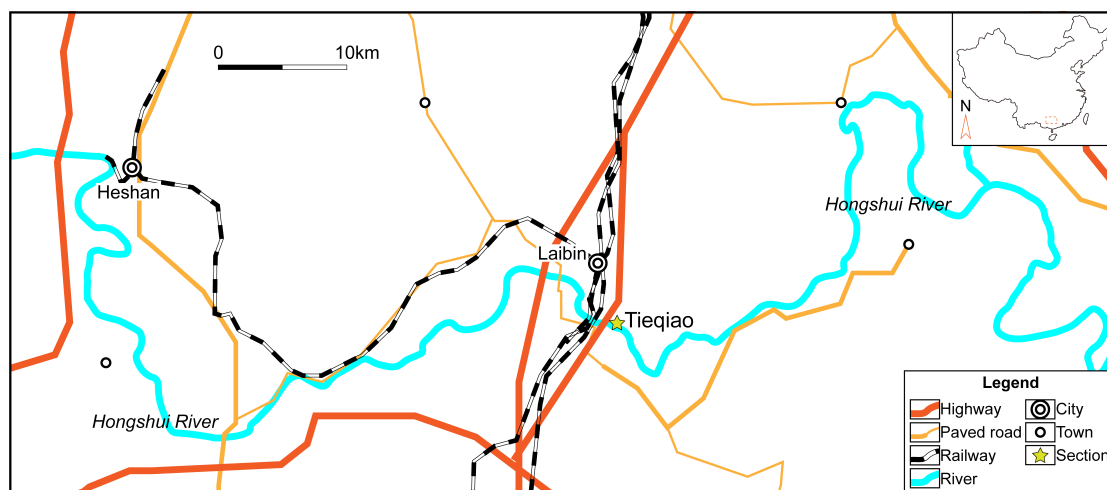


Figure 1.1. Location map of Tieqiao section in the Laibin-Heshan area.

isolated carbonate platform is one of them. This study was carried out on the Tieqiao section, deposited on the margin of the Laibin-Heshan isolated platform during the Late Permian Wuchiapingian Stage.

Age (Ma)	Stage	Conodont Zone	Conodonts	South China				Central/ West Europe	North America	
				Laibin					Guadalupe Mountains	Delaware Basin
Lithostratigraphic units										
250	Early Triassic	I2	<i>Isarcicella isarcica</i>	LuoLou Fm.	Feixianguan Fm.	Yinkeng Fm.	Dongchuan Fm.	Buntsandstein Gp.		
252		I1	<i>Hindeodus parvus</i>							
254	Changhsingian	L10	<i>Clarkina changxingensis</i>	Talung Fm.	Changhsing Fm.	Talung Fm.	Kayitou Fm.			Dewey Lake Fm.
254		L9	<i>Clarkina subcarinata</i>							
254		L8	<i>Clarkina wangi</i>							
256	Wuchiapingian	L7	<i>Clarkina orientalis</i>					Zechstein Gp.		Rustler Fm.
256		L6	<i>Clarkina transcaucasica</i>	Wuchiaping/Heshan Fm.	Wuchiaping Fm.	Longtan Fm.	Xuanwei Fm.			Salado Fm.
258		L5	<i>Clarkina guangyuanensis</i>							
258		L4	<i>Clarkina leveni</i>							
258		L3	<i>Clarkina asymmetrica</i>							
258		L2	<i>Clarkina dukouensis</i>							
258		L1	<i>Clarkina postbitteri postbitteri</i>							
260	Capitanian	G7	<i>Jinogondolella hongshuiensis</i>				Emeishan basal			
260		G6	<i>Jinogondolella granti</i>							
262		G5	<i>Jinogondolella xuanhanensis</i>							
262		G4	<i>Jinogondolella prexuanhanensis</i>							
262		G4	<i>Jinogondolella altudaensis</i>							
262		G4	<i>Jinogondolella shannoni</i>							
264	Wordian	G3	<i>Jinogondolella postserrata</i>	Maokou Fm.	Maokou Fm.	Kuhfeng Fm.	Maokou Fm.	Rotliegend Gp.	Capitan Fm. (Capitan Reef Complex)	Bell Canyon Fm.
266		G2	<i>Jinogondolella aserrata</i>							Cherry Canyon Fm.
270	Roadian	G1	<i>Jinogondolella nankingensis</i>							Brushy Canyon Fm.
272										Cutoff Fm.

Figure 1.2 Correlation of chronostratigraphic units, lithostratigraphic units and conodont zones. Note: age, conodont zone, conodonts, and lithostratigraphic units of South China are modified from Shen et al. (2018), Lithostratigraphic units of Laibin is modified from Sha et al. (1990), lithostratigraphic units of Central/West Europe and North America is modified from Menning et al. (2006) and Kerans and Tinker (1999). Fm.: Formation; Gp.: Group.

The Tieqiao section (109.251°E; 23.704°N) is located 5km southeast from the center of Laibin city, Guangxi Zhuang Autonomous Region, China, along the northern bank of Hongshui

river (Fig. 1.1). It is an auxiliary section for the Global Stratotype Section and Point (GSSP) of Guadalupian/Lopingian (G/L) boundary. The GSSP Penglitan section is 10 km east from the Tieqiao section. The strata of the Tieqiao section were subdivided by Sha et al.(1990) into 15 Members and subsequent 139 Beds, which including the Maping, Chihhsia (Qixia), Maokou, Heshan (Wuchiaping or Wujiaping) and Talung (Dalong) Formations (Figure 1.2), spanning Asselian (Early Permian) to the Permian/Triassic boundary. The subdivision of strata from Sha et al., (1990) was applied in the present study to allow the correlation with other studies.

1.3 General methodology

The scenario of post-extinction reef recovery should be scripted within both the temporal and spatial framework. In this study, biostratigraphic, sedimentologic, and palaeoecological methods were used to explore the nature of the Wuchiapingian reef evolution. Firstly, to constrain the reef development following the Middle Permian (Capitanian) mass extinction, a conodont biostratigraphic study from Early to Late Permian was applied on the Tieqiao section. This step is essential as conodonts provide a standard framework which can be correlated globally. Secondly, to understand the reef recovery process timely and spatially, a sedimentological study based on detailed semi-quantitative 2D outcrop mapping was applied on the Wuchiapingian Tieqiao section, including observation on the weathered/acid-etched surfaces of the outcrop, on polished slabs, and thin sections. Lastly, to further study the factors, including but not limited to sedimentological and ecological ones, which controlled or impacted the reef recovery process, quantitative biocommunity and rock composition analyses on the point-counting data of thin sections were applied on selected samples from the Wuchiapingian Tieqiao section.

1.4 Organization of the thesis

This doctoral thesis is divided into five chapters, of which chapters 2, 3, and 4 are published or submitted research papers presenting the main results of this study. Three different

perspectives are studied in these three papers to approach the nature of the recovery of reefs following the Middle Permian (Capitanian) mass extinction.

Chapter 2 includes a revised conodont stratigraphic study through the Artinskian to the Wuchiapingian Stage on the Tieqiao section. Detailed description of twenty main conodont zones, seven subordinate conodont zones, and new species are presented in this chapter. Although it is challenging to recover the conodonts directly from the shallow-water deposits, through investigations in the deep-water deposits below and above the reef settings, conodonts have been found to constrain the time of post-extinction reefs.

In chapter 3, a semi-quantitatively sedimentological study was carried out on the Wuchiapingian Tieqiao section. A manual grid mapping and a remote photogrammetry mapping using a drone (Commercial UAV Dji Phantom 4 pro) were applied on the outcrop to recognize individual reef bodies. The intensive acid-etched outcrop surfaces and thin sections were made for detailed lithofacies studies. The timing and pattern of reef recovery after the Middle Permian (Capitanian) mass extinction was updated through these investigations. In addition, the reef growth cycles with different biotas were also revealed.

Chapter 4 was designed to enhance the understanding of reef recovery from semi-quantitative studies. Quantitative analyses were applied on the point-counting data of selected thin sections. The ecology and functioning of reef-building organisms were discussed to evaluate their contribution to the post-extinction reef evolution through the analyses of skeletal grains. Furthermore, the analyses of whole-rock components were applied to investigate the contribution of additional components that important to the reef construction. Environmental factors that impacted the reef recovery were also discussed in this chapter.

Finally, in chapter 5, the results were summarized and discussed in the synthesis section, and the main results were generalized as conclusions of this thesis.

Chapter 2 has been published in 2017 in *Palaeogeography, Palaeoclimatology, Palaeoecology* (Sun, Y.D, Liu, X.T., Yan, J.X., Li, B., Chen, B., Bond, D.P.G., Joachimski, M.M., Wignall, P.B., Wang, X., Lai, X.L., 2017. Permian (Artinskian to Wuchiapingian) conodont biostratigraphy in the Tieqiao section, Laibin area, South China. *Palaeogeography, Palaeoclimatology, Palaeoecology*. 465, 42–63. <https://doi.org/10.1016/j.palaeo.2016.10.013>). Chapter 3 has been published in 2019 in *Global and Planetary Change* (Wang, X., Foster, W.J.,

Yan, J.X., Li, A.Z., Mutti, M., 2019. Delayed recovery of metazoan reefs on the Laibin-Heshan platform margin following the Middle Permian (Capitanian) mass extinction. *Global and Planetary Change*. 180, 1–15. <https://doi.org/10.1016/j.gloplacha.2019.05.005>). Chapter 4 has been submitted to *Palaeogeography, Palaeoclimatology, Palaeoecology* (Wang, X., Foster, W.J., Yan, J.X., Meng, Q., Mutti, M., Quantifying ecosystem functioning in post-extinction reef communities: a test of ecological restructuring after the Middle Permian mass extinction.).

Chapter 2

Permian (Artinskian to Wuchiapingian) conodont biostratigraphy in the Tieqiao section, Laibin area, South China

Published in 2017 in *Palaeogeography, Palaeoclimatology, Palaeoecology*,
<https://doi.org/10.1016/j.palaeo.2016.10.013>

Abstract

Permian strata from the Tieqiao section (Jiangnan Basin, South China) contain several distinctive conodont assemblages. Early Permian (Cisuralian) assemblages are dominated by the genera *Sweetognathus*, *Pseudosweetognathus* and *Hindeodus* with rare *Neostreptognathodus* and *Gullodus*. Gondolellids are absent until the end of the Kungurian stage—in contrast to many parts of the world where gondolellids and *Neostreptognathodus* are the dominant Kungurian conodonts. A conodont changeover is seen at Tieqiao and coincided with a rise of sea level in the late Kungurian to the early Roadian: the previously dominant sweetognathids were replaced by mesogondolellids. The Middle and Late Permian (Guadalupian and Lopingian Series) witnessed dominance of gondolellids (*Jinogondolella* and *Clarkina*), the common presence of *Hindeodus* and decimation of *Sweetognathus*.

Twenty main and seven subordinate conodont zones are recognised at Tieqiao, spanning the lower Artinskian to the middle Wuchiapingian Stage. The main (first appearance datum) zones are, in ascending order by stage: the *Sweetognathus* (*Sw.*) *whitei*, *Sw. toriyamai*, and *Sw. asymmetrica* n. sp. Zones for the Artinskian; the *Neostreptognathodus prayi*, *Sw. guizhouensis*, *Sw. iranicus*, *Sw. adjunctus*, *Sw. subsymmetricus* and *Sw. hanzhongensis* Zones for the Kungurian; the *Jinogondolella* (*J.*) *nankingensis* Zone for the Roadian; the *J. aserrata* Zone for the Wordian; the *J. postserrata*, *J. shannoni*, *J. altudaensis*, *J. prexuanhanensis*, *J. xuanhanensis*, *J. granti* and *Clarkina* (*C.*) *hongshuiensis* Zones for the Capitanian and the *C. postbitteri* Zone and *C. transcaucasica* Zone for the base and middle of the Wuchiapingian. The subordinate (interval) zones are the *Pseudosweetognathus* (*Ps.*) *costatus*, *Ps. monocornus*, *Hindeodus* (*H.*) *gulloides*, *Pseudohindeodus ramovsi*, *Gullodus* (*G.*) *sicilianus*, *G. duani* and *H. excavates* Zones.

In addition, three new species, *Gullodus tieqiaoensis* n. sp., *Pseudohindeodus elliptica* n. sp. and *Sweetognathus asymmetrica* n. sp. are described. Age assignments for less common species (e.g., *G. duani*, *H. catalanoi* and *Pseudosweetognathus monocornus* etc.) are reassessed based on a rich conodont collection.

2.1. Introduction

Conodonts are important index fossils in the Palaeozoic and Triassic, due to their high speciation rates, geographically widespread distribution and in part high abundance in marine

sediments. Conodont biostratigraphy provides the best method for high-resolution, supra-regional correlations of Permian strata, because other key taxa such as ammonoids are often scarce in many locations, whilst foraminifers and brachiopods are generally long ranging and facies controlled and thus less useful for age diagnosis. As a consequence, Permian conodont taxonomy and biostratigraphy have been the topics of extensive study since the 1950s (e.g., Youngquist et al., 1951; Clark and Behnken, 1971; Ritter, 1986; Wardlaw and Grant, 1990; Mei et al., 1994b; Wardlaw, 2000; Nestell et al., 2006; Lambert et al., 2010; Shen et al., 2012). The importance of conodonts in stratigraphy is exemplified by their use at Global Boundary Stratotype Section and Points: as of 2016, conodonts define the bases of all but three of the 29 stages between the Pragian (Lower Devonian) and Rhaetian (Upper Triassic), 15 of which have been ratified by the International Commission on Stratigraphy.

The diversity of Permian conodonts is generally low in comparison to that observed for other time periods, with typically fewer than five genera and two dozens of species occurring in any given Permian stage. Conodont zones are also relatively long for some intervals. For instance, though substantial investigations have been carried out in West Texas (e.g., Wardlaw, 2000; Nestell et al., 2006; Nestell and Wardlaw, 2010a; Wardlaw and Nestell, 2010), only one standard conodont zone has been established for the Roadian and Wordian stages (Henderson et al., 2012). This reflects a true low point in the diversity of conodonts during their long evolutionary history. A further complication is that minor changes in Permian conodont morphology require a careful taxonomic examination of different species. New species are rarely reported from regions other than West Texas and South China, perhaps owing to a decrease in research effort and a substantial loss of expertise in recent years.

Establishing a robust biostratigraphic scheme in different areas is essential for supra-regional correlation. Permian conodonts have been most often studied in the Urals of Russia (Early Permian), West Texas (Middle Permian) and South China (Late Permian and the Permian-Triassic boundary) (e.g., Chuvashov et al., 1990; Mei et al., 1994a; Zhang et al., 1995; Wardlaw, 2000; Lambert et al., 2002; Chernykh, 2005; Jiang et al., 2007; Nestell and Wardlaw, 2010b). The Early to Middle Permian of South China has attracted comparatively little research attention and is less systematically studied (Wang et al., 2016).

This study presents a higher-resolution conodont record for the Tieqiao section, Guangxi, South China. New data, spanning the Artinskian (Early Permian) to the middle Wuchiapingian (Late Permian), substantially improve existing records of the section, first described two decades ago in the context of the Capitanian-Wuchiapingian (Guadalupian-Lopingian) transition (Mei et al., 1994c; Henderson et al., 2002; Wang, 2002).

2.2. Geological setting

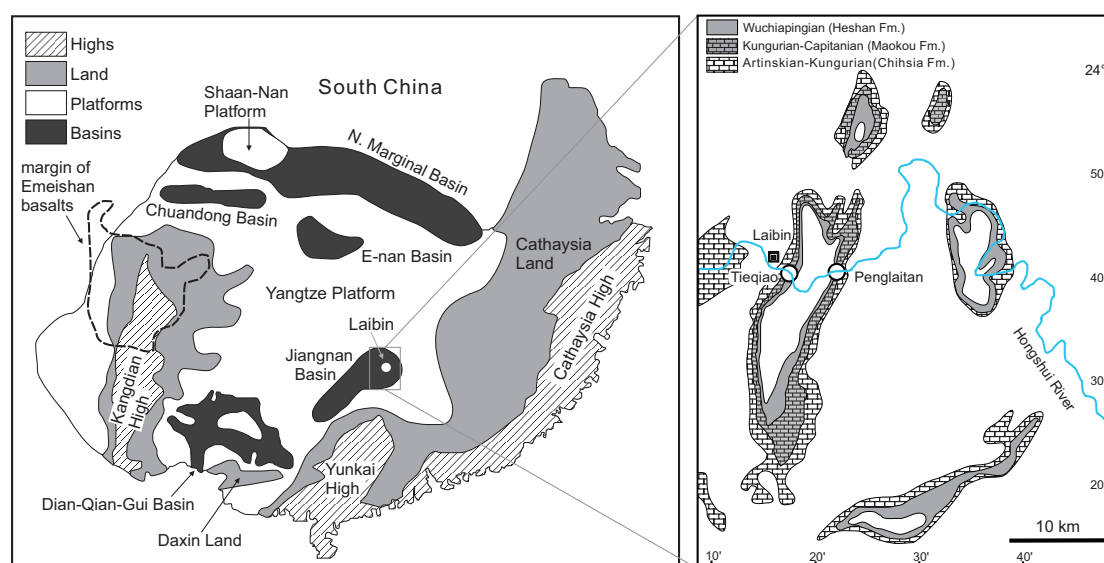


Figure 2.1: Middle Permian palaeogeographic reconstructions of South China and Permian lithologic units in Laibin area (after Wang and Jin, 2000; Shen et al., 2007).

The Yangtze region was a large isolated platform situated within the Permian equatorial Tethys (Figure 2.1) with extensive carbonate deposits and diverse sedimentary facies. It is an ideal location for conodont studies. The Laibin area is located in the Dian-Qian-Gui Basin towards the southwestern margin of the Yangtze Platform (Wang and Jin, 2000). A series of superb sections are exposed along the banks of Hongshui River (Shen et al., 2007) and these have been comprehensively studied for the Capitanian-Wuchiapingian transition (e.g., Mei et al., 1994c; Wang et al., 2004; Jin et al., 2006; Wignall et al., 2009b; Chen et al., 2011).

The Permian strata of the region consist of thick Early Permian platform carbonates, subordinate Middle Permian slope to basinal carbonates and cherts. Late Permian rocks are geographically more variable, including coal seams, reef build-ups and radiolarian cherts (Sha et al., 1990; Shen et al., 2007; Qiu et al., 2014).

The studied section at Tieqiao ($23^{\circ} 42.733' \text{ N}$, $109^{\circ} 13.533' \text{ E}$) is exposed on the northern bank of the Hongshui River, southeast of the town of Laibin (Figure 2.1, 2.2). The Permian

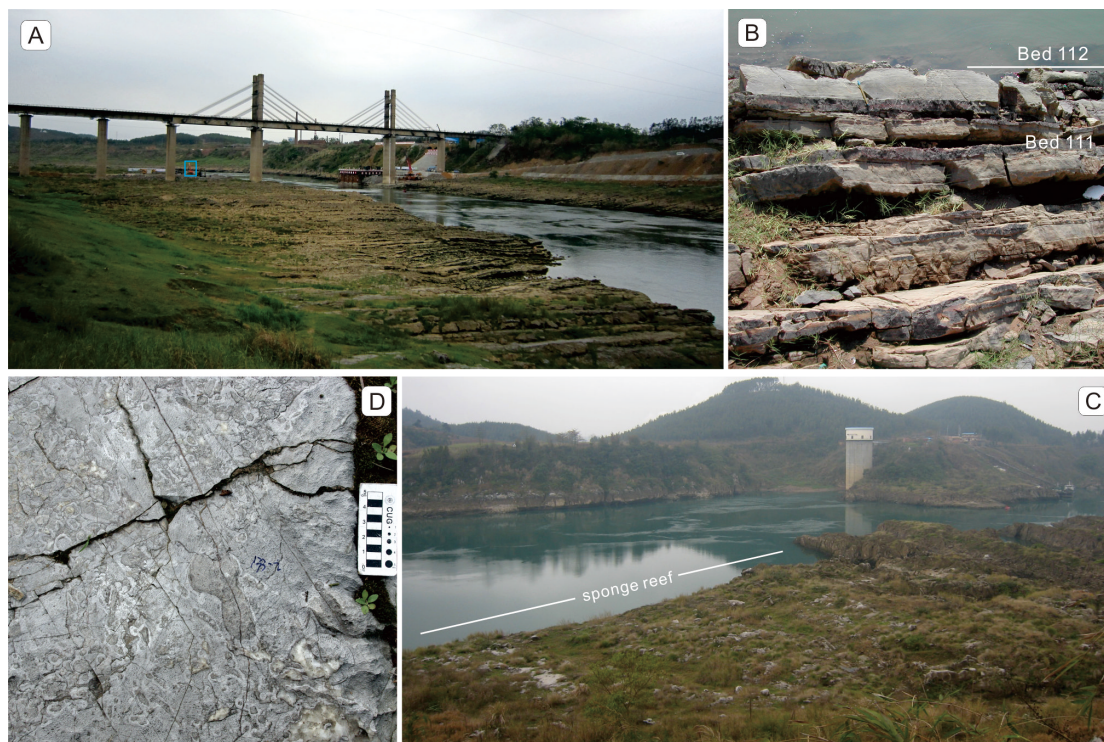


Figure 2.2: Field photographs of the studied section. A, an overview of the Chihhsia Fm. in the lower part of the section. A digger in the far side (blue square) as scale. B, a close review of fine laminated Bed 111–112 transition (Roadian-Wordian boundary interval). The pen (~15 cm long) as scale. C, an overview of the Wuchiapingian sponge reef at Tieqiao. D, Photograph shows a high diversity, *in situ* framework of sponges (bafflestone) in Bed 133.

strata measure 1307 m thick and comprise the Maping, Chihhsia, Maokou, Wuchiaping (Heshan) and Talung Formations, spanning the earliest Permian (Asselian) to the Permian-Triassic boundary (Sha et al., 1990). The section is very fossiliferous, with foraminifers, calcareous algae, crinoids, sponges and corals being prolifically abundant (e.g., Wang and Sugiyama, 2000; Bucur et al., 2009; Zhang et al., 2015), whilst bivalves and ammonoids occur less frequently. Well-preserved *Zoophycos* trace fossils are also abundant (Gong et al., 2010).

Sha et al. (1990) pioneered the study of the Tieqiao section and subdivided the section into 15 Members and 139 Beds. Our study follows these subdivisions (Figures 2.3–2.5) for consistency and focuses on the stratigraphy and conodont zonation of the Chihhsia, Maokou and Wuchiaping formations (Bed 1 to Bed 134). The Chihhsia Fm. generally records deposition in a carbonate ramp setting, whilst the Maokou Fm. comprises slope to basin transition facies. The two formations are 710 m thick in total and range from the Sakmarian (?) to the Capitanian-

Wuchiapingian boundary (Figures 2.3–2.5). The Wuchiaping Fm. records a shift in depositional environments from a deep water basin (Beds 120–122) to a sponge reef (Beds 123–133).

2.3. Materials and Methods

The section was sampled over four field campaigns between 2005 and 2010. During the spring of 2010, the water of the Hongshui River fell to its lowest level of the past ten years due to a severe drought, which allowed us to describe and sample several normally submerged parts of the section (e.g., Bed 17 and Bed 112). A total of 374 rock samples were collected with a sampling resolution of ~1–2 m for most parts of the section. Cherts and grainstones bearing abundant corals and fusulinid foraminifers were avoided during sampling due to complications in conodont extraction and low conodont yields. Each sample weighed between 2.5 and 8.0 kg.

Three hundred and eleven samples were processed in the micropaleontology laboratory at China University of Geosciences (Wuhan) and 63 samples were processed at the GeoZentrum Nordbayern, Universität Erlangen-Nürnberg. All samples were dissolved using 7–10% diluted acetic acid, wet sieved through 20# and 160# meshes (openings are ~850 and 97 μm , respectively) and air-dried. The insoluble residues were separated by using heavy liquid fractionation (bromoform-acetone solution at Wuhan and sodium polytungstate-water solution at Erlangen, both with density 2.82 g/cm^3). Conodont specimens were handpicked using binocular microscopes. Conodonts from Tieqiao are generally well preserved with colour alternation index ranging from 1.5 to 2.5. A total of 8733 specimens were obtained at Wuhan and about ~3000 specimens were recovered at Erlangen. Results from both laboratories were cross checked.

Please note that references first appearance datum (FAD) in this study are based on the current sampling effort and represents local first occurrence (FO).

2.4. Stratigraphy and conodont zonation

2.4.1. *Sakmarian* (?)

The lowermost part of the studied section (Beds 1 to 16, Chihhsia Fm.) consists mainly of thin-to-medium bedded dark-grey bioclastic micrites, marls and black shales (Figure 2.2). Brachiopods, gastropods, crinoids, bryozoans and sponges are the most abundant fossils. The

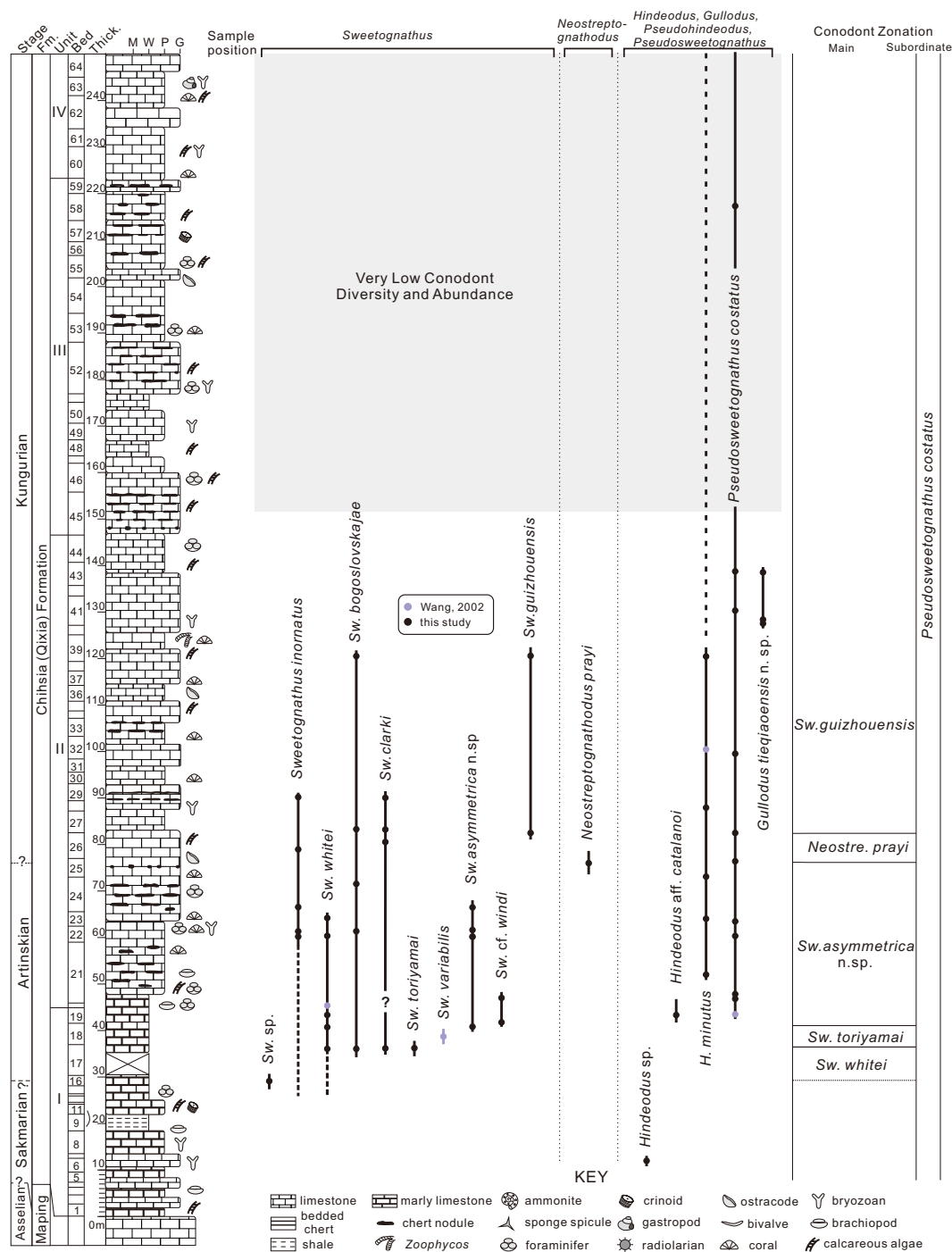


Figure 2.3: Log of the lower part of Tieqiao section (Asselian to Kungurian) with conodont ranges and zonation.

age assignment for this part of the section is controversial. Sha et al. (1990) suggested an Asselian age for the underlying Mapping Fm. and reported the occurrence of the fusulinacean

foraminifers *Eoparafusulina* sp., *Nankinella* sp., *Pamirina* sp., *Staffella* sp., and *Pseudofusulina* sp. from Bed 1 to Bed 16, implying a possible Sakmarian age for the unit. Mei et al. (1998) inferred this unit to be of “Longlinian” age — a Chinese equivalent of the Artinskian by original definition (Sheng and Jin, 1994; Jin et al., 1997), now re-defined as Sakmarian (Figure 4.1 in Henderson et al., 2012). Based on consideration of all published fossil materials, Shen et al. (2007) tentatively assign this part of the section to the Artinskian.

Few conodonts were recovered from this part of the section, despite great efforts. One *Hindeodus* specimen was obtained from Bed 6 whilst many ramiform elements were recovered from Bed 8. But none of these is age-diagnostic. These ramiform elements are Ellisonids, but unlikely belonging to *Sweetognathus* or *Hindeodus* (e.g., Wardlaw et al., 2015). Bed 16 yields a poorly preserved *Sweetognathus* specimen. The precise age of this unit remains unresolved.

2.4.2. Artinskian

Beds 17 to 26 consist mainly of dark-grey to grey bioclastic pack- and grainstones. The conodont assemblage is dominated by *Sweetognathus whitei* and affinitive species and thus indicates an Artinskian age (Plate 1 and Plate 2). *Neostreptognathodus* and *Hindeodus* are rare whilst gondolellids are absent. The base of the Artinskian stage cannot be precisely defined because the FO of *Sweetognathus whitei* cannot be ascertained due to the inaccessibility of the submerged lower part of Bed 17 and the absence of diagnostic conodonts from beds below this level. In ascending order, three conodont zones were established for the Artinskian:

1) *Sweetognathus whitei* Zone (?30–36.5 m, Bed 17)

The lower limit of this zone is not defined. The upper limit is defined by the FAD of *Sweetognathus* (*Sw.*) *toriyamai*.

Sweetognathus whitei was one of the most cosmopolitan conodont species during the Early Permian (Mei et al., 2002). It is known e.g., from North and South China, Japan, U.S.A., Canada and Colombia. (Rhodes, 1963; Igo, 1981; Orchard, 1984; Ritter, 1986; Ding and Wan, 1990; Ji et al., 2004; Boardman et al., 2009) and is considered a good marker for the base of Artinskian.

2) *Sweetognathus toriyamai* Zone (36.5–41 m, Beds 17–18)

Lower limit: FAD of *Sw. toriyamai* in the uppermost Bed 17. Upper limit: FAD of *Sw. asymmetrica* n. sp. The FAD of *Sw. bogoslovskajae* occurs in this zone. *Sw. bogoslovskajae* is known to co-exist with *N. pequopensis* in Nevada and has a range restricted to the upper “Baigendzhinian” (equivalent to uppermost Artinskian to lower Kungurian) (Ritter, 1986). Wang (2002) reported the occurrence of *Sw. variabilis* in this zone (in Bed 18). We have found morphotypes which are similar to *Sw. variabilis* but the specimens are not sufficiently well-preserved to make an identification.

3) *Sw. asymmetrica* n. sp. Zone (41–76 m, Beds 18–25)

Lower limit: FAD of *Sw. asymmetrica* n. sp. Upper limit: FAD of *Neostreptognathodus prayi*. *Hindeodus catalanoi* and *Sw. cf. windi* co-occur in this zone. This Zone likely straddles the Artinskian-Kungurian boundary due to the absence of the *N. pnevi* Zone at Tieqiao.

2.4.3. Kungurian

Kungurian rocks, spanning from Bed 25 to the lower part of Bed 109, consist mainly of medium-to-thick bedded fossiliferous pack- and grainstones with common chert nodules in the lower part. Medium to thin bedded lime mudstones and wackestones were gradually developed higher in the Kungurian strata, with a notable shift in fossil assemblages from a bryozoan- and calcareous algae-dominated shallow water facies (Beds 89–99) to a sponge spicule and radiolarian rich deeper water facies (Beds 100–111). In the latest Kungurian, conodont faunas change from *Hindeodus-Pseudohindeodus-Sweetognathus*-dominated and gondolellid-free assemblages (Plate 3 and Plate 4) to gondolellid-dominated assemblages in Bed 109 (Plate 5). This shift in conodont assemblage coincides with a lithological change from thick- and medium- bedded wackestones to more cherty, medium- to thin- bedded wackestones and micritic mudstones.

The conodont biostratigraphy of the basal Kungurian Stage has been a matter of debate (Wang et al., 2011). Kozur (1995) suggested the cline *Neostreptognathodus (N.) pequopensis-N. pnevi* to be suitable for a definition for the Artinskian-Kungurian boundary. Mei et al. (2002) proposed the FAD of *N. pequopensis* or *Sw. guizhouensis* to define the base of the Kungurian

whereas Chuvashov et al. (2002) formally proposed the FAD of *N. pnevi* as diagnostic of the base of the Kungurian, a definition that has been generally accepted (Henderson et al., 2012).

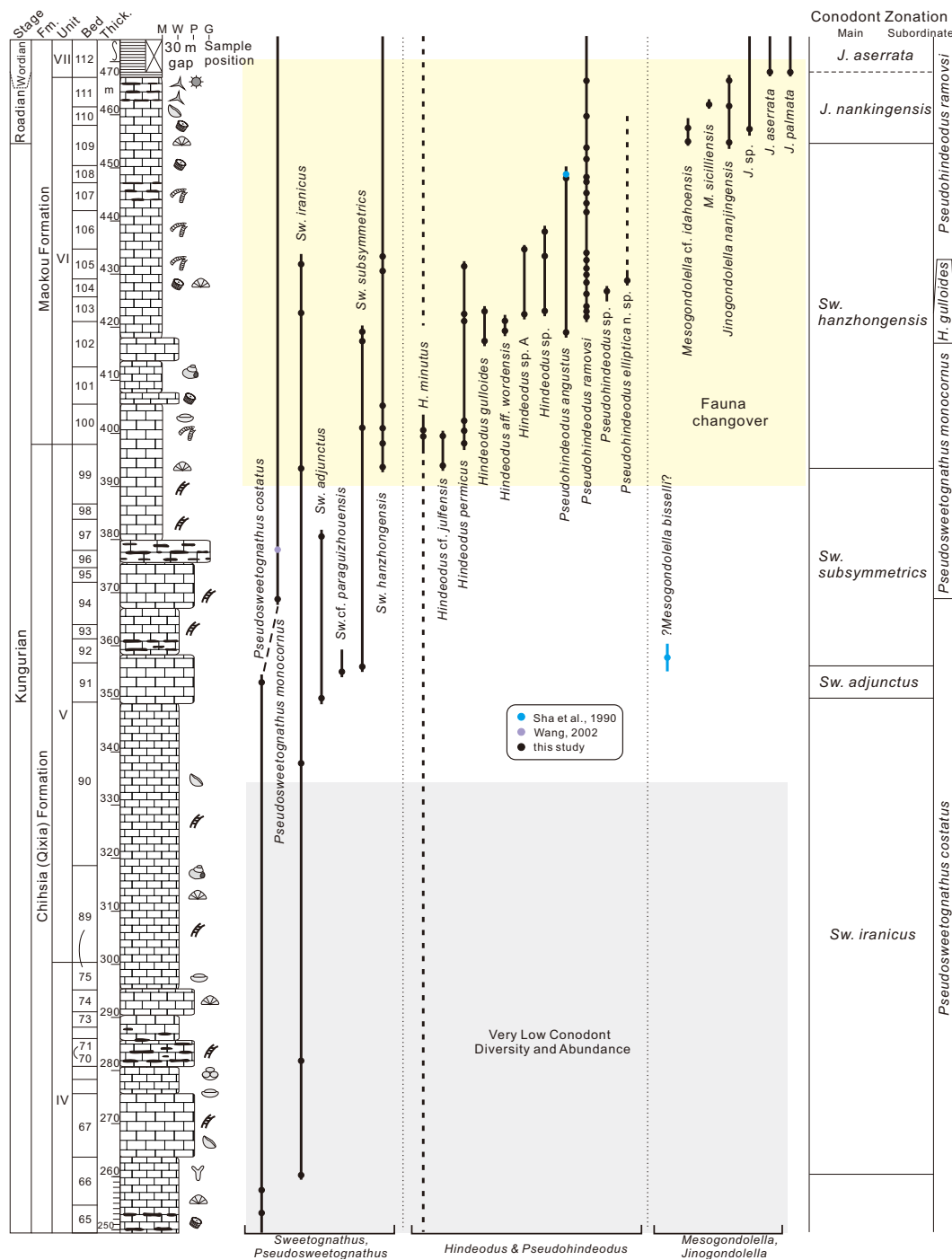


Figure 2.4: Log of the middle part of Tieqiao section (Kungurian to Wordian) with conodont ranges and zonation. Keys are the same as in Figure 2.3. Note that the reported occurrence of *Mesogondolella bisselli* in Bed 91 (Sha et al., 1990) cannot be confirmed by our dataset (for details see discussion of the *Sw. adjunctus* zone). Keys are the same as in Figure 2.3.

However, due to the absence of *N. pnevi* at Tieqiao, we suggest alternatively using the FAD of *N. prayi* or *Sw. guizhouensis* to correlate the lower Kungurian. The Kungurian strata at Tieqiao

is rather expanded (roughly 300 m thick) and is ideal for studying conodont zonation for this Stage. Six conodont zones have been established, described in ascending order below:

4) *Neostreptognathodus prayi* Zone (76–82.5 m, Beds 25–26)

Lower limit: FAD of *N. prayi*. Upper limit: FAD of *Sw. guizhouensis*. Behnken (1975) described the zonal element *N. prayi* and illustrated a full growth series for the species. At Tieqiao, we recovered a few specimens which fit into Behnken's (1975) description for gerontic growth stage of *N. prayi* (Figure 18 of Plate 2 in Behnken, 1975; the same specimen is re-illustrated in Kozur, 1987). In addition, gerontic *N. prayi* and *Pseudosweetognathus costatus* can be easily differentiated due to their distinctive platform shoulders and different carina decorations.

The *N. prayi* Zone is the second oldest zone of the Kungurian in the standard Permian conodont zonation (Henderson et al., 2012) and so the *N. prayi* Zone at Tieqiao most probably does not indicate the “true” earliest Kungurian (Figure 2.6). *Sw. clarki*, a species most commonly seen in the late Artinskian (Beauchamp and Henderson, 1994), also extends to this zone.

5) *Sw. guizhouensis* Zone (82.5–260.5 m, Beds 26–66)

Lower limit: FAD of *Sw. guizhouensis*. Upper limit: FAD of *Sw. iranicus*. Except for in the lower part of this ~180 m thick conodont zone, conodonts are relatively rare. The long-ranging species *Pseudosweetognathus costatus* is the only species that was sparsely recovered in the upper part of this zone.

Sweetognathus guizhouensis is a cosmopolitan species that has high potential for supra-regional correlation. It is known from South China (Wang et al., 1987; Mei et al., 2002), Japan (Shen et al., 2012), Pamir Mountains (Kozur, 1994) and Sicily (Catalano et al., 1991), although it is not recorded in the north America.

6) *Sw. iranicus* Zone (260.5–350 m, Beds 66–91)

Lower limit: FAD of *Sw. iranicus*. Upper limit: FAD of *Sw. subsymmetricus*. As with the *Sw. guizhouensis* Zone, both conodont diversity and abundance are very low. A major stratigraphic complication at this level of the section is that Beds 76–88 are a tectonic repetition of older beds (also see Sha et al., 1990).

7) *Sw. adjunctus* Zone (350–356 m, Bed 91)

Lower limit: FAD of *Sw. adjunctus*. Upper limit: FAD of *Sw. subsymmetricus*. *Sw. cf. paraguizhouensis* appears in this zone. Sha et al. (1990) reported the occurrence of “*Neogondolella*” *bisselli* in this zone (Bed 91). However, “*N.*” *bisselli* is an older species which often co-occurred with the Artinskian *Sw. whitei* group (e.g., Behnken, 1975; Clark et al., 1979; Orchard, 1984; Wang, 1994; Mei et al., 2002). The occurrence of *bisselli* obviously contradicts a Kungurian age of the host strata and also is not confirmed by our dataset.

Sw. adjunctus is also known from the uppermost Victorio Peak Formation from Texas and the upper Pequop Formation from Nevada, USA (Behnken, 1975) as well as from south-central British Columbia, Canada (Orchard and Forster, 1988): All of these occurrences are dated to be of late Leonardian age in the Permian regional stratigraphy (= middle to late Kungurian). Because of the geographically wide distribution of *Sw. adjunctus*, this zone therefore has high potential for super-regional correlation.

8) *Sw. subsymmetricus* Zone (356–393 m, Beds 91–99)

Lower limit: FAD of *Sw. subsymmetricus*. Upper limit: FAD of *Sw. hanzhongensis*. This zone correlates to the Kungurian “*M. siciliensis*-*Sw. subsymmetricus*” Zone in southern Guizhou (Mei et al., 2002).

Sw. subsymmetricus is well known from the Kungurian of Guizhou and Guangxi in South China, as well as from Thailand and Oman (Mei et al., 2002 and this study; Henderson and Mei, 2003; Metcalfe and Sone, 2008; Burrett et al., 2015). The report of the co-occurrence of *Sw. subsymmetricus* and *J. nankingensis* in the Nanjing area (Wang, 1995) suggests that the range of *Sw. subsymmetricus* extends at least to the earliest Roadian. However, the assertion that *Sw. subsymmetricus* is only restricted to the Roadian (Kozur, 1993) is incorrect.

9) *Sw. hanzhongensis* Zone (393–454.5 m, Beds 99–109)

Lower limit: FAD of *Sw. hanzhongensis*. Upper limit: FAD of *M. idahoensis*. The FAD of *Pseudohindeodus augustus* and *Pseudohindeodus ramovsi* occurs in the middle part of this zone. A turnover in the dominant conodont fauna initiated during this zone. *Hindeodus* becomes abundant whilst the abundance and the diversity of *Sweetognathus* decreases. *Hindeodus permicus*, *H. gulloides* and *H. aff. wordensis* all occur in this zone.

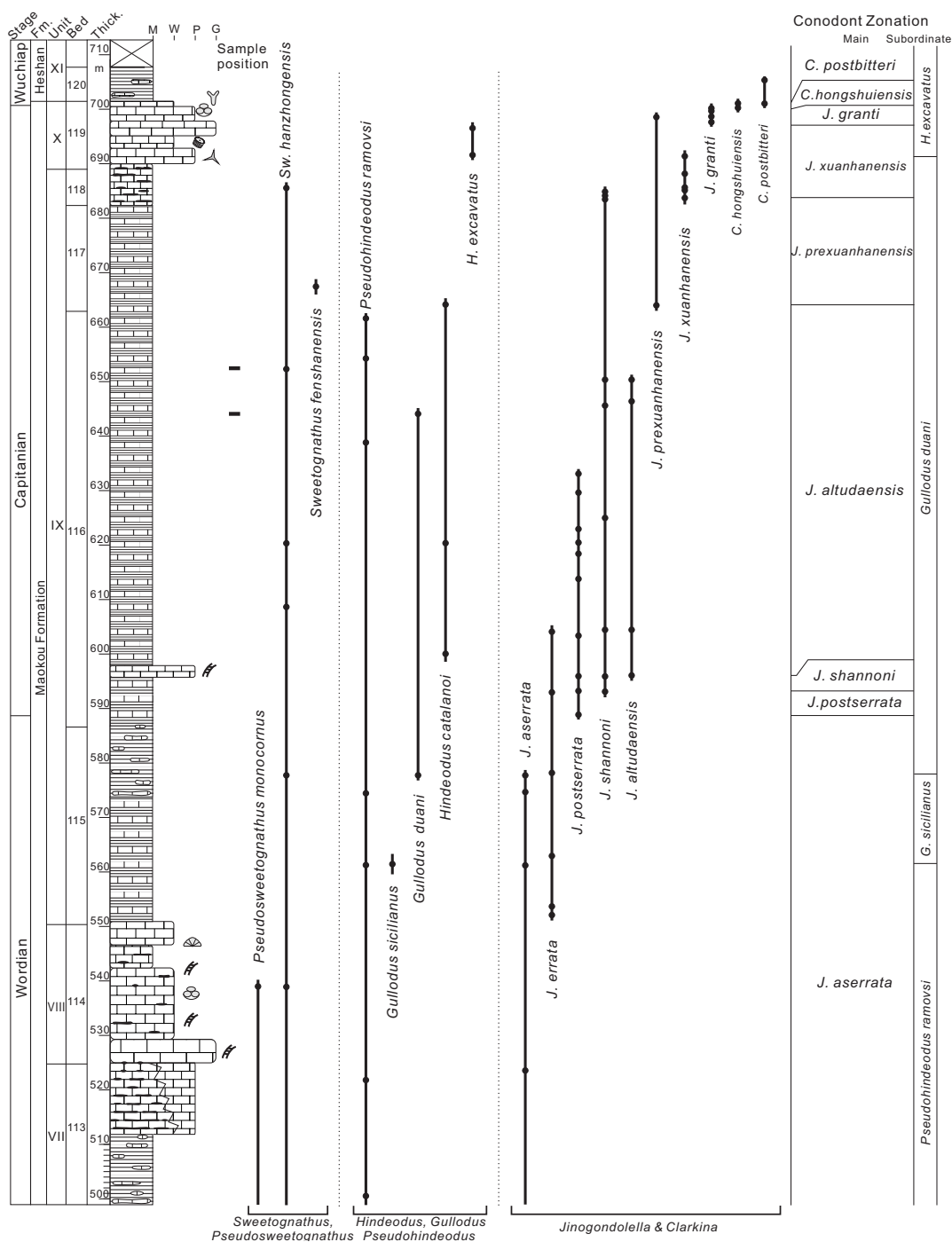


Figure 2.5: Log of the upper part of Tieqiao section (Wordian to Wuchiapingian) with conodont ranges and zonation. Keys are the same as in Figure 2.3.

2.4.4. Roadian

The Roadian strata consist of 15 m of weakly bioturbated but still finely laminated micritic mudstones starting in Bed 109 (Figure 2.2B). In Beds 110–111, strata are more thinly bedded with an increasing abundance of sponge spicules and radiolarian tests, indicating

deepening and a relative sea level rise was ongoing throughout the Roadian. A major sea-level rise is known from the Early-Middle Permian transition and is manifest at Tieqiao by a transition to thinly bedded radiolarian cherts by Bed 112 (Wordian age). By this time, deep, basinal sedimentation was established in the region. The minor thickness of the Roadian strata may be attributed either to condensation during this sea level rise or to hiatus resulting in a loss of strata (due to sudden loss of carbonate production below the carbonate compensation depth). Only one conodont zone is recognised (Plate 5).

10) *Jinogondolella nankingensis* Zone (454.5–468 m, Beds 109–111)

Lower limit: FAD of *J. nankingensis*. Upper limit: FAD of *J. aserrata*. *Pseudohindeodus ramovsi* are abundant. Disrupted lamination in the upper (Roadian) part of Bed 111 indicates weak bioturbation.

2.4.5. Wordian

Wordian strata are presented by Bed 112 to lowermost part of Bed 116. The sediments consist of thinly bedded radiolarian cherts in the lower part (Beds 112–113), thickly bedded bioclastic wacke- and packstones in the middle (Bed 114, also known as “the Great White Bed”) and alternation of cherts and lime mudstones in the upper part (Bed 115–116). One conodont zone is recognised (Plate 5).

11) *J. aserrata* Zone (468–588.5 m, Beds 112–116)

Lower limit: FAD of *J. aserrata*. Upper limit: FAD of *J. postserrata*. The FAD of *J. palmata* occurs at the same level as the FAD of *J. aserrata*. This is generally consistent with the record in west Texas where the FAD of *J. palmata* was reported very close to the FAD of *J. aserrata* (Nestell and Wardlaw, 2010a). Several species, such as *J. errata*, *Gullodus duani* and the long ranging species *Sw. hanzhongensis* and *Pseudohindeodus ramovsi* appear in the middle-upper part of this zone.

2.4.6. Capitanian

The Capitanian (Beds 116–119) is the most intensively studied interval in the Laibin area (Mei et al., 1994c; Jin et al., 2006; Chen et al., 2009; Wignall et al., 2009b). Strata of this age consist of medium bedded alternating cherts and lime mudstones in the lower part (Beds 116–118) overlain by pack- to grainstones (Laibin Limestone Member, Bed 119). Here we only give a brief description of the conodont zones of this stage since they have been well studied. Conodont specimens are shown in Plate 5 and Plate 6.

12) *J. postserrata* Zone (588.5–593 m, Bed 116)

Lower limit: FAD of *J. postserrata*. Upper limit: FAD of *J. shannoni*.

13) *J. shannoni* Zone (593–596 m, Bed 116)

Lower limit: FAD of *J. shannoni*. Upper limit: FAD of *J. altudaensis*.

14) *J. altudaensis* Zone (596–664 m, Beds 116–117)

Lower limit: FAD of *J. altudaensis*. Upper limit: FAD of *J. prexuanhanensis*. This interval is characterised by extinctions amongst marine fauna and flora as well as the onset of Emeishan volcanism (Wignall et al., 2009a; Bond et al., 2010a; Sun et al., 2010). Losses include many foraminifers, calcareous algae and brachiopods in the equatorial realm, and the latter also suffered comparable losses in the Boreal realm (Bond et al., 2010a; Bond et al., 2015). Though there are no obvious lithological changes in the *J. altudaensis* Zone at Tieqiao, the last appearances of several long-ranging species, such as *Gullodus duani*, *Sw. hanzhongensis* and *Pseudohindeodus ramovsi*, are all recorded in this zone.

15) *J. prexuanhanensis* Zone (664–683.8 m, Beds 117–118)

Lower limit: FAD of *J. prexuanhanensis*. Upper limit: the FAD of *J. xuanhanensis*. This zone has not been recognised in western Texas (Lambert et al., 2002). However, it is distinguishable at Tieqiao (Guangxi, this study) and Dukou (Sichuan, Mei et al., 1994b). In condensed sections in Guizhou, *J. prexuanhanensis* zone is often combined with the younger *J. xuanhanensis* zone as the *J. prexuanhanensis*-*J. xuanhanensis* assemblage zone (Sun et al., 2010).

Sw. fengshanensis occurs in this zone. *Sw. fengshanensis* was established in the late Capitanian strata at Fengshan, northwestern Guangxi (Mei et al., 1998). In the Penglitan section, *Sw. fengshanensis* spans the upper *J. postserrata* zone to the lower *J. xuanhanensis*

zone, representing the last in the evolutionary lineage of sweetognathids in South China (Mei et al., 2002).

16) *J. xuanhanensis* Zone (683.8–697 m, Beds 118–119)

Lower limit: FAD of *J. xuanhanensis*. Upper limit: FAD of *J. granti*. Many mature morphotypes of *J. shannoni* occur in the lowermost part of this zone and are very similar to their counterparts from West Texas (Lambert et al., 2002; Wardlaw and Nestell, 2010). There is an influx of volcanoclastic material during this zone and it becomes more common in the overlying *J. granti* Zone, where it presumably derived from large scale explosive eruptions of the Emeishan Traps (Wignall et al., 2009b; Sun et al., 2010).

17) *J. granti* Zone (697–700 m, Bed 119)

Lower limit: FAD of *J. granti*. Upper limit: FAD of *Clarkina hongshuiensis*. Conodonts are prolific in this zone with a typical yield rate of ~100 specimens per kg rock.

18) *Clarkina hongshuiensis* Zone (700–701.5 m, Bed 119)

Lower limit: FAD of *C. hongshuiensis*. Upper limit: FAD of *C. postbitteri*.

2.4.7. *Wuchiapingian*

The early Wuchiapingian (Bed 120) is characterised by deposition of extensive bedded cherts with intercalated pinkish limestone lenses. Evidence for a relative sea level fall towards the end of Wuchiapingian is indicated by a reduction of chert thickness up-section with carbonate sedimentation increasing. Eventually, this basinal setting evolved into a sponge reef facies in the later Wuchiapingian in which conodonts are barren (Figure 2.2 C, D). Two conodont zone are established for the earliest and the middle Wuchiapingian:

19) *Clarkina postbitteri* Zone (701.5–? m, Bed 120)

Lower limit: FAD of *C. postbitteri*. Upper limit: not determined.

20) *Clarkina transcaucasica* Zone (Bed 134 and upsection)

Lower limit: FO of *C. transcaucasica*. Upper limit: not determined.

Clarkina transcaucasica is found in Bed 134 (Plate 6). Sha et al. (1990) reported the occurrence of *C. bitteri* in Bed 133. Although we cannot confirm this finding, *C. bitteri* occurs

above the *C. asymmetrica* Zone and can extend to the *C. transcaucasica* Zone (Jin and Shang, 2000) and so the observations of Sha et al. (1990) are consistent with our interpretation.

The *C. transcaucasica* Zone at Tieqiao immediately overlies a sponge reef (Beds 123–133, partially in Bed 134). The Wuchiapingian is known for paucity of reefs (Wang and Jin, 2000; Weidlich, 2002a) and the Tieqiao reef is one of a handful of known Wuchiapingian reefs in South China. In terms of the standard zonation of Permian (Figure 2.6), the Tieqiao reef can be constrained to the early to middle Wuchiapingian, possibly ranging from the *C. dukouensis* Zone to the *C. guangyuanensis* Zone. The demise of the reef occurs in the *C. transcaucasica* Zone.

2.5. Subordinate zones and reassessment for age assignments of rare species

Series Age/Ma	Stage	Standard zonation, Henderson et al. 2012	Nashui, Mei et al. 2002	Tieqiao, this study	
Lop. 260	Wuchiapingian	<i>C. transcaucasica</i> <i>C. guangyuanensis</i> <i>C. asymmetrica</i> <i>C. dukouensis</i> <i>C. postbitteri</i>		<i>C. transcaucasica</i> <i>C. postbitteri</i>	4
	Capitanian	<i>C. hongshuiensis</i> <i>J. granti</i> <i>J. xuanhanensis</i> <i>J. prexuanhanensis</i> <i>J. altudaensis</i> <i>J. shannoni</i>	<i>J. xuanhanensis</i> <i>J. prexuanhanensis</i> <i>J. altudaensis</i> <i>J. shannoni</i>	<i>C. hongshuiensis</i> <i>J. granti</i> <i>J. xuanhanensis</i> <i>J. prexuanhanensis</i> <i>J. altudaensis</i> <i>J. shannoni</i>	
		<i>J. posterrata</i>	<i>J. posterrata</i>	<i>J. posterrata</i>	
	Wordian	<i>J. aserrata</i>	<i>J. aserrata</i>	<i>J. aserrata</i>	
Roadian					3
		<i>J. nankingensis</i>	<i>J. nankingensis</i>	<i>J. nankingensis</i>	
Kungurian		<i>M. lamberti</i> - <i>N. sulcopicatus</i> - <i>M. idahoensis</i>	<i>M. idahoensis</i> - <i>Sw. subsymmetricus</i> <i>M. siciliensis</i> - <i>Sw. subsymmetricus</i>	<i>Sw. hanzhongensis</i> <i>Sw. subsymmetricus</i> <i>Sw. adjunctus</i> <i>Sw. iranicus</i> <i>Sw. guizhouensis</i> <i>N. prayi</i>	2
		<i>Sw. guizhouensis</i> <i>N. prayi</i> <i>N. pnevi</i>	<i>M. intermedia</i> - <i>Sw. guizhouensis</i>	<i>Sw. guizhouensis</i> <i>N. prayi</i>	
		<i>N. pequopensis</i>	<i>N. exsculptus</i> - <i>N. pequopensis</i>	<i>Sw. asymmetrica</i> n. sp. <i>Sw. toriyamai</i>	
		<i>Sw. clarki</i>			
Artinskian		<i>Sw. whitei</i>	<i>Sw. whitei</i> - <i>M. bisselli</i>	<i>Sw. whitei</i>	1

Figure 2.6: Correlation chart of the Early-Middle Permian with standard conodont zonation (Henderson et al., 2012), Tieqiao (this study) and Nashui (Mei et al., 2002). Zonation abbreviation: 1, *Pseudosweetognathus monocornus*; 2., *Hindeodus gulloides*; 3., *Gullodus sicilianus*; 4., *Hindeodus excavates*.

Seven subordinate zones are established at Tieqiao, representing interval zones based on occurrences of long ranging species. The subordinate zones are less effective for stratigraphic correlation but can provide a valuable reference for cases when a single conodont assemblage is obtained from an age-ambiguous lithologic unit (e.g., Burrett et al., 2015).

In the following section, we first describe the ranges of these subordinate zones in the Tieqiao section, followed by comments on the ranges of the zonal species. A correlation with main conodont zones is shown in figure 2.6. Conodont specimens are shown in Plate 4 and Plate 7. Note that the range of the species can be much longer than the respective zone.

1) *Pseudosweetognathus (Ps.) costatus* Interval Zone

Lower limit: FAD of *Ps. costatus*. Upper limit: FAD of *Ps. monocornus*. The *Ps. costatus* Zone spans the early Artinskian to middle Kungurian (Bed 19 to Bed 94). Elements of long-ranging species *H. minutus* are abundant in the lower part of this zone and there is a single occurrence of *H. aff. catalanoi* in the lowermost.

Pseudosweetognathus costatus was established in Artinskian strata of South China (Wang et al., 1987) and also reported from Thailand, co-existing with a typical Kungurian taxon *Sw. subsymmetricus* (Metcalf and Sone, 2008). Our data confirm former observations and indicate that the range of *Ps. costatus* extends from the Artinskian *Sw. asymmetrica* n. sp. Zone to the Kungurian *Sw. adjunctus* Zone. The *Ps. costatus*-*Ps. monocornus* lineage occurs as an anagenetic one at Tieqiao. In the middle Kungurian, *Ps. costatus* evolved into *Ps. monocornus*.

2) *Pseudosweetognathus monocornus* Interval Zone

Lower limit: FAD of *Ps. monocornus*. Upper limit: FAD of *H. gulloides*. This zone comprises Bed 94 to Bed 102 at Tieqiao, and is of late Kungurian age.

Li et al. (1989) established *Ps. monocornus* (under the genus “*Sichuanognathodus*”) from the upper part of Maokou Fm. at Shangsi. A later and detailed study of the same section reported a *Jinogondolella* and *Hindeodus* dominated fauna which indicates an early Capitanian age for the upper Maokou Fm. (Sun et al., 2008).

Pseudosweetognathus monocornus is found in the upper part of Chihhsia Fm. and lower part of Maokou Fm. at Tieqiao and here is reassigned a middle-Kungurian to early-Roadian age. This species only occurred with shallow water, high energy assemblage composed of calcareous algae, corals and foraminifers found in thickly bedded bioclastic pack- and

grainstones (e.g., in Bed 114, the Great White Bed). We thus speculate that the occurrence of *Ps. monocornus* might be facies-related, and its presence in Wordian to lower Capitanian strata elsewhere (Li et al., 1989) cannot be excluded.

Pseudosweetognathus monocornus superficially resembles gerontic morphotypes of *N. prayi* (Figure 8 in Plate 2; also see figure 18 of Plate 2 in Behnken, 1975). The main differences between the two species are the shapes of the platform shoulders and carina ornaments. However, taxonomical discussion on these two species is beyond the scope of this paper and will be included in another study.

3) *Hindeodus gulloides* Interval Zone

Lower limit: FAD of *H. gulloides*. Upper limit: FAD of *Pseudohindeodus (Ph.) ramovsi*. This zone occupies Bed 102 and correlates to the middle part of *Sw. hanzhongensis* Zone, representing a Late Kungurian age.

The species *H. gulloides* Kozur and Mostler, 1995, ranges from upper Kungurian to Roadian. In northeast Thailand, *H. gulloides* occurs at an age-equivalent level as in South China and co-existed with a typical late Kungurian assemblage which consists of species *Mesogondolella siciliensis*, *Ph. oertlii* (= *angustus*? our brackets) and *Sw. subsymmetricus* (Burrett et al., 2015). In west Texas, the species was recovered from the upper part of Road Canyon Fm., representing a late Roadian age (Kozur and Mostler, 1995).

4) *Pseudohindeodus ramovsi* Interval Zone

Lower limit: the FAD of *Ph. ramovsi*. Upper limit: the occurrence of *Gullodus sicilianus*. This zone spans from Bed 103 to Bed 115, representing a latest Kungurian to Wordian age.

The species *Ph. ramovsi* Gullo and Kozur, 1992 has a much longer range than the Interval Zone. Wardlaw (2000) reported sporadic occurrences of this species from the Kungurian to Capitanian. Our data are consistent with Wardlaw (2000), suggesting that *Ph. ramovsi* spanned from the late Kungurian *Sw. hanzhongensis* Zone to the middle Capitanian *J. altudaensis* Zone.

Another associate species in this zone is *Ph. augustus* (Igo, 1981). This species has been reported from coeval Kungurian strata in Japan (Igo, 1981; Shen et al., 2012), but can also occur in much older strata such as in the Artinskian (Orchard and Forster, 1988). However, Artinskian occurrences of *Ph. augustus* is not yet known from South China.

5) *Gullodus sicilianus* Interval Zone

Lower limit: FO of *G. sicilianus*. Upper limit: FAD of *Gullodus duani*. This zone covers the middle part of Bed 115, representing a middle-late Wordian age.

Gullodus sicilianus (Bender and Stoppel, 1965) ranges from the Roadian to Wordian (Kozur, 1993). It is a rare taxon that is known mostly from the Tethys realm during the Wordian (Kozur, 1995).

6) *Gullodus duani* Interval Zone

Lower limit: FAD of *Gullodus duani*. Upper limit: prolific occurrence of *H. excavatus*. This zone comprises Bed 115 to Bed 118 and includes much of the Capitanian strata.

Gullodus duani Mei et al., 2002 is a rather rare species in the Guadalupian. This species was originally recovered from the Maokou Fm. from Guangxi and is only known from South China. At Tieqiao, this species is known from uppermost Wordian to middle Capitanian strata.

An associated taxon *Hindeodus catalanoi* ranges through the upper part of this zone. Though Gullo and Kozur (1992) assigned a Wordian age for *H. catalanoi*, this form is found in the Capitanian at Tieqiao, suggesting a longer range of the species than its original definition.

7) *Hindeodus excavatus* Interval Zone

Lower limit: the prolific occurrence of *H. excavatus*. Upper limit: FAD of *C. postbitteri* (the Capitanian-Wuchiapingian boundary). At Tieqiao, this zone is represented by the Laibin Limestone Member (Bed 119) of a late Capitanian age.

Hindeodus excavatus is another long-ranging species in the Permian, but its use as a zonal fossil derives from its prolific abundance in the late Capitanian.

2.6. Systematic palaeontology

2.6.1. Genus *Gullodus* Kozur, 1993

Emended diagnosis: Spathognathodiform elements with a medium to long anterior blade and a posteriorly positioned, strongly expanded basal cavity. Denticles occur on the blade and above the basal cavity and are in most cases without ornamentations. Denticles are generally 10–18 in number and those above the basal cavity can be expanded and form a carina-like structure or narrow transverse ridges. Small coalesced denticles are sometimes developed on

the anterior edge forming an “anterior blade”. Length/height ratio is between 1.5 and 3. Basal cavities are expanded, non-ornamented and occupy 1/3 to 2/3 of the full body.

Remarks: the diagnosis of this genus (Kozur, 1993) should be emended because it is often hard to differentiate between *Gullodus* and *Hindeodus*. The emended diagnosis also includes wider variability of *Gullodus* species. Basal cavities of *Gullodus* are more expanded than most *Hindeodus* species but not as greatly expanded as *Pseudohindeodus*. Key differences between *Gullodus* and *Hindeodus* are the shape and position of the basal cavity and the length/height ratio: *Hindeodus* has a more centrally positioned basal cavity and lower length/height ratio. A key difference between *Gullodus* and *Sweetognathus* is that denticles of *Gullodus* are not ornamented whilst those of *Sweetognathus* develop pustules. *Gullodus* can be differentiated from *Pseudohindeodus* because the basal cavity of the latter is more horizontally expanded and ornamented with a surface apron (i.e., a crimp around the fringe of the basal cavity) and occupies $\geq 2/3$ of the full element length.

Based on the revised diagnosis, *Gnathodus sicilianus* Bender and Stoppel, 1965 should remain as *Gullodus sicilianus* as suggested by Kozur (1993). However, *Pseudohindeodus catalanoi* Gullo and Kozur (1992) and *Gullodus hemicircularis* Kozur, 1993 should be assigned to *Hindeodus*, rather than *Pseudohindeodus* or *Gullodus*.

Occurrence: Kungurian to Capitanian.

2.6.1.1. *Gullodus tieqiaoensis* n. sp. Sun and Lai

Plate 4, figures 6, 7

No reported specimens are similar to this species.

Etymology: From the name of the section from where the species is described.

Holotype: Specimen S1_060 (Plate 4, figure 6) from sample 41–1 of Bed 41, Chihsia Fm., Tieqiao Section, South China.

Paratype: Specimen S1_062 (Plate 4, figure 7) from sample 41–2 of Bed 41, Chihsia Fm., Tieqiao Section, South China.

Type locality: specimens were obtained from Bed 40 to 44 in the lower Chihsia Fm., Tieqiao, South China.

Type interval: lower *Sw. guizhouensis* Zone, early Kungurian.

Diagnosis: A *Gullodus* species with a high length/height ratio of ~2 and a robust cusp.

Description: Body slim and elongated. Length/height ratio is ~2. The cusp is erected, tall, wide and robust, normally twice as high as the denticles and three times wider than the denticles. 13–17 densely arranged denticles decrease in height posteriorly. Posterior denticles above the basal cavity are more expanded and thus wider than the rest. They can be lower and more fused. The basal cavity is expanded, leaf or irregular shaped and occupies the posterior 2/3 of the element. The widest point is in the posterior 1/4 to 1/3.

Remarks: This species has a very high length/height ratio and a posteriorly positioned, expanded but non-ornamented basal cavity that extends to the posterior end. It thus belongs to *Gullodus* rather than *Hindeodus* or *Pseudohindeodus*.

Occurrence: lower Chihhsia Fm. (early Kungurian), Tieqiao, South China.

2.6.2. Genus *Hindeodus* Rexroad & Furnish, 1964

2.6.2.1. *Hindeodus catalanoi* Gullo and Kozur, 1992

Plate 7, figures 6–8

Pseudohindeodus catalanoi n. sp. Gullo and Kozur, 1992 p. 225, plate 5, figure A.

Hindeodus gulloides Kozur and Mosher, 1995; Burrett et al., 2015, p. 111–113, Figure 6, figures J–I.

Diagnosis: A *Hindeodus* species that is triangular shaped (in lateral view) with 2 to 3 anterior coalesced denticles and 12–15 densely arrayed denticles.

Remarks: The species resembles its Artinskian-Kungurian and “Roadian” predecessors *H. hemicircularis* Kozur, 1993 and *H. gulloides* Kozur and Mostler, 1995. They all have two to three anterior denticles. However, *H. hemicircularis* is sub-semicircular shaped and has fewer but wider denticles whilst *H. gulloides* is more elongated and has a much broader cusp than the current species.

H. catalanoi was previously known only from the Wordian of Sicily (Gullo and Kozur, 1992). Our collections from Tieqiao extend the range of the species to the *J. altudaensis* Zone

of middle Capitanian.

Occurrence: upper Maokou Fm. (middle-late Capitanian), Tieqiao, South China; Wordian of Sicily.

2.6.2.2. *Hindeodus* sp. A

Plate 4, figures 23, 26

Diagnosis: A *Hindeodus* species whose outline is close to that of an isosceles triangle.

Description: Body triangular shaped (lateral view) with a long anterior edge. Anterior angle is around 45°-60°. Two or three small coalesced denticles may develop on the anterior edge. Medium sized cusp followed by three low denticles. Posterior denticles are taller and wider and decrease in height towards the posterior end. The basal cavity is medially expanded and central positioned.

Remarks: The species resembles *H. permicus* but differs by its outline and shapes of denticles.

Occurrence: upper Kungurian, basal Maokou Fm. of South China.

2.6.3. Genus *Pseudohindeodus* Gullo and Kozur, 1992

2.6.3.1. *Pseudohindeodus elliptica* n. sp. Sun and Lai

Plate 4, figure 13; Plate 7, figure 14

Pseudohindeodus sp. Wang, 1995, plate 1, Figure 1a, b.

Etymology: From the oval shape of the basal cavity of the species.

Holotype: Specimen S7_001 (Plate 7, figure 14) from sample 104-2 of Bed 104, Maokou Fm., Tieqiao Section, South China.

Paratype: Specimen S2_075 (Plate 4, figure 13) from sample 104-2 of Bed 104, Maokou Fm., Tieqiao Section, South China.

Type locality: specimens were obtained from Bed 104 in the lower Maokou Fm., Tieqiao, South China.

Type interval: *Sw. hanzhongensis* Zone to *J. nankingensis* Zone; late Kungurian to Roadian.

Diagnosis: A *Gullodus* species with an asymmetrical basal cavity that is near oval in shape.

Description: Element is small and rounded. Cusp is large, robust and higher and broader than any following denticles. The 5–8 denticles immediately behind the cusp are thin and more fused with each other and thus can appear as a ridge. The last 4–6 denticles are the largest amongst all denticles. They are lower, more rounded in shape and relatively evenly spaced with each other with a small gap in between. The basal cavity is decorated with a surface apron, horizontally expanded, asymmetrical and very rounded. The outline of the basal cavity is close to an oval.

Remarks: the species resembles *Ph. ramovsi*. However, *ramovsi* has a near triangular basal cavity whilst *Ph. elliptica* n. sp. has a more rounded basal cavity.

The *Ph.* sp. reported by Wang (1995) is assigned to *Ph. elliptica* n. sp. It co-occurs with Roadian element *J. nankingensis* at Longtan, Nanjing area (Wang, 1995).

Occurrence: basal Kufeng Fm. and lower Maokou Fm. of South China.

2.6.4. Genus *Sweetognathus* Clark, 1972

2.6.4.1. *Sweetognathus asymmetrica* n. sp. Sun and Lai.

Plate 1, figures 1, 7, 14, 17.

Sweetognathus anceps Chernykh, Chernykh, 2006 plate XIII, figure 1.

Sweetognathus whitei (Rhodes), Chernykh, 2006 plate XIII, figure 2.

Etymology: The species name refers to its asymmetric anterior transverse ridges.

Holotype: Specimen S1_018 (Plate 1, figure 1) from sample 18-1 of Bed 18, Chihhsia Fm., Tieqiao Section, South China.

Paratypes: Specimen S1_037 (Plate 1, figure 7) from sample 22-2 of Bed 22, Chihhsia Fm., Tieqiao Section, South China.

Type locality: specimens were obtained from Beds 18 to 24 in the lower Chihhsia Fm., Tieqiao, South China.

Type interval: middle Artinskian to the earliest Kungurian.

Diagnosis: A Type III sweetognathid (definition follows Ritter, 1986) with short blade and asymmetric anterior transverse ridges.

Description: Short blade, often bearing 4–6 denticles; the first anterior blade denticle is moderately big. The second denticle is the biggest and very often fused with the first denticle and forms a high robust denticle; the other denticles are much smaller, lower and more fused towards the carina. The first two denticles are occasionally both very high, robust and triangular in shape. Commonly 7–10 transverse ridges are developed and clearly incised. The first one or two ridges are always asymmetrically developed—in most cases the left ridges are missing. The widest part of the carina is in the middle or, in rare cases, near the posterior. The basal cavity is leaf- to heart-shaped and moderately expanded, occupying the posterior half of the full element length.

Remarks: This species is similar to *Sw. subsymmetricus*. Both species developed asymmetric anterior transverse ridges. However, the current species differs from *Sw. subsymmetricus* by: 1) the length ratio of free blade/carina b_1 (most commonly $1/2$ to $1/4$), whereas that of *Sw. subsymmetricus* generally ranges from $1/2$ to ≥ 1 ; 2) the first denticle on the anterior blade is large, tall and robust, whereas that of *Sw. subsymmetricus* is moderately large, compared with other denticles on the blade; 3) an apparent low ridge between blade and carina; *Sw. subsymmetricus* has small and low denticles connecting blade and carina; 4) *Sw. subsymmetricus* has a less expanded basal cavity and a narrower carina, therefore appears more “slim”; 5) gaps between transverse ridges are more or less evenly spaced, whereas those of *Sw. subsymmetricus* become larger towards the posterior end.

Though *Sw. subsymmetricus* and *Sw. asymmetrica* n. sp. may have close affinities, *Sw. asymmetrica* n. sp. is restricted to the Artinskian to earliest Kungurian whereas *Sw. subsymmetricus* is found in younger rocks of late Kungurian to Roadian age (Kozur, 1995). Many reported occurrences of *Sw. subsymmetricus* in pre-middle-Kungurian strata (most of which have not been illustrated) should be reassessed.

The paratype shares a few common features with *Sw. variabilis*. They both have two big triangular-shaped denticles on the blade. The key difference is the position of the basal cavity. *Sw. variabilis* has a basal cavity near the posterior end. In addition, *Sw. variabilis* has a long

blade (blade/carina ratio ≥ 1) and five transverse ridges with the widest being near the posterior end. *Sw. asymmetrica* n. sp. has a blade/carina ratio always ≥ 1 , and usually seven or more transverse ridges whilst the widest occurs near the middle of the body. In addition, *Sw. subsymmetricus* and *Sw. variabilis* are rather distinctive species and should preferably not be considered as synonyms of *Sw. paraguizhouensis* and *Sw. guizhouensis* (Shen et al., 2012).

Figures 1 and 2 on Plate XIII in Chernykh (2006) are both from the Bursevian horizon in the lower Artinskian *Sw. whitei* Zone, have short blades and asymmetrically developed anterior transverse ridges and are assigned to *Sw. asymmetrica* n. sp.

Note: The specimen shown in figure 3 in Plate 4 seemingly has a gap between blade and carina. This is an artefact of photography.

2.6.4.2. *Sweetognathus bogoslovskajae*

Plate 1, figure 11; Plate 2, figures 1, 2, 4, 9.

Sweetognathus bogoslovskajae n. sp. Kozur; Kozur and Mostler, 1976, p. 18–19, plate 3, figures 7, 8.

Sweetognathus whitei (Rhodes, 1963); Kang et al., 1987, plate IV, figures 12, 14.

Sweetognathus bogoslovskajae Kozur; Mei et al., 2002, figure 12.5; Figure 10.13.

Remarks: The current species has a slim carina. The maximum width is uniquely in the front third to the middle of the carina. A gap likely develops between the blade and the carina. The node-like denticles on the carina rarely develop into broad transverse ridges and are widely spaced. Such space between denticles increases towards the posterior end.

Sweetognathus binodosus Chernykh, 2005 also has widely spaced node-like denticles on the carina. However, *Sw. binodosus* has a maximum width in the middle of the carina and several densely arrayed denticles between the carina and the blade.

2.6.4.3. *Sweetognathus hanzhongensis* (Wang, 1978)

Plate 3, figures 15–18; Plate 7, figures 9–10

Gnathodus hanzhongensis n. sp. Wang, 1978, p. 217, plate I, figures 33–35, 40–41.

Sweetognathus hanzhongensis (Wang), Wang and Dong, 1991, plate III, Figures 6–8.

Sweetognathus iranicus hanzhongensis (Wang, 1978), Mei et al., 2002, p. 85, Figure 10, Figures 6–7 (only).

Description (direct translation from Wang, 1978): the element consists of a near-rectangular blade (if viewed laterally) and a relatively elongated, two way pointed ovate basal cup. The front edge of the blade is almost vertical and forms a right anterior angle together with the lower blade edge. The blade is of 1/3 of the full element in length and consists of 4–6 fused denticles. The basal cavity is thin and is of 2/3 of the element length. The maximal width is near the middle or slightly in front. The lower edge (of the basal cavity, our brackets) is often broken due to incomplete preservation. The basal cavity is empty inside and unornamented on the surface. A moderately high carina is developed in the middle and is composed of almost completely fused denticles (i.e., node-like denticles with pustulose ornamentations, our brackets). The carina has a smooth upper outline.

Remarks: Specimens illustrated in Wang (1978) each have 4–6 denticles on the blade and the first three (in one case four) denticles are about the same size, and larger than the later denticles. In one specimen (Plate I, figure 35 in Wang, 1978), the second anterior blade denticle is the largest. One of the key features of this species is that the fused node-like denticles form a smooth middle carina (lateral view) and this smooth part extends at least to the middle of the basal cavity and occasionally to near the posterior end (e.g., Plate I, figure 33 in Wang, 1978).

2.6.4.4. *Sweetognathus inornatus* Ritter, 1986

Plate 1, figure 10; Plate 7, figure 2

Sweetognathus whitei (Rhodes, 1963); Clark et al., 1979, plate 1, figure 15.

Sweetognathus aff. *whitei* (Rhodes, 1963); Orchard, 1984, p. 213, plate 23.1 figures 1?, 2.

Sweetognathus inornatus n. sp. Ritter, 1986, p. 150, plate 3, figures 1, 6-7, 12-15; plate 4, figures 2, 9, 13, 14.

Remarks: Mei et al. (2002) considered the current species to be a synonym of *Sw. whitei*. However, Boardman et al. (2009) considered most of the Mei's specimens to be *Sw. merrilli*. We emphasise that *Sw. inornatus* is a distinct species. A key feature of the current species is

that 2 to 3 slim denticles are often partially or completely merged together to form a short ridge connecting the blade and the carina. Neither *Sw. whitei* nor *Sw. anceps* has this feature.

The current species is very similar to *Sw. iranicus* in outline. However, the maximum width of the current species is in the middle of the carina whilst the carina of *Sw. iranicus* increases in width posteriorly and the maximum width is near the posterior 1/3 to 1/4. Denticles between the blade and the carina of *Sw. iranicus* are low and merged together to form a gap, not a higher ridge as in *Sw. inornatus*.

2.6.4.5. *Sweetognathus* sp. A

Plate 1, figure 9

Diagnosis: A Type III sweetognathid with tall and slim denticles and narrow ridges.

Description: Body elongated with a height/length ratio $\approx 1/2$. The first anterior blade denticle is tall and slim, at least twice as high as any following denticles, and is immediately followed by five to six very slim denticles. The second and fourth denticles are the lowest. A gap is developed between the fifth and sixth denticles. Pustules are short, forming 5–7 low and generally evenly spaced ridges.

2.6.4.6. *Sweetognathus toriyamai* (Igo, 1981)

Plate 1, figures 12, 15

Neostreptognathodus toriyamai n. sp. Igo, 1981, p. 42–43, plate 6, figures 1–16.

Sweetognathus whitei (Rhodes, 1963) Igo, 1981, plate 7, figure 7?

Remarks: The denticles on the anterior blade of this species point forwards. The carina is lens-shaped—thus the widest is near the middle. There is a short and narrow ridge connecting the blade and carina. The ridge is relatively high anteriorly and decreases in height posteriorly towards the carina, thus giving a triangular shape if laterally viewed.

Comparisons: The short narrow ridge between the free blade and carina is one of the most distinguishable features of this species. The current species and *Sw. behnkeni* both have a broad, lens-like carina with a maximum width in the middle. However, the latter species has “ledge-like” decorations on the carina, whereas *Sw. toriyamai* is decorated by lower transverse ridges.

Occurrence: Artinskian, basal Chihhsia Fm. of South China and Kuchibora Fm. of Japan.

2.7. Conclusions

A detailed conodont biostratigraphic and taxonomic study of the Permian strata at Tieqiao, South China has enabled recognition of 20 main and 7 subordinate conodont zones from the Artinskian stage to the Wuchiapingian stage. Three new species (namely, *Gulloodus tieqiaoensis* n. sp., *Pseudohindeodus elliptica* n. sp. and *Sweetognathus asymmetrica* n. sp.) are established. The following conclusions can be drawn:

1) The Tieqiao strata record a change in conodont faunas from Early Permian *Sweetognathus* dominated assemblages to Middle Permian gondolellids dominated assemblages from the latest Kungurian onwards. This shift coincided with a relative sea-level rise and change to deeper water facies.

2) The Early Permian *Sweetognathus* fauna represents an important evolutionary lineage and a shallower (surface?) water group, which evolved in parallel to the contemporary but possibly deeper (cooler?)-dwelling *Mesogondolella* fauna.

3) The Chihhsia Fm., which had been in many cases erroneously regarded as a Middle Permian unit, is of Early Permian age. It spans the Artinskian to the late Kungurian whilst the overlying Maokou Fm. straddles the Early and Middle Permian from the late Kungurian to latest Capitanian. The Chihhsia/Maokou lithological boundary is thus locally not suitable for defining the Early-Middle Permian boundary (Kungurian-Roadian stage boundary).

4) Diversity of conodonts is generally low in the Middle Permian. Except for an extinction of a few long-ranging species, conodonts did not suffer significant losses during the mid-Capitanian Crisis.

5) Species such as *J. palmata* and *J. errata* occur at time-equivalent stratigraphic levels at Tieqiao as in west Texas, suggesting that they can be used for intercontinental correlations.

6) Our conodont biozones constrain the age of the Late Permian sponge reef at Tieqiao to the early and middle Wuchiapingian (from the *C. dukouensis* Zone to *C. transcaucasica* Zone).

Acknowledgements

Many colleagues helped with field and lab work, including H.S. Jiang (Wuhan), F. Li (now Chengdu), Q. Li (now Qingdao), D. Lutz (Erlangen), F. Nanning (now Münster), W. Pan (now Guangzhou), L. N. Wang (now Shijiazhuang), Y.J. Yan (now Lianyungang) and W.Q. Xue (Wuhan). V. Chernykh, H. Igo and B. R. Wardlaw are thanked for providing conodont literature. Constructive comments of reviewers Y.L. Chen (Xi'an) and C.M. Henderson (Calgary) have improved this study. We thank Editor D. Bottjer for professional editorial work. Y.D. Sun acknowledges the Alexander von Humboldt Foundation for a fellowship. This study is supported by the National Key Research and Development Program of China (grant no. 2016YFA0601104), the Chinese Fundamental Research Funds for the Central Universities (CUG130615), the Natural Science Foundation of China (grants no. 41602026; 41472087; 41572002), the 111 Project (B08030), and the State Key Laboratory of Palaeobiology and Stratigraphy (Nanjing Institute of Geology and Palaeontology, CAS) (no. 163112). D.P.G. Bond acknowledges funding from the UK Natural Environment Research Council (grant NE/J01799X/1). This is a contribution to IGCP 630.

Plate Caption

Plate 1. SEM images of Tieqiao conodonts—genus *Sweetognathus*. Bar scale for 100 μm , ‘a’ for oral view, ‘b’ for lateral view. Default is oral view. 1, 7, 14, 17. *Sweetognathus asymmetrica* n. sp., 1, holotype, S1_018 (18-1); 7, paratype, S1_037 (22-2); 14, S_001 (18-1); 17, S_006 (24A); 2, 16. *Sweetognathus whitei* (Rhodes, 1963), 2, S1_019 (18-1); 16, S_005 (23A), this specimen shows a transition from *Sw. whitei* to *Sw. guizhouensis*; 3, 8. *Pseudosweetognathus costatus* Wang et al., 1987, 3, S1_021 (19-2), 8, S1_025 (21-2). 4. *Sweetognathus* sp., S1_023 (19-2); 5. Transitional form from *Sw. inornatus* to *Sw. asymmetrica* n. sp., S1_038 (22-2); 6. *Sweetognathus* sp., S1_031 (22-1). 9. *Sweetognathus* sp. A., S1_026 (21-2); 10. *Sweetognathus inornatus* Ritter, 1986, S1_030 (22-1); 11. *Sweetognathus* cf. *bogoslovskajae* Kozur in Kozur and Mostler, 1976, S1_020 (18-1); 12, 15. *Sweetognathus toriyamai* (Igo, 1981), 12, S_002 (17c), 15, juvenile form, S_003 (17c); 13. *Sweetognathus clarki* (Kozur, 1976), S_004 (17c).

Plate 2. SEM images of Tieqiao conodonts—genera *Sweetognathus*, *Pseudosweetognathus*, *Neostreptognathodus* and *Hindeodus*. Scale bar is for 100 μm , ‘a’ for oral view, ‘b’ for lateral view. Default is oral view. 1, 2, 4, 9. *Sweetognathus bogoslovskajae* Kozur in Kozur and Mostler, 1976, 1, S1_039 (22-2), 2, S1_043 (24-3), 4, juvenile, S1_057 (39-1), 9, S1_051 (27-1); 3, 12. *Sweetognathus guizhouensis* Bando et al., 1980, 3, S1_048 (26-3), 12, S1_055 (39-1); 5–7. *Pseudosweetognathus costatus* Wang et al., 1987, 5, S1_047 (26-2), 6, S1_049 (26-4), 7, S1_045 (25-2); 8. *Neostreptognathodus prayi* Behnken, 1975, gerontic form, note the completely different platform shoulders compared to *Ps. costatus*, S1_046 (25-2); 10. *Sweetognathus clarki* Morphotype I, (Kozur, 1976), S1_050 (27-1); 11. *Sweetognathus inornatus* Ritter, 1986, S1_053 (29-1); 13. *Hindeodus* aff. *Catalanoi*, S1_022 (19-2); 14, 16, 17. *Hindeodus minutus* (Ellison, 1941), 14, S1_044 (25-1), 16, S1_056 (39-1), 17, S1_052 (28-1); 15. *Hindeodus* sp. S1_042 (23-3).

Plate 3. SEM images of Tieqiao conodonts—genera *Sweetognathus* and *Pseudosweetognathus*. Scale bar is for 100 μm , ‘a’ for oral view, ‘b’ for lateral view. Default is oral view. 1–3. *Pseudosweetognathus costatus* Wang et al., 1987, 1, S1_065 (52-2); 2, S1_066 (58-1), 3, S1_068 (65-2); 4, 5. *Sweetognathus iranicus* Kozur, 1975, 4, S1_069 (66-3), 5, S1_071 (71-1); 6. *Pseudosweetognathus monocornus* (Dai and Zhang, 1989), S2_001 (94-2); 7, 9, 19. *Sweetognathus* sp. 7, S1_072 (90-7), 9, S2_002 (97-2), 19, S2_020 (100-1); 8, 10, 11. *Sweetognathus adjunctus* (Behnken, 1975), 8, S2_004 (97-2), 10, S2_005 (97-2), 11, S1_076 (91-1); 12. *Sweetognathus* cf. *paraguizhouensis* S1_078 (91-3); 13. Transitional form between *Sweetognathus iranicus* and *Sweetognathus hanzhongensis*, S2_007 (99-4); 14. *Sweetognathus subsymmetrics* Wang et al., 1987, S2_039 (100-3); 15–18. *Sweetognathus hanzhongensis* (Wang, 1978), 15, S2_038 (100-5), 16, S2_018 (100-1), 17, S2_010 (100-1), 18, S2_028 (100-3).

Plate 4. SEM images of Tieqiao conodonts—genera *Sweetognathus*, *Gulldodus*, *Hindeodus* and *Pseudohindeodus*. Scale bar is for 100 μm , ‘a’ for oral view, ‘b’ for lateral view. Default is oral view. 1. *Sweetognathus* sp. S2_049 (102-2); 2–4. *Sweetognathus subsymmetrics* Wang et al., 1987, 2, S2_051 (102-3); 3, S2_056 (102-4); 4, S2_058 (102-4); 5, 15. *Sweetognathus iranicus* Kozur, 1975, 5, S2_082 (105-3), 15, S2_072 (103-2); 6–7. *Gulldodus tieqiaoensis* n. sp., 6, holotype, S1_060 (41-1), 7, paratype, S1_062 (41-2); 8. *Gulldodus sicilianus* (Bender and Stoppel, 1956), S3_020 (115-4); 9, 10, 16, 18. Transitional forms between *Hindeodus* and *Pseudohindeodus*. Note that these elements developed weak apron structures on basal cavities. 9, S1_074 (91-1), 10, S1_075 (91-1), 16, S2_057 (102-4), 18, S2_053 (102-3); 11, 12. *Gulldodus duani* Mei et al., 2002, 11, S1_013 (TQ-28), 12, S3_022 (115-7); 13. *Pseudohindeodus elliptica* n. sp. Sun and Lai, paratype,

S2_075 (104-2); 14. *Pseudohindeodus ramovsi* Gullo and Kozur, 1992, S2_073 (103-4); 17. *Hindeodus* cf. *wordensis* Wardlaw, 2000; 17, S2_060 (102-5); 19, 20. *Hindeodus* cf. *julfensis* 19, S2_014 (100-1), 20. S2_011 (100-1); 21. *Hindeodus* cf. *permicus*, S2_050 (102-2); 22, 36. *Hindeodus* sp. 22, S2_061 (102-5), 36, S2_022 (100-3); 23, 26. *Hindeodus* sp. A. 23, S2_068 (103-2); 26, S2_084 (106-1). 24, 25, 27, 30–32, 34, 35. *Hindeodus permicus* (Igo, 1981) 24. S2_081 (105-3), 25. S2_034 (100-4), 27. S2_026 (100-3), 30. S2_083 (105-3), 31. S2_016 (100-1), 32. S2_062 (103-1), 34. S2_071 (103-2); 35, S2_067 (103-2). 28, 29. *Hindeodus minutus* (Ellison, 1941), 28. S2_027 (100-3); 29. S2_021 (100-2); 33. *Hindeodus golloides* Kozur and Mostler, 1995, S2_066 (103-2).

Plate 5. SEM images of Tieqiao conodonts—genera *Mesogondolella* and *Jinogondolella*. Scale bar is for 100 μm , ‘a’ for oral view, ‘b’ for lateral view. Default is oral view. 1, 7. transitional type between *M. lamberti* to *J. nankingensis*, 1, S3_001 (109-2), 7, S3_012 (113-2); 2, 5, 9. *Jinogondolella nankingensis* (Ching, 1960), 2. S3_002 (109-2); 5. S3_007 (111-1); 9. S3_011 (111-5); 3, 8. *Jinogondolella* sp., 3. S3_004 (109-3), 8. S3_013 (113-7); 4. *Mesogondolella?* cf. *idahoensis* (Youngquist et al., 1951), S3_005 (110-2); 6. *Mesogondolella sicilliensis* (Kozur, 1975), S3_006 (111-1); 10–11. *Jinogondolella errata* Wardlaw and Nestell, 2000, 10. S3_019 (115-3), 11. S3_017 (115-2); 12. *Jinogondolella aserrata* (Clark and Behnken, 1979), S3_021 (115-4); 13, 16. *Jinogondolella* sp., 13. SP_051 (115-3), 16, S3_037 (116-7); 14, 15. *Jinogondolella postserrata* (Behnken, 1975), S3_028 (116-1); 15. S3_036 (116-7); 17, 18. *Jinogondolella shannoni* (Wardlaw, 1994), 17. S3_040 (116-8); 18, S3_030 (116-2); 19. *Jinogondolella altudaensis* (Kozur, 1992), S3_033 (116-3).

Plate 6. SEM images of Tieqiao conodonts—genera *Jinogondolella* and *Clarkina*. Scale bar is for 100 μm , ‘a’ for oral view, ‘b’ for lateral view and ‘c’ for back view. Default is oral view. 1. *Jinogondolella prexuanhanensis* (Mei and Wardlaw, 1994), S4_004 (TQ-11); 2. *Jinogondolella* cf. *prexuanhanensis* SP_010 (118-2); 3–5. *Jinogondolella shannoni* (Wardlaw, 1994), 3. S3_062 (118-2); 4. S4_006 (TQ-17+); 5. SP_014 (118-2); 6, 17. *Jinogondolella* sp., 6, SP_013 (118-2), 17, S_035 (119A); 7. *Jinogondolella xuanhanensis* (Mei and Wardlaw, 1994), 06-70_023 (TQ-6f); 8–11. *Jinogondolella granti* (Mei and Wardlaw, 1994), 8. 06-70_024 (TQ-6f), 9. 06-70_022 (TQ-6f), 10. TQ6f_010 (TQ-6f), 11. 06-70_027b (TQ-6f); 12–13. *Clarkina postbitteri* Mei and Wardlaw, 1994, 12. S6_054 (TQ-1), 13. C6_040a (TQ-1). 14. *Clarkina* sp., S6_055 (TQ-1); 15. *Clarkina transcaucasica* Gullo and Kozur, 1992, S4_003 (134-9); 16. *Clarkina hongshuiensis* Henderson, Mei and Wardlaw, 2002, S_029 (TQ-1).

Plate 7. SEM images of Tieqiao conodonts—genera *Hindeodus*, *Jinogondolella*, *Mesogondolella*, *Pseudohindeodus* and *Sweetognathus*. Scale bar is for 100 μm , ‘a’ for oral view, ‘b’ for lateral view. Default is oral view. 1, transitional form between *Sweetognathus bogoslovskajae* and *Sweetognathus inornatus*, S_007 (24A); 2. *Sweetognathus inornatus* Ritter, 1986, S_008 (26C); 3. *Sweetognathus fengshanensis* Mei and Wardlaw, 1998, S_016 (117-3); 4. *Jinogondolella* cf. *idahoensis* (Youngquist et al., 1951), S_009 (109-2); 5. *Jinogondolella palmata* (Nestell and Wardlaw, 2010a), S_025 (111-1-2); 6–8. *Hindeodus catalanoi* (Gullo and Kozur, 1992), 6, S3_052 (117-2), 7, S3_052 (117-2), 8, S3_043 (116-12); 9–10. *Sweetognathus hanzhongensis* (Wang, 1978), 9, S4_012 (TQ-25), 10, S_025 (115-8). 11–12. *Pseudohindeodus augustus* (Igo, 1981), 11, S7_007 (102-4), 12, S7_005 (102-4). 13. *Pseudohindeodus* sp. S7_003 (104-2). 14. *Pseudohindeodus elliptica* n. sp. Sun and Lai, holotype, S7_001 (104-2).

Plate 1

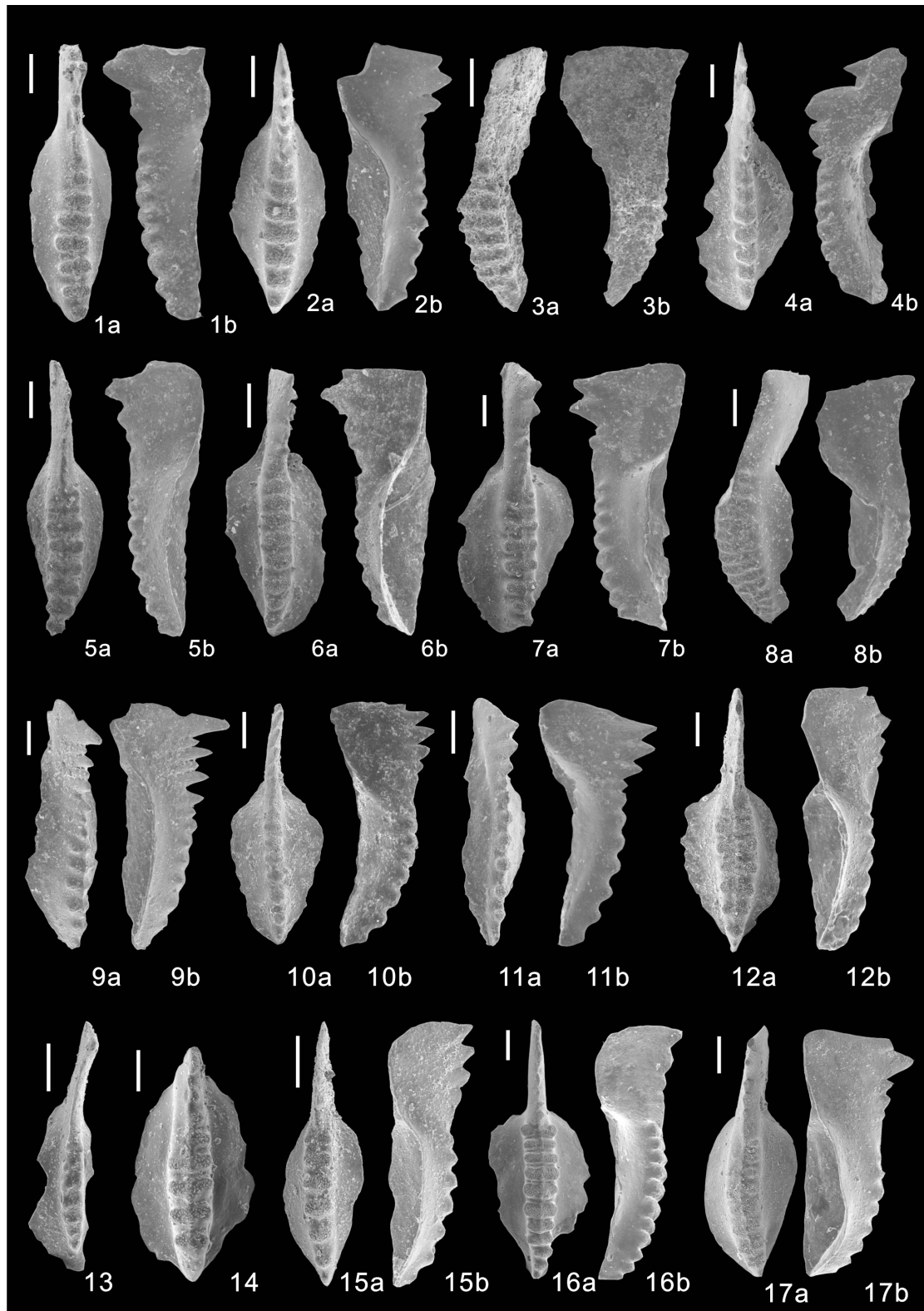


Plate 2

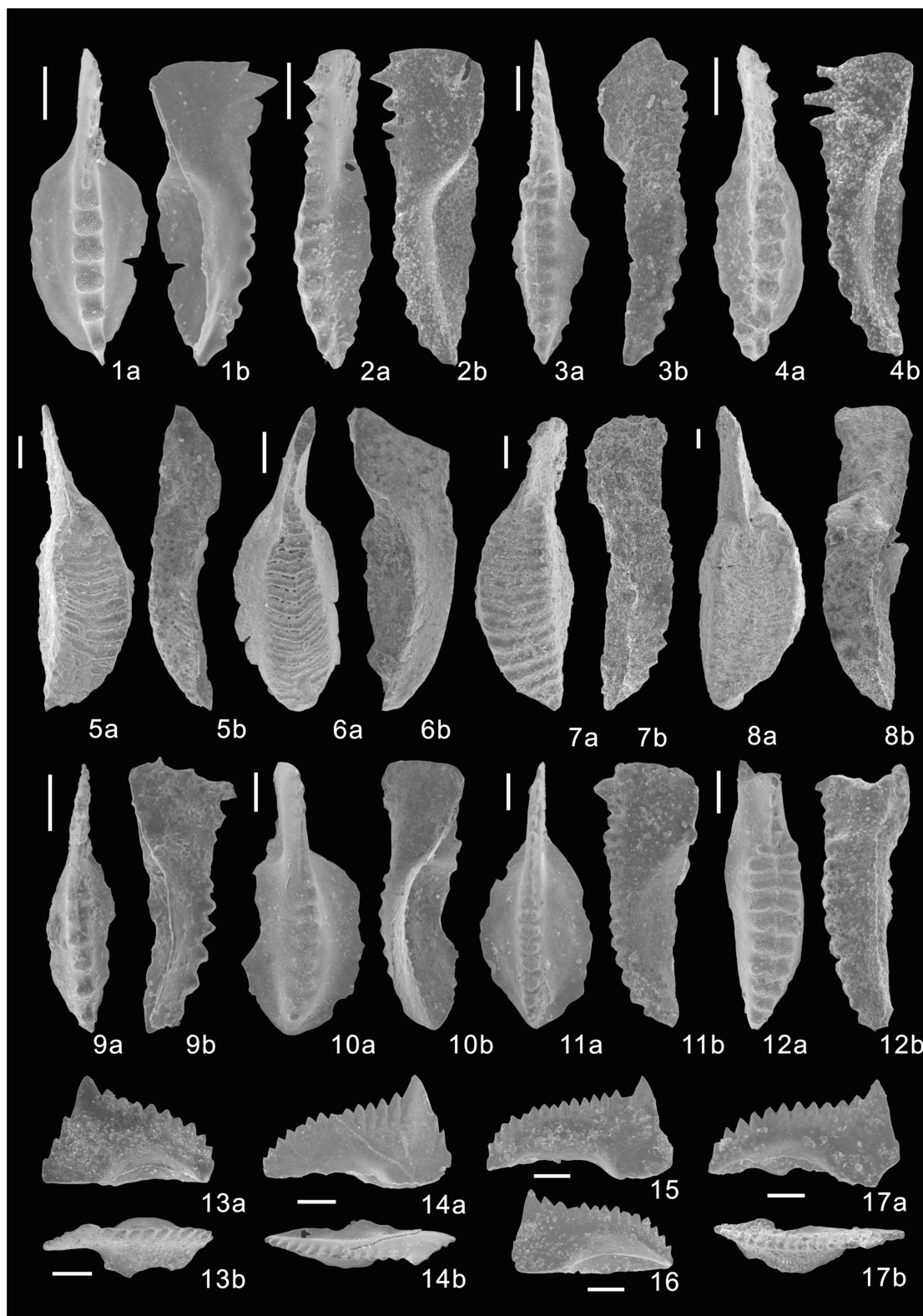


Plate 3

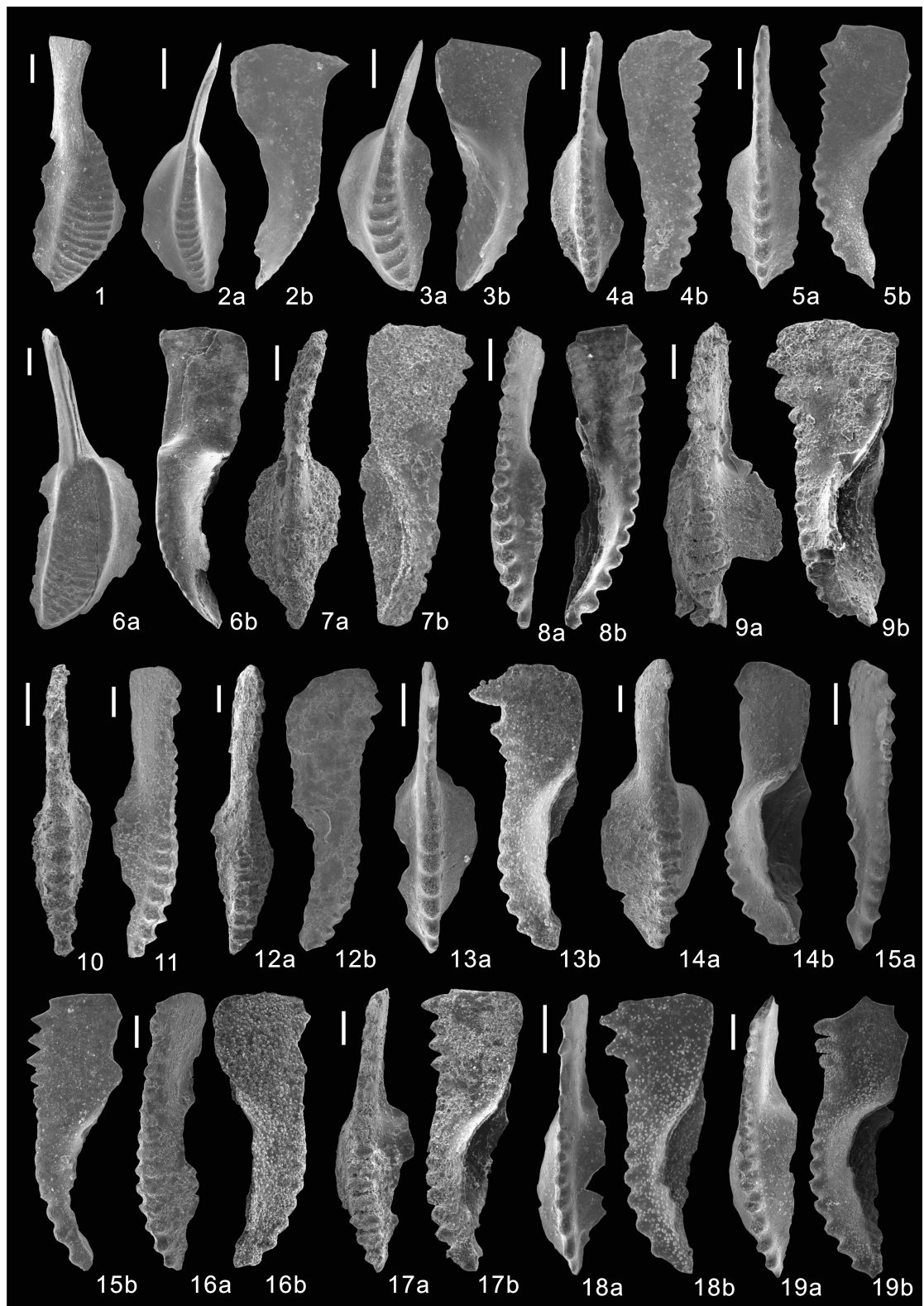


Plate 4

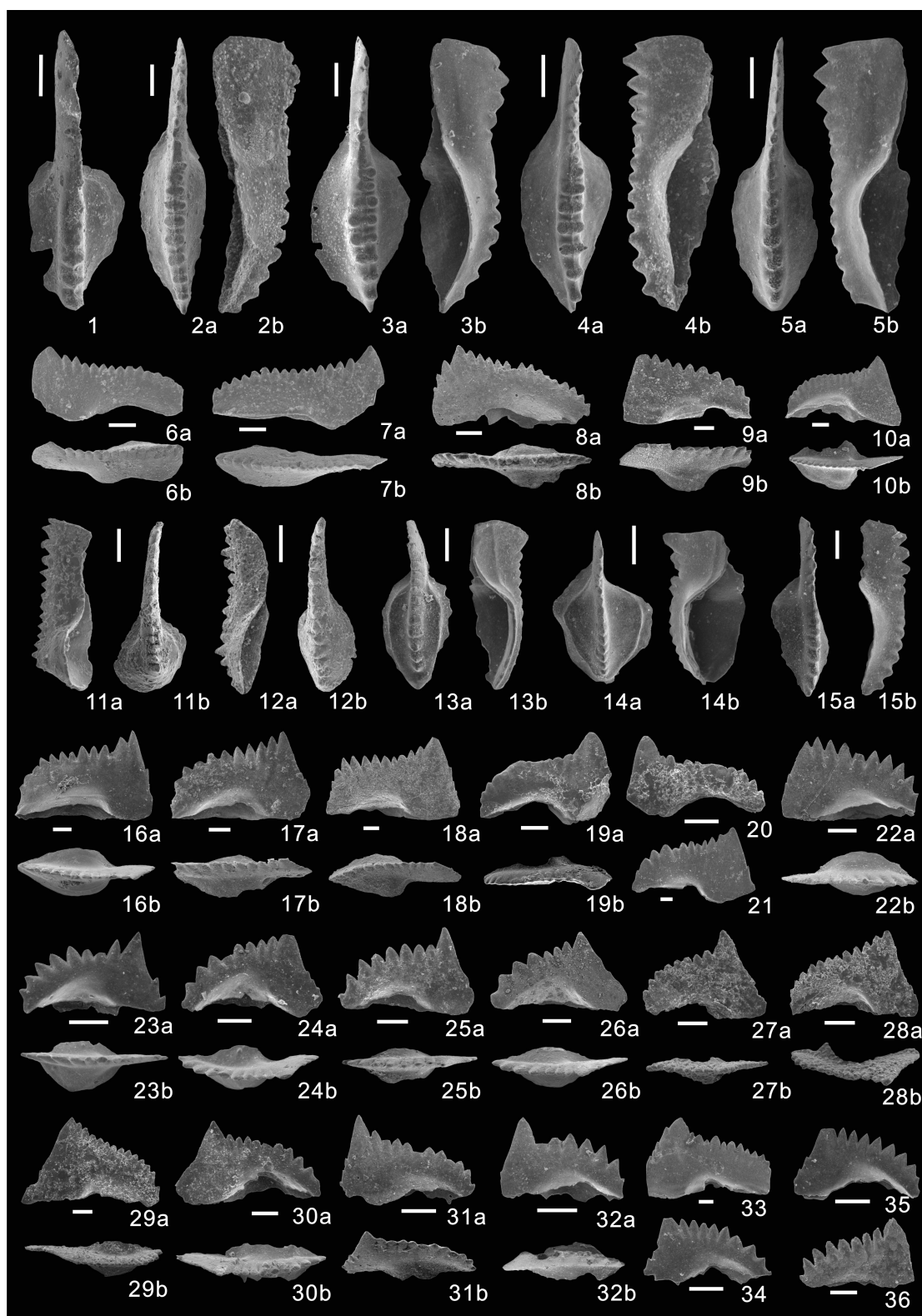


Plate 5

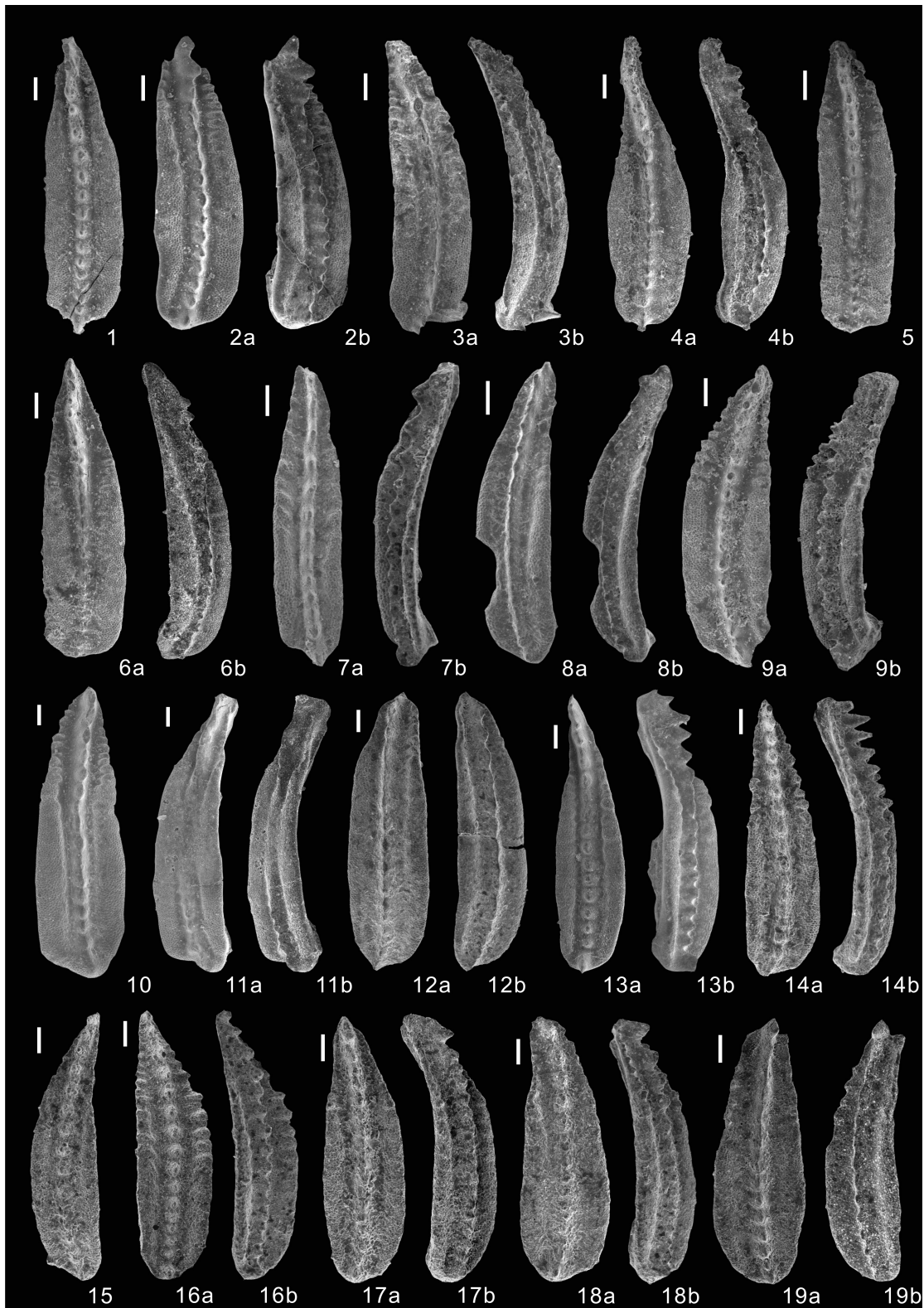


Plate 6

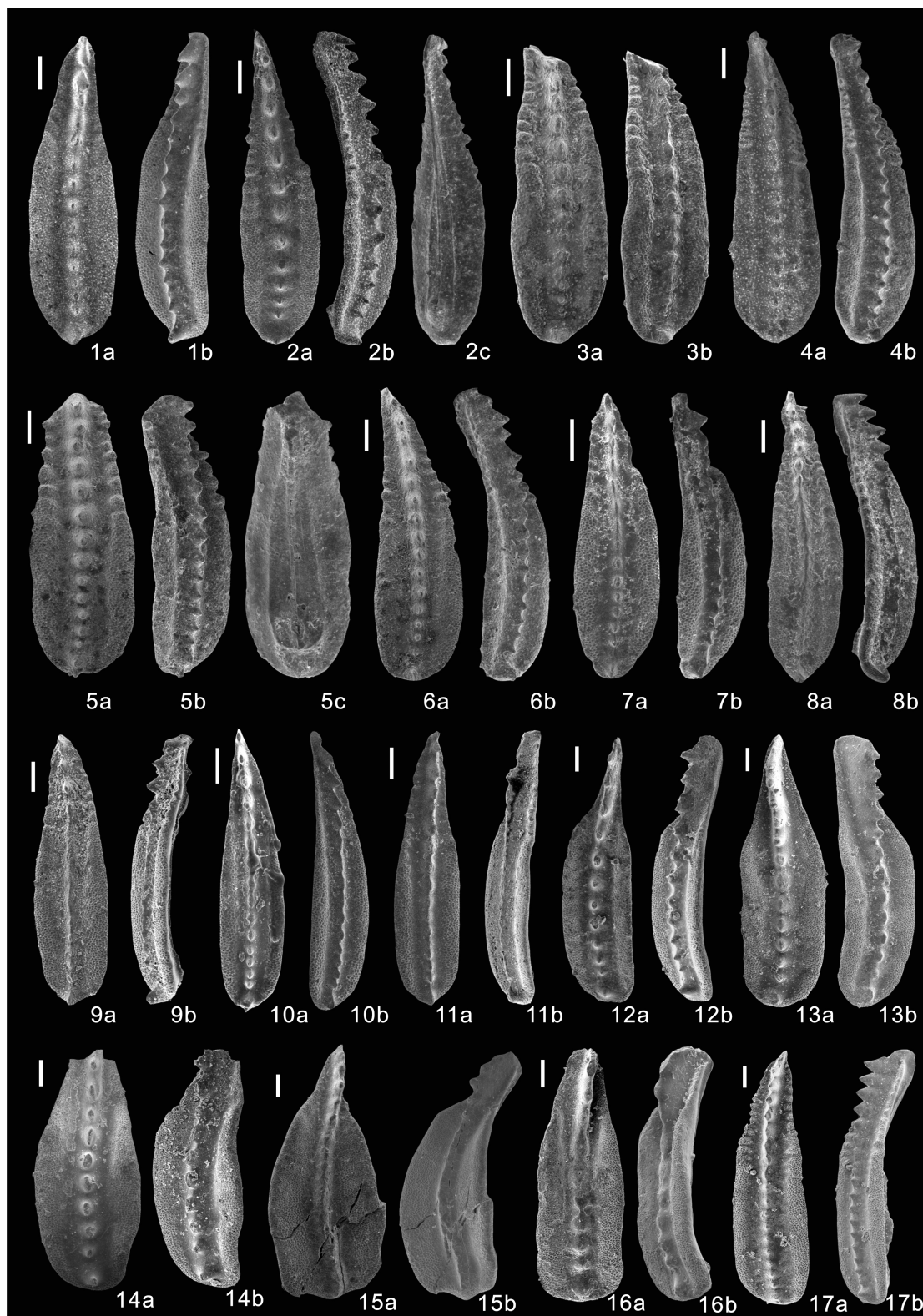
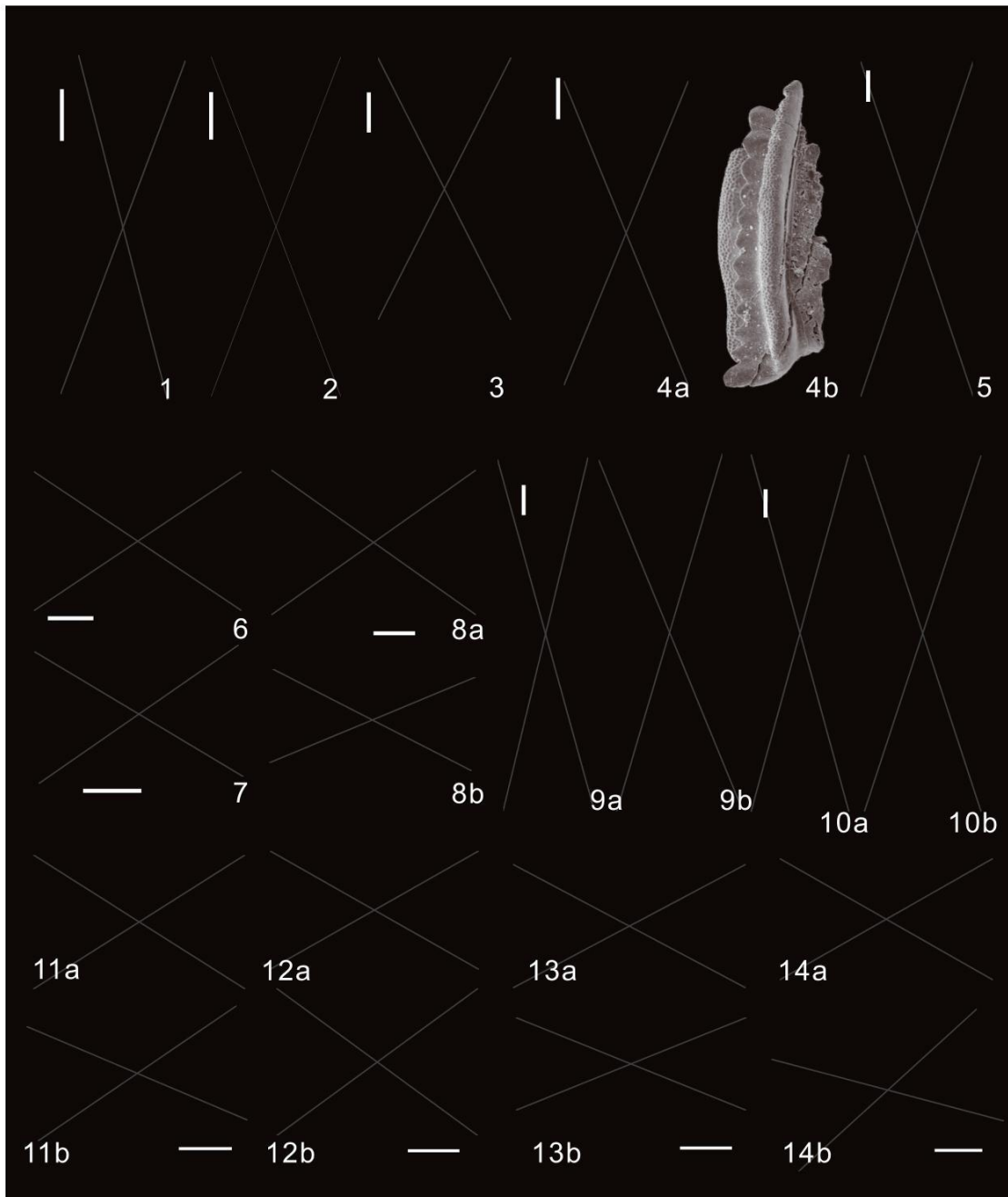


Plate 7



Chapter 3

Delayed recovery of metazoan reefs on the Laibin-Heshan platform margin following the Middle Permian (Capitanian) mass extinction

Published in 2019 in *Global and Planetary Change*,
<https://doi.org/10.1016/j.gloplacha.2019.05.005>

Abstract

Following the Middle Permian (Capitanian) mass extinction there was a global ‘reef eclipse’, and this event had an important role in the Paleozoic-Mesozoic transition of reef ecosystems. Furthermore, the recovery pattern of reef ecosystems in the Wuchiapingian of South China, before the radiation of Changhsingian reefs, is poorly understood. Here, we present a detailed sedimentological account of the Tieqiao section, South China, which records the only known Wuchiapingian reef setting from South China. Six reef growing phases were identified within six transgressive-regressive cycles. The cycles represent changes of deposition in a shallow basin to a subtidal outer platform setting, and the reefal build-ups are recorded in the shallowest part of the cycles above wave base in the euphotic zone. Our results show that the initial reef recovery started from the shallowing up part of the 1st cycle, within the *Clarkina leveni* conodont zone, which is two conodont zones earlier than previously recognized. In addition, even though metazoans, such as sponges, do become important in the development of the reef bodies, they are not a major component until later in the Wuchiapingian in the 5th and 6th transgressive-regressive cycles. This suggests a delayed recovery of metazoan reef ecosystems following the Middle Permian extinction. Furthermore, even though sponges do become abundant within the reefs, it is the presence and growth of the encrusters *Archaeolithoporella* and *Tubiphytes* and abundance of microbial micrites that play an important role in stabilizing the reef structures that form topographic highs.

3.1. Introduction

The Permian-Triassic transition represents a critical time interval for the evolution of modern reef ecosystems, as it experienced the extinction of the main Paleozoic reef builders and the evolution of animals and their symbiotic relationships that dominate reef-building today, e.g., Scleractinian corals and their symbiotic dinoflagellates (Stanley Jr, 2006). Even though the extinction of Paleozoic reef builders is typically attributed to the end-Permian mass extinction, the Middle Permian (Capitanian) mass extinction was also significant in the initial demise of Paleozoic reef ecosystems (Kiessling, 2005). The Middle Permian extinction

occurred prior to the end-Permian mass extinction and was catastrophic to reef-building and reef-dwelling animals, e.g., significant diversity declines for fusulinid foraminifera (Shen and Shi, 2002; Wignall et al., 2009a), brachiopods (Shen and Shi, 2009), Paleozoic corals (Shen and Shi, 2009; Wang and Sugiyama, 2000), and giant alatoconchid bivalves (Aljinović et al., 2008; Chen et al., 2018; Isozaki and Aljinović, 2009). In addition, the Middle Permian extinction caused changes in the dominant reef types, paleogeographic distribution and diversity of reefs (Weidlich, 2002a, 2002b).

Even though the Middle Permian extinction is recognized as an important event in the evolution of reef ecosystems, our understanding in precisely how the extinction affected the composition of reef ecosystems is limited because during the subsequent Wuchiapingian stage only a few locations have been reported for reef development (Weidlich, 2002b). Wuchiapingian algae-sponge reefs have been reported from margin of Tethys (e.g., Flügel and Reinhardt, 1989), and the central Europe Zechstein basin is famous for its ecologically diverse bryozoan reefs and stromatolite reefs (Hollingworth and Tucker, 1987; Paul, 1995; Peryt et al., 2012; Fheed et al., 2015; Raczynski et al., 2017). However, those locations that do record post-extinction reef development are poorly-constrained stratigraphically. In South China, Wuchiapingian coral biostromes with in-situ compact fasciculate corals and microbial carbonates have been reported from the southern margin of the Yangtze platform, but these biostromes are not considered reefs because they lack lateral topographic relief (Shen and Xu, 2005).

Here, we investigated the development of a recently discovered platform margin reef in the Tieqiao section, Laibin, which sheds new light on the development of a stratigraphically well-constrained reef following the Middle Permian extinction, and the timing of recovery of metazoan reef ecosystems. In addition to a continuously deposited vertical succession, the Tieqiao section is around 50–100m wide, so we have the opportunity to investigate the geometry of reef/bioherm bodies laterally. The main aim is to build upon preliminary work by Huang et al. (2019a) to provide an understanding in the spatial structure and geometry of this reef, the changes in the main reef-builders (e.g., metazoans, microbes, and problematica) during the Wuchiapingian, and how this relates to Permian-Triassic transition of reef ecosystems.

3.2. Geological and stratigraphic setting

This study investigated multiple profiles through the Tiejiao section, which is located near Laibin, Guangxi (South China) (Figures 3.1 and 3.2). The Tiejiao Section is located at the northern bank of the Hongshui River, 5 km southeast from Laibin, and 10 km east from the Penglaitan section, which is the Global Stratotype Section and Point (GSSP) of Guadalupian/Lopingian (G/L) boundary. The Tiejiao section is also the supplementary reference section of the GSSP. During the Lopingian, the Tiejiao Section was located on the eastern margin of Laibin-Heshan isolated platform (Figure 3.1) (Yao et al., 2012; Qiu et al., 2014) on the eastern side of the Dian-Qian-Gui Basin, and on the southern portion of the Yangtze block. This basin was located between the Yangtze Block and Cathaysian Block during the late Paleozoic and existed as a depression from the Middle Permian (Roadian stage) until the Early Triassic.

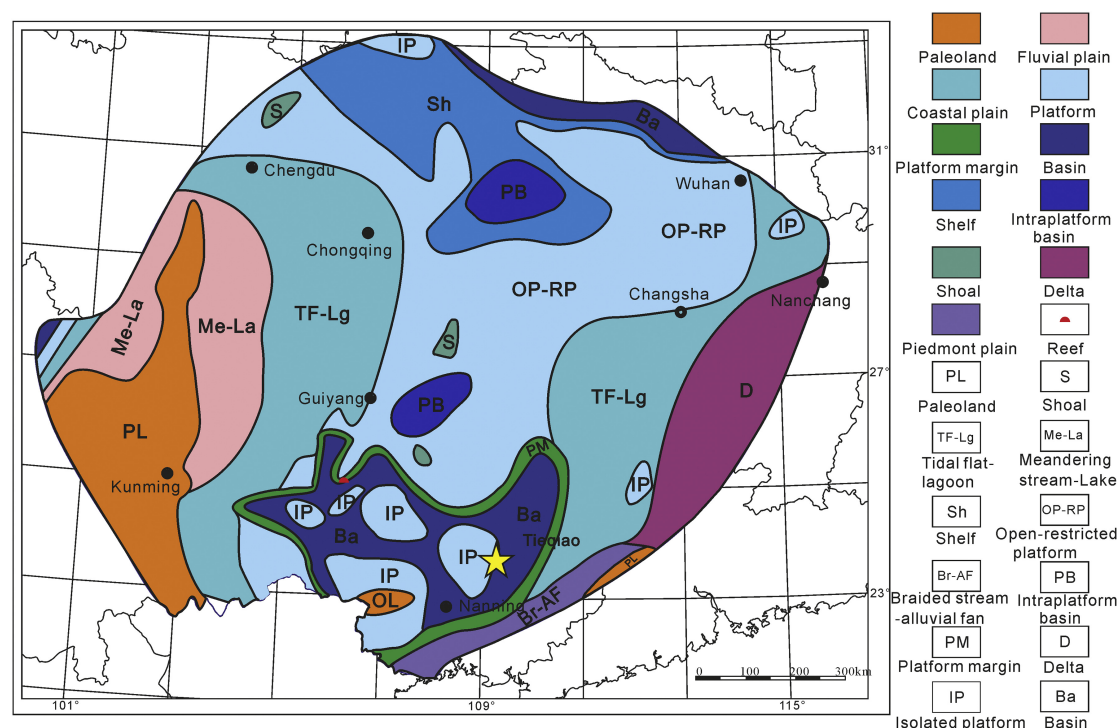


Figure 3.1: Paleogeographic map of the South China Yangtze Platform during the Wuchiapingian, modified from Liu et al. (2010). The star indicates the location of the Tiejiao section.

The Tiejiao and Penglaitan Sections are exposed on the western and eastern side of Laibin Syncline. Both sections were deposited continuously across the G/L boundary (Jin et al., 2006;

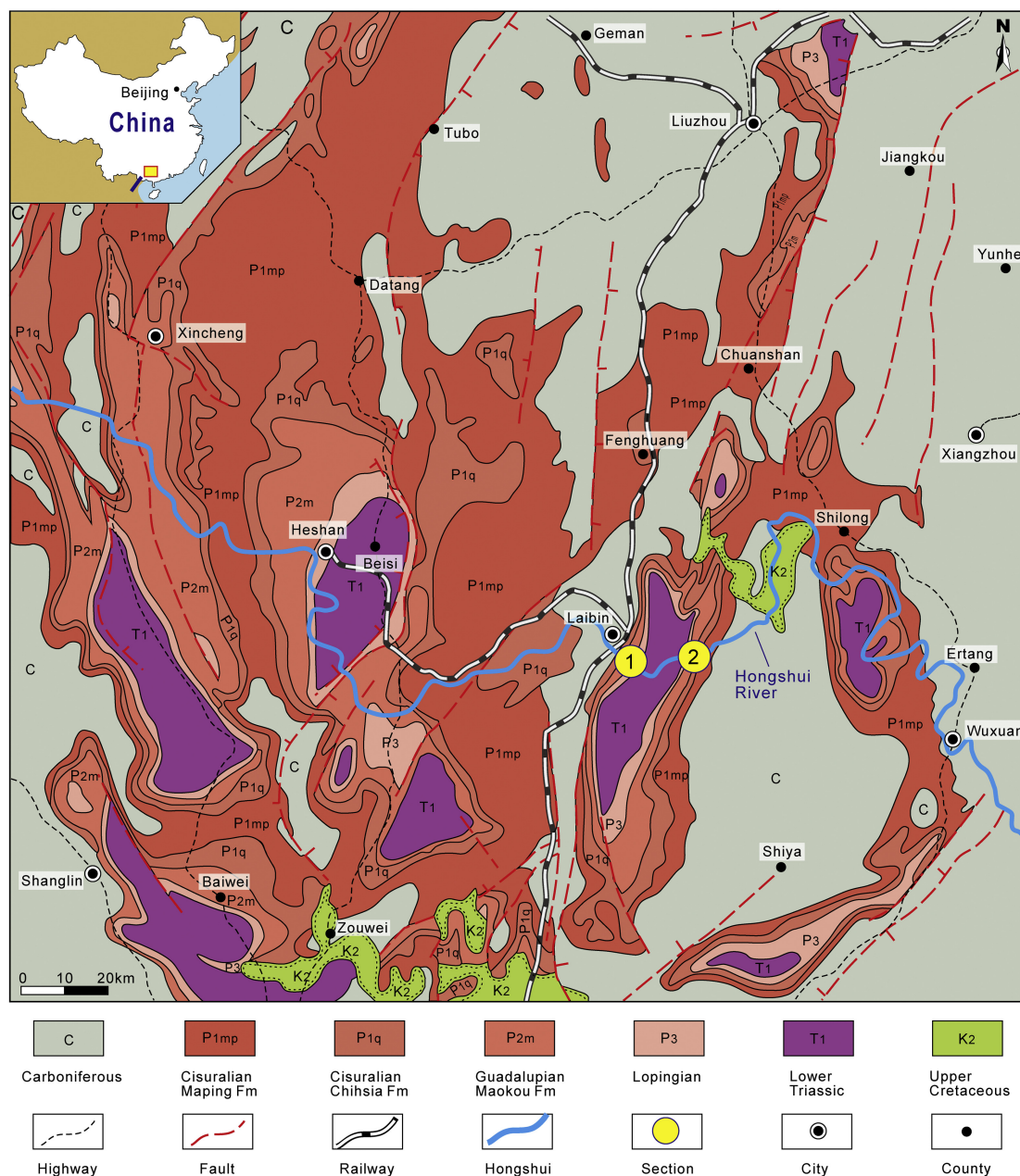


Figure 3.2: Geological map of Laibin-Heshan area, Guangxi, China. Modified from Shen et al. (2007). Section 1 is Tieqiao section (this study) and Section 2 is Guadalupian/Lopingian GSSP Penglaitan section.

Wignall et al., 2009b). In the Tieqiao section, the Permian succession is represented by the Qixia, Maokou, Heshan and Dalong formations (Sha et al., 1990). The G/L boundary is defined at the base of the conodont zone *Clarkina postbitteri postbitteri*, about 0.5m below the top of Maokou Formation (Jin et al., 2006) (Figure 3.3). The Middle Permian (Capitanian) mass extinction in the nearby Penglaitan section occurs at the upper Maokou Formation into the base of the Heshan Formation, across the G/L boundary (Huang et al., 2019b). The lower part of the Heshan Formation is characterized by thin-bedded radiolarian chert and thin-bedded limestone

interbedded with radiolarian chert or cherty limestone (Huang et al., 2019a; Qiu and Wang, 2011; Qiu et al., 2014; Shen et al., 2007). In addition, the Wuchiapingian *C. dukouensis*, *C. asymmetrica*, and *C. leveni* conodont zones, have been recorded in the lower part of Heshan Formation (Mei et al., 1998). The Heshan Formation is then made up of massive limestones sandwiched with four units of cherty limestones that have been recognized as sponge reef/bioherm in previous studies (Yang, 1987; Sha et al., 1990; Shen et al., 2007; Qiu et al., 2014; Wignall et al., 2009b; Huang et al., 2019a) which do not record conodonts, but are overlain by rocks that record the Wuchiapingian *C. transcaucasica* Conodont Zone (Sun et al., 2017).

3.3. Methods

In this study, fieldwork was undertaken to investigate the reef facies and their architecture at the Tieqiao section, Laibin, at both the macro- and micro-scale. To investigate the geometry of the reef at the macroscale a map-view orthophoto (Figure 3.4A) has been made by stitching images taken by a drone (Commercial UAV Dji Phantom 4 pro). The flying route was programmed and automatically operated from the ground station using the program Pix4D capture. A total of 308 aerial images were taken from 50m height and processed using Agisoft PhotoScan.

To understand the importance of reef-building organisms, a 5×5 m grid (Figure 3.5) was generated to describe the reef geometry. The 5×5 m grid divisions were made in the field using measuring rope (100m long), which is oriented by compass in North-South and West-East direction. All coordinate points were painted on the outcrop. The abundances of organisms were measured in the field on acid etched (using 10% hydrochloric acid) and weathered surfaces of each bed (with an area between 150 cm^2 and $20,000 \text{ cm}^2$). The abundance of sponges was quantified as absent (not observed), rare (the sponges comprised approx. <15% of the area), abundant (sponges made up approx. 15–30% of the area, and were not touching each other), and dominant (sponges made up approx. >30%, and frequently touching each other). The thickness of the encruster *Archaeolithoporella* was also quantified as absent (not observed), thin (< 1 mm), medium (1–3 mm), and thick (> 3 mm). In addition, 300+ samples were collected

along three main stratigraphic sampling profiles spanning the entire outcrop thickness and 10 auxiliary profiles in intervals of particular interests. The samples were collected in-situ to explore the contribution of different reef builders and the distribution of lithofacies (Figure 3.4A). The samples were then polished for observing the sedimentary fabrics, and 258 thin sections were produced for detailed facies study.

3.4. Results and interpretations

3.4.1. Lithofacies associations and depositional environments

Ten different lithofacies types (Lf) are differentiated according to the expanded Dunham classification (Dunham, 1962; Embry III and Klovan, 1971), rock composition (mainly skeletal and non-skeletal components), sedimentary structures and strata dimensions and geometries. The lithofacies associations and their distribution are investigated because of their importance in understanding the depositional environments associated with the development of the Laibin platform margin reefs (Figure 3.4B). The 10 lithofacies have been grouped into 5 facies associations, corresponding to different depositional settings: (1) basin-slope, (2) initial reef phase, (3) reef core facies, (4) reef cap facies, and (5) subtidal outer platform/back reef.

3.4.1.1. Slope-basin facies association

3.4.1.1.1. Lithofacies types.

Lithofacies 1: Mudstones, wackestones, and packstones alternating with cherts. Thin-bedded, tabular (up to 15 cm) alternations of mudstones and wackestones with beds of cherts (Figure 3.8M). Chert nodules and bioclasts can also occur within the calcareous beds. The bioclasts include fragments of foraminifera, ostracods, and bryozoans. Radiolarians have also previously been described from the mudstones by Qiu and Wang (2011) and comparable skeletal grains were observed in the mudstones in this study (Figure 3.6B). However, they lack key characteristics of radiolarians, such as a latticed shell, and both a consistent size and shape, which makes this identification equivocal. These putative radiolarian fossils are also restricted to the chert beds in the lower part of the section. The packstones are limited to the upper part

of this lithofacies. The bioclasts in the packstones are larger than in the mudstones and wackestones and include fragments of bryozoans, echinoderms, and brachiopods. There is no bioturbation.

3.4.1.1.2. Interpretation.

Lithofacies 1 is interpreted as the most distal facies, restricted to deep-marine areas of a low-gradient slope to basin. The occurrence of abundant putative radiolarians at the base of the section, combined with the mudstone-wackestone texture, indicate a relatively deep-water environment with a low hydrodynamic level, below storm-weather wave base, and within a basinal environment consistent with previous studies (Shen et al., 2007). Whereas the presence of packstone beds with fragmented bioclasts, indicate occasional reworking by storm currents and a shallower depositional setting closer to storm-weather wave base on the slope (Flügel, 2009). Furthermore, the absence of light-dependent organisms suggests deposition in a deeper environment below the euphotic zone. In addition, neither facies is characterized by synsedimentary slump structures indicating a relatively flat topography of the slope.

3.4.1.2. Initial reef phase facies association

3.4.1.2.1. Lithofacies types.

Lithofacies 2: Bioclastic packstone/rudstone. Medium- to thick-bedded bioclastic packstones (up to 50 cm), and thick-bedded to massive rudstones. Large sponge fragments, *Tubiphytes*, brachiopods, and crinoids are abundant in this facies (Figure 3.7F). Poorly sorted and angular lithoclasts of lime mudstones and sponges are significant components in the rudstone (Figure 3.7K).

3.4.1.2.2. Interpretation.

Packstones and rudstones of Lf2 reflect a transition between the slope-basin facies association and the reef facies associations. The occurrence of more complete and delicate shells such as brachiopods suggest a lower hydrodynamic level when compared with the packstones of the shallower facies associations. The Lf5 rudstone contains angular and poorly sorted bioclasts of fossils similar to the reef core facies association including sponges,

Tubiphytes and aggregates of encrusted sponges. So, these bioclasts are similar to the reef facies, except that they are not forming topographic highs or rigid reef structures. The presence of sparry cement in the rudstones cavity indicates the presence of high depositional porosity. Spatially, Lf2 is deposited below the reef core facies (Lf3–Lf7) and represents a transition from the slope to the platform margin reef.

3.4.1.3. Reef core facies association

3.4.1.3.1. Lithofacies types.

Lithofacies 3: Algae-Tubiphytes sponge boundstone. Massive lenticular boundstones with a height up to 2m and a width up to 15m (Figures 3.6D and 3.8A). Recrystallized bioclasts (probably calcareous algae) encrusted by *Archaeolithoporella* are the dominant components in this lithofacies. *Tubiphytes* and fragments of inozoan sponges occur sporadically, but do not have an important role in forming the boundstone fabric.

Lithofacies 4: Sponge-Tubiphytes bafflestone. Massive and massive lenticular bafflestones with a height up to 20m (Figures 3.6I and 3.7I). Toppled sponges act as a substrate for the upward growth of *Tubiphytes* that are encrusted by thin layers (<1 mm) of *Archaeolithoporella* (Figure 3.7I). The structure is principally formed by sponges and *Tubiphytes*, and these fossils trap large amounts of micritic sediments and fine-grained bioclastic material.

Lithofacies 5: Sponge-Archaeolithoporella bindstone. Massive and massive lenticular bindstones with a height up to 40m (Figures 3.6A, K, L, and 3.7N). Sponges, that are occasionally toppled, and *Archaeolithoporella* are the dominant components of this lithofacies. The sponges encrusted by medium to thick layers (>1 mm) of *Archaeolithoporella*. *Tubiphytes* are also present in this lithofacies as encrusters on the sponges, but this differs to lithofacies 4 in that the *Tubiphytes* are not freely growing upwards. Syndepositional isopachous cements filled primary pore spaces in the reef framework after the encrusting *Archaeolithoporella* (Figure 3.6K, L).

Lithofacies 6: Sponge-Algae-microbial boundstone. Massive bindstones with a height up to 10m (Figure 3.6G). Inozoan sponges are encrusted by laminated microbial micrites, and these microbial micrites also form on the roof/wall of centimeter-scale to decimeter-scale

cavities. Small sponges are also observed within the cavities, and some are attached to the roof of the cavities. Between these small sponges, the primary pore spaces are filled by syndepositional isopachous cements. In the remaining spaces of the cavity, clotted microbial sediments form crenulated laminations. Microbial micrites (crusts) (Figure 3.6G) showing micritic to fine-grained peloidal (range from 20 μ m to 30 μ m) texture, containing small undetermined tubular or spherical fossils. They also show gravity-defying orientation when they encrust the side and upper surface of other organisms, which confirmed the organic origin of these micritic-fine peloidal textures.

Lithofacies 7: Sponge-Algae framestone. Massive framestones with an exposed height up to 15m (Figure 3.7P), but it could be larger due to the small available exposure of the outcrop. This lithofacies is dominated by sponges with encrustations including *Archaeolithoporella* and microbial micrite. The occurrence of abundant cements between the reef framework is a significant feature of this lithofacies.

3.4.1.3.2. Interpretation.

Lithofacies 3–7 are all consistent with *in situ* massive or massive lenticular biologically-controlled deposition. We summarize them into a reef core facies association but the different lithofacies correspond to slightly different hydrodynamic levels and stratigraphically, expressed by different fabrics, and different phases of reef growth. The mud-rich texture in Lf3 indicates a possibly deeper environment with lower hydrodynamic level comparing with other lithofacies in this facies association, and Lf3 only occurred in the lowest part of reef setting development. In Lf4, the structure composed by sponge and upward growing *Tubiphytes* combined with the micritic sediments trapped by this structure and filling the remaining voids, and the existing of geopetal structure indicate a relatively quiet depositional environment with moderate hydrodynamic level. In Lf5, *Archaeolithoporella* is thicker comparing with other lithofacies in reef core facies. *Archaeolithoporella* entirely encrusting sponges and other organisms to form an oncoidal like fabric, which probably indicates a high-water energy environment. The Lf6 is usually developed in the uppermost part of most reef growing cycle (except the 6th transgressive-regressive cycle, described in 4.2.6), which is deposited in the shallowest part of these reef growing phases. The Lf5 locally occurred as a lens-like shape but

without a clear boundary within other reef core facies including Lf4 and Lf6, which possibly record the local changing of the hydrodynamic level. The abundant cements in the clear voids of Lf7 indicate a high hydrodynamic energy level, probably the highest in the entire reef core facies association.

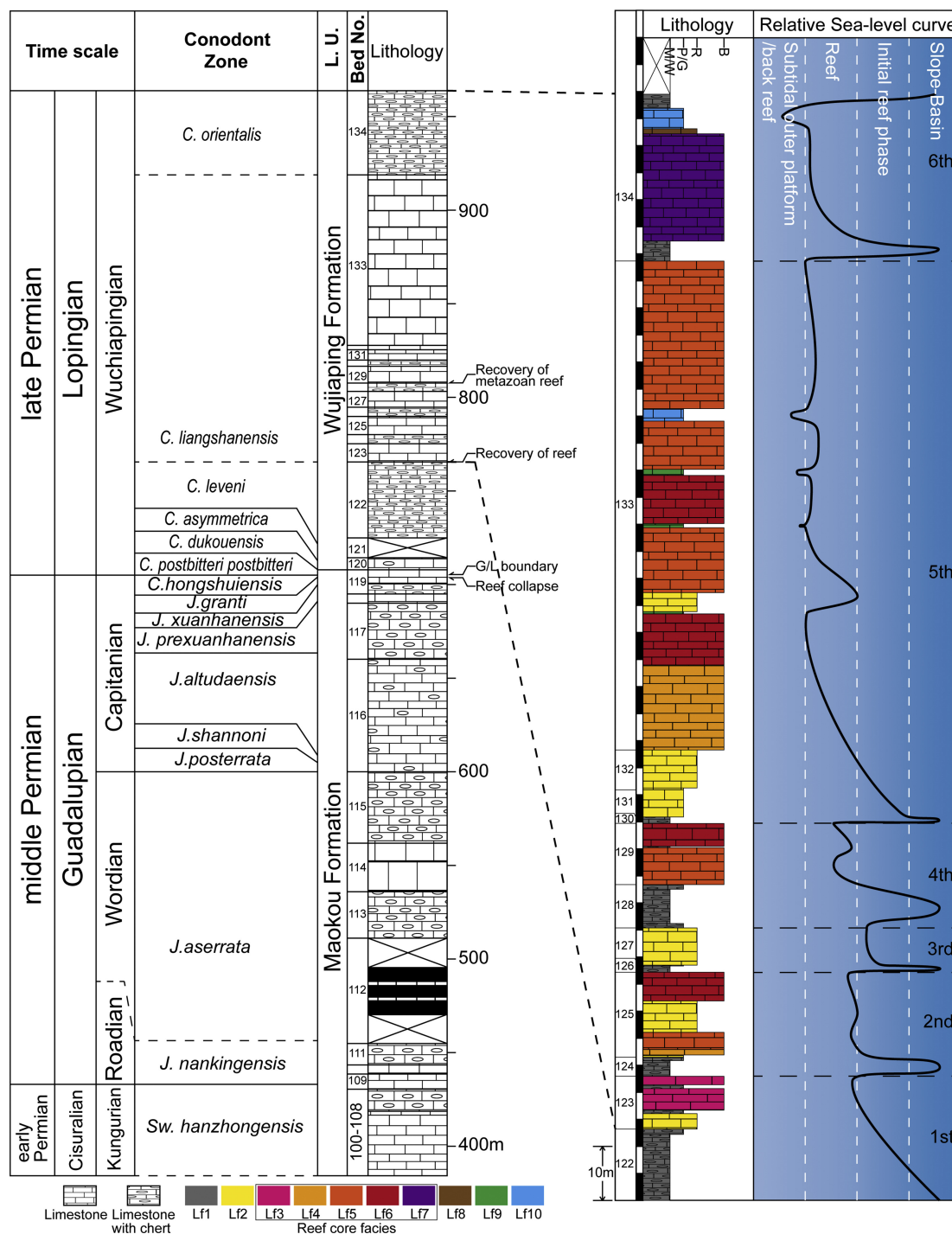


Figure 3.3: Stratigraphic succession of the Tieqiao section and relative sea-level curve. M/W=Mudstone/Wackestone, P/G=Packstone/Grainstone, R=Rudstone, B=Boundstone. Conodont zones are from Mei et al. (1998), Shen et al. (2007), and Sun et al. (2017). The bed numbers after Sha et al. (1990).

3.4.1.4. Reef cap facies association

3.4.1.4.1. Lithofacies types.

Lithofacies 8: Rudstone with breccia. Rudstones with lithoclasts of poorly sorted, angular reef debris, and wackestones with large crinoids (Figure 3.8I).

3.4.1.4.2. Interpretation.

The mixture of breccia of boundstone from reef core, breccia of wackestone and coarse clasts of crinoids within Lf8 suggest the collapse of a reef and surrounding deposition.

3.4.1.5. Subtidal outer platform/back reef facies association

3.4.1.5.1. Lithofacies types.

Lithofacies 9: Tubiphytes-crinoidal packstone-grainstone. Thin- to thick-bedded (5 cm–100 cm) parallel or laterally wedged beds of packstones and grainstones. Locally, an erosional surface occurs between this lithofacies and the underlying strata (Figure 3.8J). Bioclasts of *Tubiphytes* and echinoderms (mainly crinoids) are the main skeletal grains in this lithofacies, combined with a diverse fossil assemblage including brachiopods, bryozoans, foraminifera, *Permocalculus*, and *Gymnocodium*, within a matrix of micritized fragments, and small lithoclasts (Figure 3.7L).

Lithofacies 10: Gymnodiacean packstone and grainstone. Packstone and grainstone lenses (Figure 3.8L) (up to 1m thick) occurring within the massive reef core facies (Lithofacies 4–7). Gymnodiacean algae are the principal components in this lithofacies. Segments of *Gymnocodium* are abundant within the packstones, together with individual fragments of sponges, brachiopods, Tubiphytes and fragments of the foraminifera *Climacammina*. *Permocalculus* occurs occasionally within the packstone dominated by *Gymnocodium* but is more abundant within the grainstone together with *Tubiphytes*, crinoids (Figure 3.7M), and *Climacammina*.

3.4.1.5.2. Interpretation.

Lithofacies 9 and 10 indicate deposition in a moderate- to high-energy environment on the outer platform. Lithofacies 9 (Figure 3.8J), is characterized by beds with an erosive base and

contains subangular fragments bioclasts, indicative of reworking in a moderate to high energy environment. The Gymnodiacean packstones and grainstones of Lf10 were interpreted as back-reef facies in previous studies (e.g., Yang, 1987; Flügel, 2009) but the occurrence of the thick-shelled foraminifera *Climacammina* in the Lf10 can be an indicator of high energy environment (Zhang, 2015). The spatial distribution of Lf9 and Lf10 also suggest a shallower depositional environment compared to the reef core facies association.

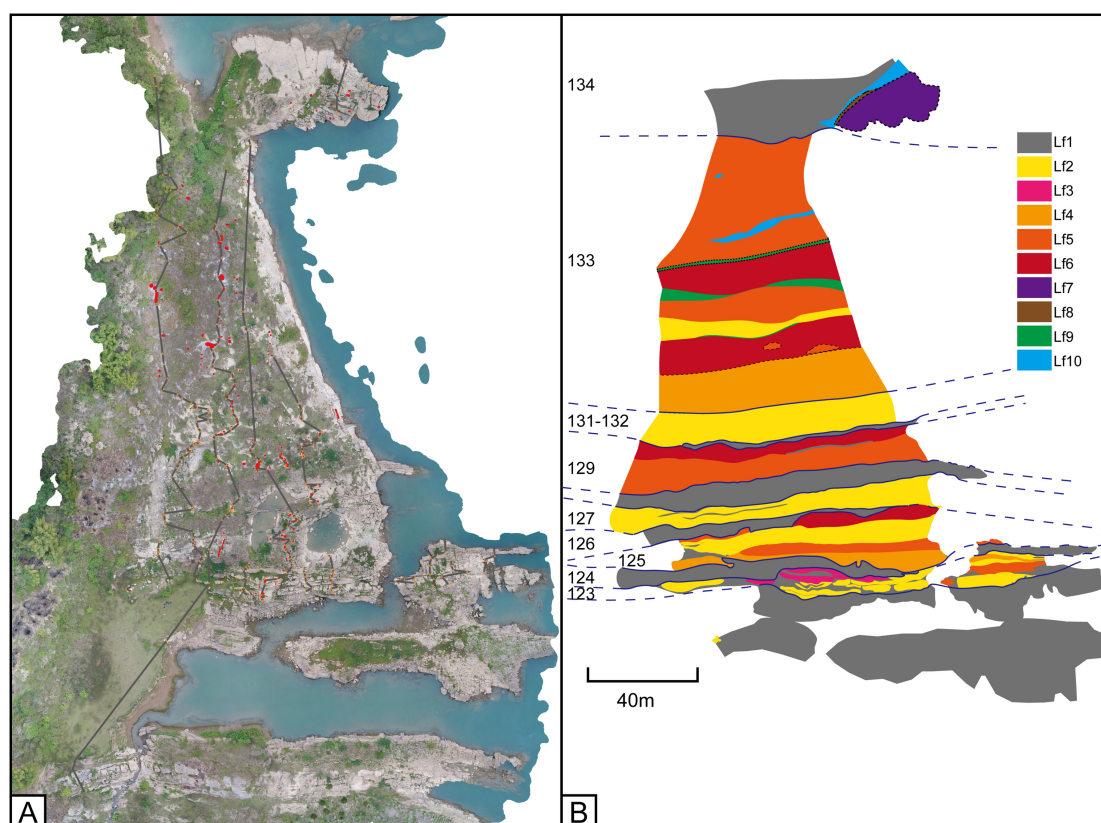


Figure 3.4: (A) Aerial drone map marked with the sample locations (orange triangle), stratigraphic profiles (gray line), and locations of acid-etched surfaces (red irregular shape); (B) distribution of lithofacies. The bed numbers after Sha et al. (1990). Note: the aerial drone map does not show the full extent of observable outcrop due to the canopy of the vegetation.

3.4.2. Spatial distribution and cyclicity

The spatial and vertical distribution of lithofacies and their geometries reveals the presence of several transgressive/regressive cycles in the section (Figures 3.3 and 3.4), deeper water cherty facies are repeatedly interbedded with reefal facies, and their onset marks the beginning

of a deepening-shallowing cycle. The six transgressive-regressive cycles are discussed in detail in the following paragraphs.

3.4.2.1. 1st transgressive-regressive cycle

Between the G/L boundary and the base of the measured section, which is 62.8m thick, the cycle is characterized by thin-bedded cherty limestones (Lf1), and just below the base of the section these transition into thin-bedded cherty limestone or nodular chert interlayered with thin- to medium-bedded packstone/rudstone that contain inozoan sponges, brachiopods and the microproblematicum *Tubiphytes obscurus* and *T. carinthiacus* (Lf1). These are then overlain by lenticular massive limestone bodies that are 10–20m wide and 1–3m thick (Figure 3.8N). The lithofacies of the lenticular bodies are boundstones (Lf3, Lf5) and surrounding the boundstones there are rudstones (Lf2), which includes debris of para-autochthonous fossils similar with the boundstone and mud and fine sediments. Rugosa corals are sporadically distributed in these rudstones (Figure 3.6E). These bioherms are relatively flat, and pinch-out horizontally. The core of the bioherms is dominantly characterized by algae-*Tubiphytes*-sponge boundstone (Lf3), whilst *Tubiphytes carinthiacus* and inozoan sponges are only a minor component (Figures 3.6D and 3.8A). Clotted microbial micrite fills the intraskeletal voids. Sponge-*Archaeolithoporella* bindstone (Lf5) occurs sporadically within the bioherm (Figure 3.6A), with the frame composed by *Archaeolithoporella* and sponges acting as a baffler for mud and matrix. These bioherms intercalated with bioclastic packstones that contain *Tubiphytes*, crinoid fossils, sponge fragments, and calcareous algae (*Gymnocodium* and *Permocalculus*), and cherty limestones.

Above the basal facies there is a decreasing abundance of cherty limestones than at the base of the measured section. The large lenticular bodies are interpreted as reefal bioherms, firstly because of their biogenetic content, which are composed by algae-*Tubiphytes*-sponge boundstone (Lf3) and *Archaeolithoporella*-sponge bindstones (Lf5). Secondly, the shapes of the lenticular bodies pinch out horizontally and are interbedded with cherty limestones (Lf1) suggesting that they are laterally restricted (Figures 8N and 4). The packstone beds occur in the upper part of calcareous limestone-chert alternation mainly composed by mudstone and

wackestone below the lenticular massive calcareous limestone, suggesting an upward shallowing of depositional environment before the development of reefal bioherm. The appearance of the packstone storm bed, reefal bioherms, and the decreasing abundance of cherty limestones are interpreted to reflect a shallowing into an upper slope environment below SWWB, but with a gentle slope.

3.4.2.2. 2nd Transgressive-regressive cycle

The second-cycle has a thickness of around 10m on the northern side of the section and 25m on the southern side. In the basal 1–7m, the succession is characterized by Lf1 which is capped by a 20 cm packstone (Lf2) (Figure 3.6H) before being overlain by two large lenticular limestone bodies. The first lenticular body covers the entire section and is 70m wide, with its the thickest part about 10 m. The second lenticular body is 60m wide and 15m thick and pinches out laterally to the north. The first lenticular massive limestone starts with a sponge-*Tubiphytes* bafflestone (Lf4) (Figure 3.6I). These then transition into an *Archaeolithoporella*-sponge bindstone (Lf5) (Figures 3.6K, L, and 3.8B) within the first lenticular massive limestone body. The two lenticular bodies are separated by an 8–10m thick interval of medium- to thick-bedded packstones and rudstones (Lf2) containing bioherm clasts (Figure 3.6J). The second lenticular massive limestone body is composed by a sponge-algae-microbial boundstone (Lf6) (Figure 3.6G). To the northern flank of the bioherms, the rocks become rudstones (Lf2) with lithoclasts (Figure 3.6C) and fragments of fossils similar to the lenticular body.

Lf1 at the base of this succession is interpreted to reflect a low-energy setting on the slope or in a basin environment. The 20 cm packstone (Lf2) bed that overlies the previous facies suggest a transition into a shallower environment. The lenticular massive limestone bodies (Lf4, Lf5, and Lf6) are interpreted to be reefal bioherms because they are constructed by frameworks built by *in situ* metazoan and encrusting organisms. Even though the two reefal bioherms have different facies, we interpret that they are a similar type of reefal bioherm, in that they are characterized by a sponge-*Tubiphytes*-microbial association. Together, these lithofacies, presence of fragmented fossils in the packstones, and the decrease in micrite in the upper part

of the bioherms indicate that the bioherm developed in an increasingly higher-energy environment, indicating shallowing upward of the environment.

3.4.2.3. 3rd transgressive-regressive cycle

The basal 2–6m of this cycle is characterized by Lf1. In the upper 50 cm of the basal part, there is a 10 cm coarsening-up grainstone, which contains fragments of *Tubiphytes*, calcareous algae (*Permocalculus* and *Gymnocodium*), bryozoans, and gastropods (Figure 3.7A). These are then overlain by medium- to thick-bedded packstones (Lf2) and on the northern flank are interlayered with thin-bedded cherty limestones. In between these beds, there is a thick-bedded *Tubiphytes carinthiacus* rudstone (Lf2) that is 4m thick and becomes thinner laterally. Unlike in the packstones, there are only *Tubiphytes* with a minor crinoid and inozoan sponge component (Figure 3.7B). Within the rudstone lithofacies, there are also small microbial columnar structures (Figures 3.7C and 3.8C) and sponges, which are encrusted by *Archaeolithoporella*.

Lithofacies 1 at the base of this succession marks the onset of the third transgressive-regressive cycle into a low-energy setting on the slope or in a basin. The transition from wackestone into packstones (Lf1) suggests shallowing into a high-energy environment probably close to the storm wave base. The *Tubiphytes*-rudstone is not interpreted as a reef but a biostrome, because even though the *Tubiphytes* are abundant and are locally forming a boundstone fabric, this is only at the cm-scale and not laterally restricted, therefore, is not forming an overall reefal structure (following the definition of reefs by Wood (1999)).

3.4.2.4. 4th transgressive-regressive cycle

In the basal 8–15m of this cycle is characterized initially by alternations of thin-bedded cherty-limestones and medium-bedded packstones (Lf1). These transition into thicker beds of cherty-limestones and from medium-bedded packstones to thin-bedded mudstones indicating a deepening into lower energy environment. The uppermost 50 cm there is a 5–10 cm packstone (Lf1). Overlaying the Lf1 there is a 10–15m massive limestone that does not show any relief over the width of the investigated section. This massive limestone is divided into two parts by

a 10–15 cm layer of cherty limestone. The lower part is characterized by sponge-*Archaeolithoporella* bindstone (Lf5). These sponges are encrusted by the *T. carinthiacus* and thick-layers of *Archaeolithoporella* that form a bindstone (Figures 3.7D and 3.8D). Clotted microbial micrites are typical interstitial filling between the sponge-*Archaeolithoporella* aggregates (Figure 3.7E). The upper part of the massive limestone is made up of sponge-algae-microbial boundstone (Lf6). The sponges are the primary component and bound by the *Archaeolithoporella* and microbial micrites. The remaining voids are filled by calcisparite, micrite and bioclasts, but microbial precipitation around the sponges makes up >40% of the rock volume (Figure 3.8E).

The massive limestones (Lf5 and Lf6) are interpreted as large reefal biostromes because we do not recognize any topographic relief. In addition, the high-abundance of sponges that are encrusted and bounded together by *Tubiphytes* and *Archaeolithoporella* suggests that the construction of the biostromes is biologically-controlled. The reefal biostromes is interpreted as developing in a shallow, high-energy environment above wave base on the outer platform. The high-energy environment is indicated by the abundance of clotted microbial micrites and the cements that fill the voids between the reef frame (Flügel et al., 1984). In addition, we infer that because of the high-abundance of *Archaeolithoporella* (algal *Archaeolithoporella* in Kirkland et al., 1998) that this reefal biostrome developed in the euphotic zone, high-energy environment (Nakazawa et al., 2015, 2012).

3.4.2.5. 5th transgressive-regressive cycle

The first meter in the southern part, and first 3m in the northern part of the section of this cycle, is characterized by Lf1. In the top 20 cm of this unit, there is a 10 cm packstone that spans the width of the section. The next unit is ~15m thick and characterized by medium to thick-bedded packstones (Lf2) (Figure 3.7F) that grade into a sparry rudstones (Lf2) containing fragments of small sphinctozoan and inozoan sponges, which are encrusted by *Tubiphytes* and *Archaeolithoporella* (Figure 3.7G). These are then overlain by partly dolomitized rudstones (Lf2) that contain abundant aggregates of sponge fragments encrusted by *Archaeolithoporella* (Figure 3.7H).

Above this unit, there is a 90m thick massive limestone. The southern part of this massive limestone is cut by the river and the northern part of the outcrop is covered by vegetation, so the size of reef core is wider than the 60–80m width that is exposed. There is also no obvious change from the reef core to the reef flank that can be observed in this phase and no overall topographic relief is observed. Within the upper part, however, boundstone overlapped by Gymnociacean-packstones and grainstones indicate a meter-scale relief in this part of the reef (Figure 3.8J, L). Within this massive limestone unit, there are also temporal transitions in lithofacies, relating to the rock fabric and the fossils. This massive limestone is characterized by boundstones with high-abundance of sponges, and the abundance of sponges increases upwards in this unit, but the distribution of sponges is uneven (Figure 3.5B). The base of this unit is dominated by sponge-*Tubiphytes* bafflestones (Lf4) with the encrusters *Archaeolithoporella* and microbial micrites, with mud filling the voids (Figure 3.7I). Then as the abundance of sponges and *Tubiphytes* and other encrusters increased upward, the lithofacies changes to a sponge-algae-microbial boundstone (Lf6) (Figure 3.8F), sporadically developed lenticular bodies of *Archaeolithoporella*-sponge bindstones (Lf5) (Figures 3.4 and 3.7J). In the central part of the section above this lithofacies is a 20 cm *Tubiphytes*-crinoidal packstone-grainstone (Lf9) lens (Figure 3.7L). The subsequent lithofacies is characterized by a 5m rudstone (Lf2) interval with fragments of sponges, *Tubiphytes*, and rare lithoclasts (Figure 3.7K). After this, *Archaeolithoporella*-sponge bindstone (Lf5) becomes the dominated lithofacies. In between this lithofacies and the next, there are lenses of packstone-grainstones (Figure 3.8K) (Lf9) that are overlain sponge-algae-microbial boundstones (Lf6). In the upper part of this lithofacies the abundance of sponges decreases (Figure 3.5B) and the lithofacies transitions to a *Tubiphytes*-crinoidal packstone-grainstone (Lf9) (Figure 3.8J). After this, a sponge-*Archaeolithoporella* bindstone (Lf5) becomes the dominant lithofacies (Figure 3.7N). This is intercalated by a 3m thick Gymnociacean packstone-grainstone (Lf10) lens (Figures 3.7M and 3.8L). In the uppermost 25–30m of the massive limestone (Lf5), there are large chambered sphinctozoans that become abundant, and the length of biggest sphinctozoan is over 30 cm (Figure 3.8G). Then sponge-*Archaeolithoporella* bindstone (Lf5) containing inozoans and small sphinctozoan sponge (Figure 3.7O) become dominant again in the uppermost 8 m, with sporadically occurring Gymnociacean packstones and grainstones (Lf10).

Lithofacies 1 that makes up the base of this cycle are interpreted to reflect deepening back into a low-energy environment, on the lower slope. Based on the presence of sparry calcite in the overlying 15m bedded rudstone interval, a transition into a high-energy environment in a shallower setting above wave base is inferred. The massive limestone unit is inferred to represent the largest phase of reef growth in the studied section, consistent with previous studies (Huang et al., 2019a; Sha et al., 1990; Shen et al., 2007; Yang, 1987). We interpret a reef environment, because of the presence of m-scale relief structures between the different lithofacies, the primary cements succeeding the reef-building organisms indicating an initial rigid structure of the reef fabric, and the construction of a biological framework by sponges, and encrusters. In the upper part of the reef core the thickness of the *Archaeolithoporella* encrustations gets thicker (Figure 3.5), and this is interpreted to reflect shallowing into either a more light-intense environment within the euphotic zone or faster growth rates in shallower warmer water.

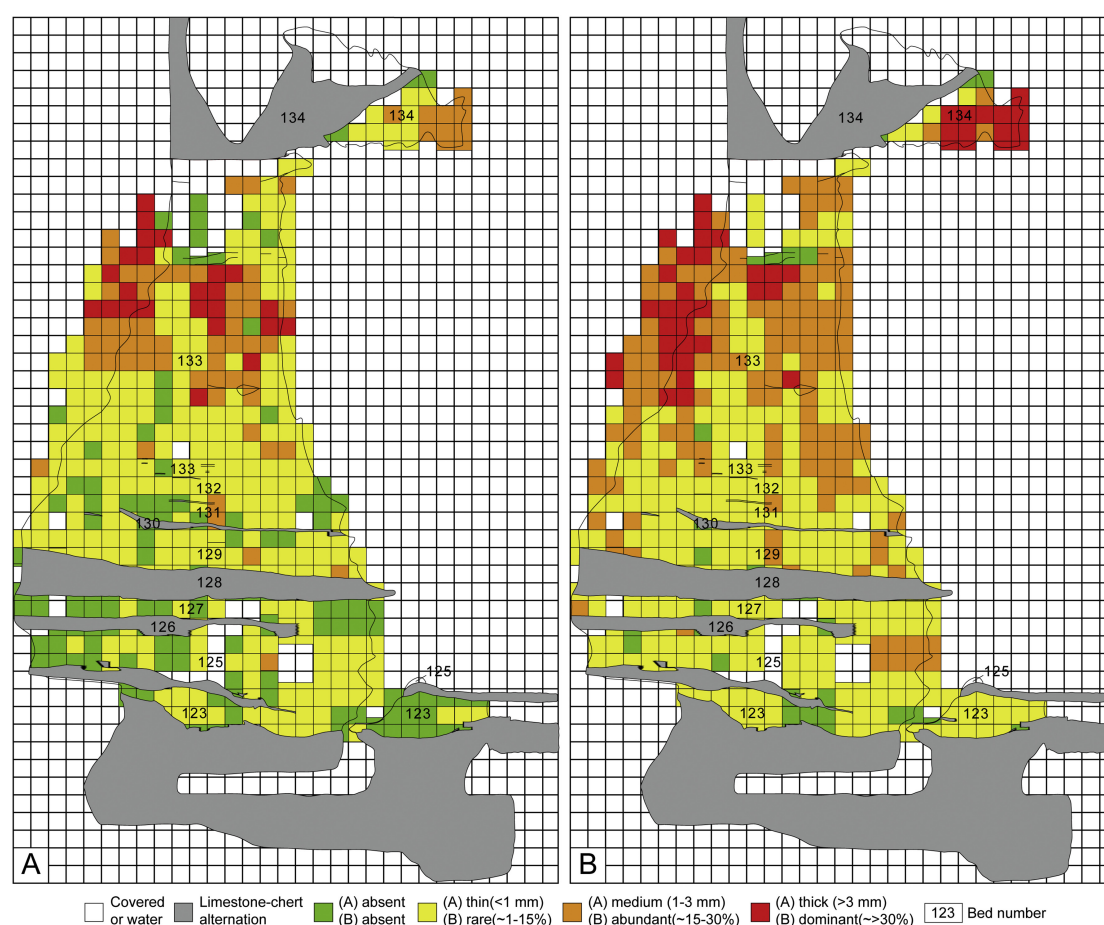


Figure 3.5: The grid map showing the abundance of the encruster *Archaeolithoporella* (A) and sponges (B). Size of an individual grid is 5m × 5 m. The bed numbers after Sha et al. (1990).

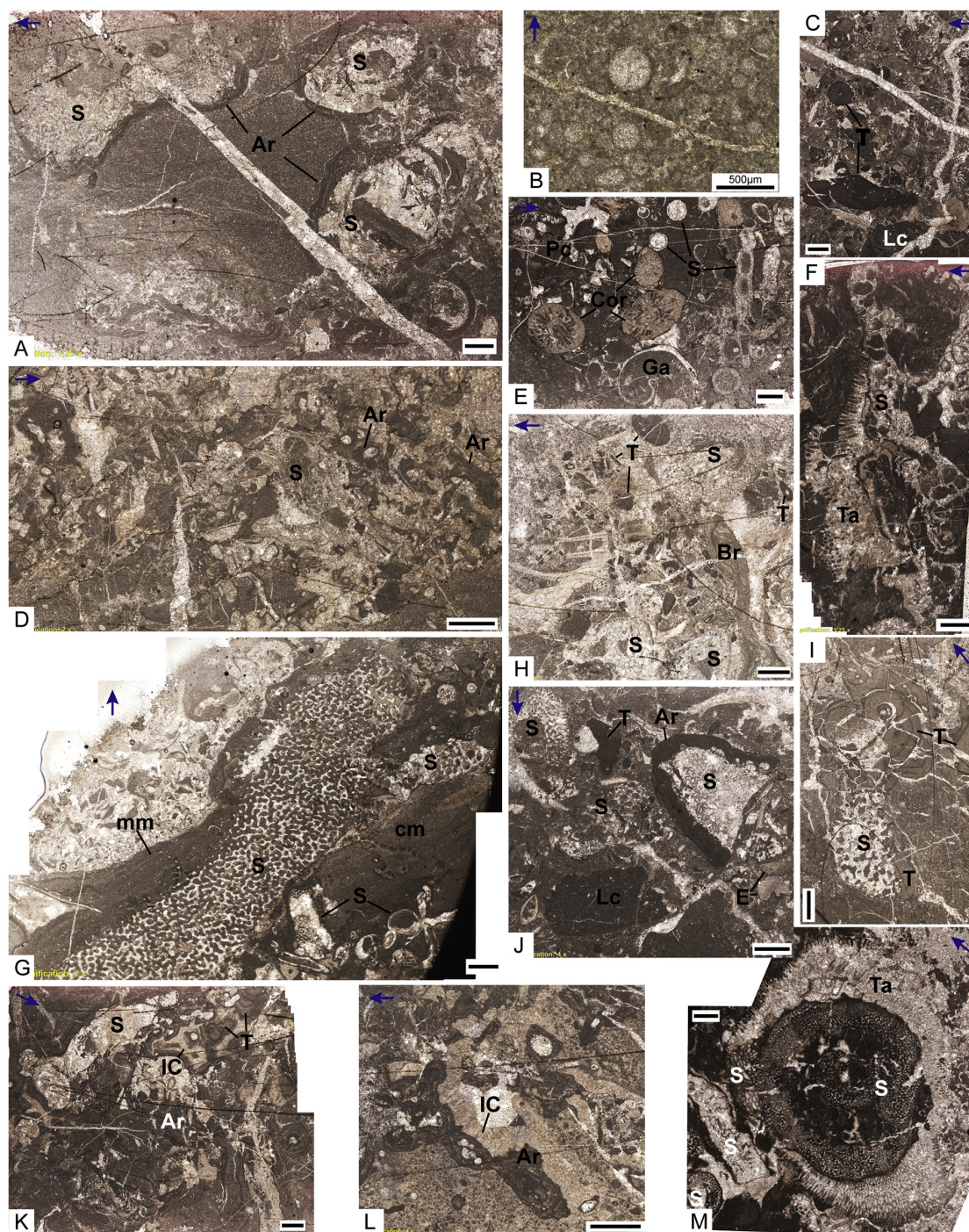
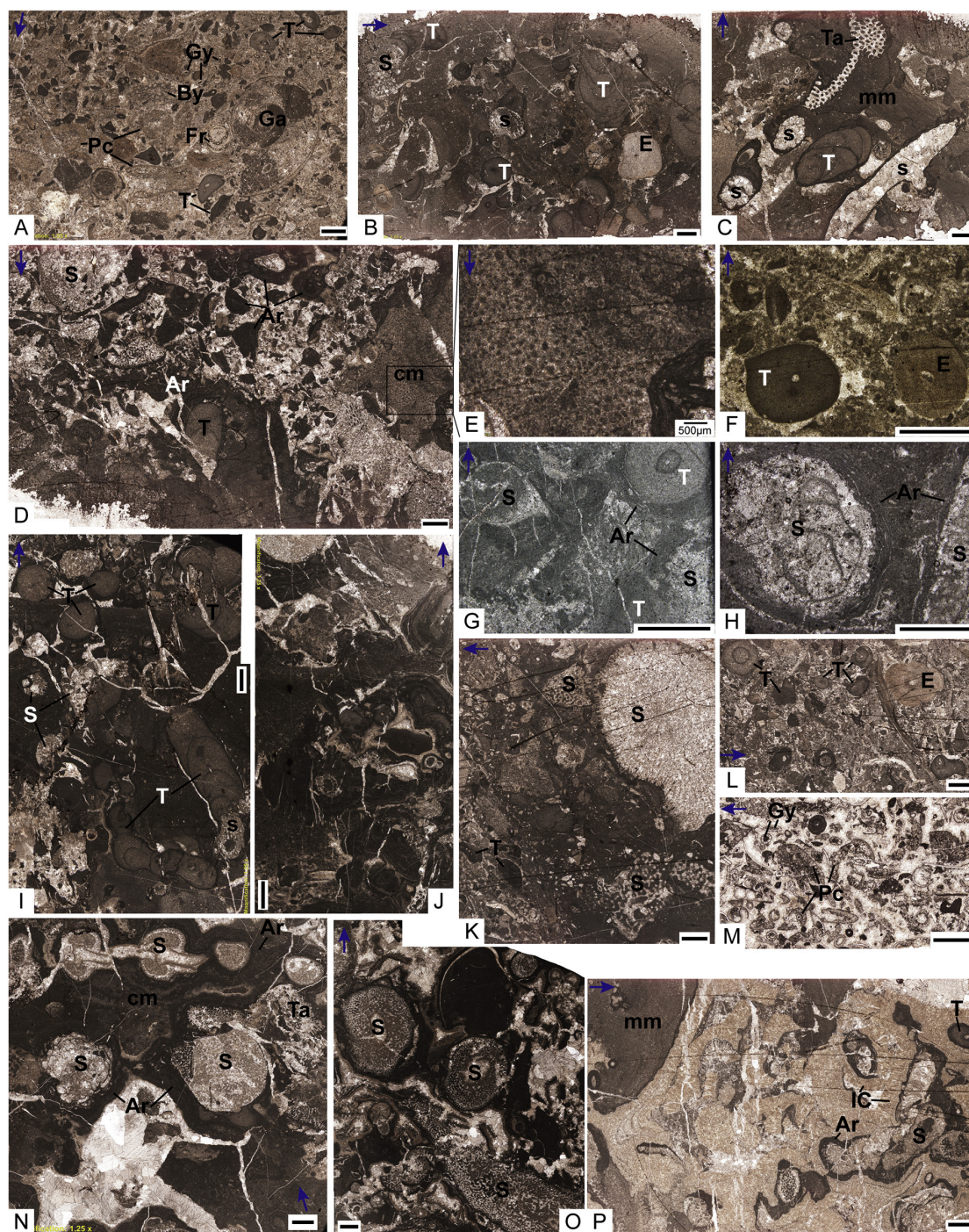


Figure 3.6. Thin-section photomicrographs of 1st, 2nd and 5th cycle. (A, K, L) sponge-*Archaeolithoporella*-bindstone; (D) Algae-*Tubiphytes*-sponge boundstone; (G) sponge-algae-microbial boundstone; (I) sponge-*Tubiphytes* bafflestone; (B) wackestone with putative radiolarians from the lowermost part of 1st cycle; (C, J) rudstones with large fragments of sponges, *Tubiphytes* and lithoclasts; (H) packstone with poorly sorted skeletal grains; (E) rudstone with sponges, rugosa corals, *Permocalculus* and gastropods; (F, M) Tabulozoan encrusting sponges. A, B, D and E is from the 1st cycle; C, G, H, I, J, K and L is from the 2nd cycle. F and M are from the 5th cycle. S: Sponge; T: *Tubiphytes*; Ar: *Archaeolithoporella*; Ta: Tabulozoan; Lc: Lithoclasts; Br: Brachiopods; Ga: Gastropods; Cor: Coral; Pc: *Permocalculus*; IC: Isopachous cements; mm: microbial micrites (crusts); cm: clotted microbial micrites. Scale bar is 2mm except B. Blue arrows indicate the stratigraphic top.



3.4.2.6. 6th transgressive-regressive cycle

This final cycle is laterally variable. In the central and northern part, this cycle is made up of thin-bedded cherty limestones alternating with thin-bedded mudstones containing thin shelled brachiopods (LF1) (Figure 3.8H), and this has a clear lateral contact with a massive limestone. The massive limestone is only 35m wide and 20m thick because the southern part has been eroded away by the river. Where the massive limestone can be observed in the same

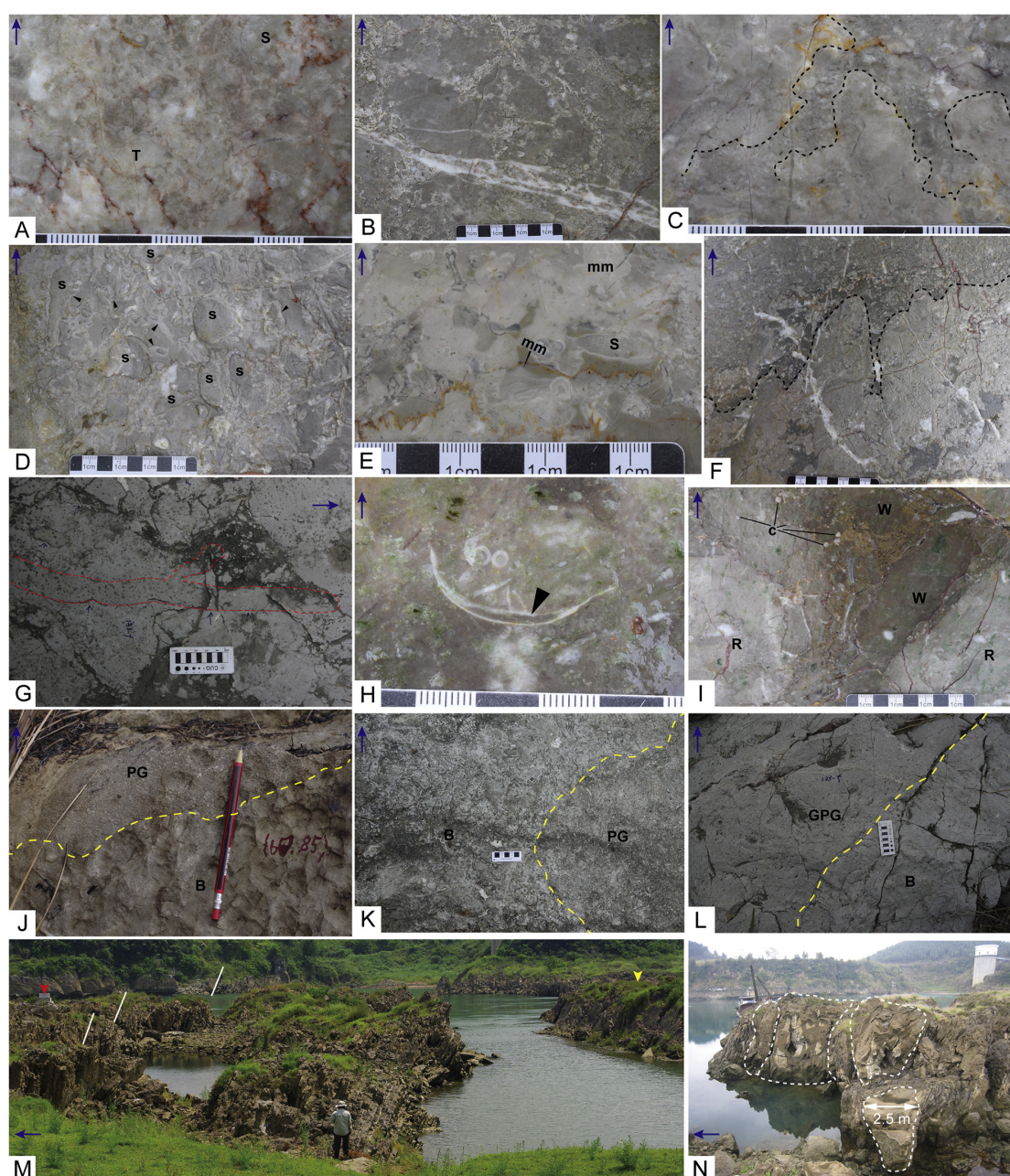
stratigraphic profile with the underlying cycle, the two are separated by a 5m interval of thin-bedded cherty limestones (Lf1) (Figure 3.4). The northern flank of this massive limestone is steep with a 40° slope. The lithofacies of the massive limestone is sponge-algae-framestone (Lf7) that is made up of abundant sponges with microbial crusts and *Archaeolithoporella*. Within this framestone lithofacies, there are abundant isopachous radial cements (Figure 3.7P). The framestone is then overlain by rudstone made up of breccia and crinoid fragments

←**Figure 3.7: Thin-section photomicrographs of 3rd to 6th cycles.** (A) packstone within lithofacies 1; (B) rudstone with abundant *Tubiphytes*; (C) rudstone with large fossil fragments encrusted by microbial crusts. (D) Sponge-*Archaeolithoporella* bindstone; (E) is enlargement of the marked area in D; (F) packstone with fragments of *Tubiphytes* and crinoids; (G, H) aggregates of sponge and *Tubiphytes* encrusted by *Archaeolithoporella* within the rudstone; (I) Sponge-*Tubiphytes* bafflestone; (J) sponge-*Archaeolithoporella*-bindstone; (K) rudstone with fragments of sponges, *Tubiphytes*, and lithoclasts; (L) *Tubiphytes*-crinoidal packstone-grainstone; (M) Gymnodiacean packstone-grainstone; (N) sponge-*Archaeolithoporella* bindstone, note the missing of *Archaeolithoporella* on the lower surface of the sponge in the upper part of this picture; (O) sponge-*Archaeolithoporella* bindstone; (P) sponge-algae framestone. A, B and C is from the 3rd cycle; D and E is from the 4th cycle; F to O is from the 5th cycle; P is from the 6th cycle. S: Sponge; T: *Tubiphytes*; Ar: *Archaeolithoporella*; Ta: Tabulozoan; Lc: Lithoclasts; Br: Brachiopods; Ga: Gastropods; Cor: Coral; Pc: *Permocalculus*; Gy: *Gymnocodium*; By: Bryozoan; IC: Isopachous cements; mm: microbial micrites (crusts); cm: clotted microbial micrites. Scale bar is 2mm except E. Blue arrows indicate stratigraphic top.

→**Figure 3.8: Close-up photos of acid etched surfaces of the outcrop (A-F, H, I), weathered surfaces of the outcrop (G, J-L) and the outcrop (M, N).** (A) algae-*Tubiphytes* sponge boundstone in the 1st cycle, note the sporadically distributed *Tubiphytes* and inozoan sponge; (B) *Archaeolithoporella*-sponge bindstone in the 2nd cycle; (C) microbial columnar structures within the rudstone in 3rd cycle, black dotted line indicates the boundary of microbial columnar structure; (D) sponge-*Archaeolithoporella* bindstone in 4th cycle; (E) sponge-algae-microbial boundstone in 4th cycle, note the laminated and columnar shape of microbial micrite. (F) sponge-algae-microbial boundstone in 5th cycle, black dotted line indicates the columnar shape of boundstone fabric; (G) large chambered sphinctozoan sponge (red dotted line) in 5th cycle; (H) mudstones containing thin-shelled brachiopods (black arrow) in 6th cycle; (I) rudstone with breccia in 6th cycle; (J) yellow dotted line indicates the erosional surface between the *Tubiphytes*-crinoidal packstone-grainstone and underlying boundstone; (K) yellow dotted line indicates the lenticular shape of packstone-grainstone; (L) yellow dotted line indicates the inclined contact between Gymnodiacean packstone-grainstone and the sponge-*Archaeolithoporella* bindstone, which indicate a local relief of the bindstone reef core facies; (M) alternations of mudstones and wackestones with beds of cherts in the lower part of 1st cycle; yellow arrow points out the position of G/L boundary; red arrow points out the southeast boundary marker of the protected-area of GSSP auxiliary section; white short lines indicate the base of bioherm in the 1st cycle; (N) white dotted lines indicate the lenticular shape of massive limestone in 1st cycle. Each black/white interval of the scale in A to F, and H, I, K is 1 cm. Each black/white interval of the scale in G and L is 0.5 cm. Pencil in J is about 15 cm. The person standing in M is about 1.6m tall. Blue arrows indicate stratigraphic top.

(Lf8) (Figure 3.8I). The rudstone with breccia is then covered by Gymnocodiacean packstone-grainstone (Lf10).

The framestone (Lf7) built by in-situ sponges, encrusters and cements, combining with the laterally restricted relief of the massive limestone which confined by the overlapping rudstone (Lf8) and thin layered cherty limestone and mudstone alternation (Lf1) in the northern flank, indicate that this massive limestone in this cycle is a reef. The overlying Lf8 is the capping facies of the reef. Above the Lf10, the overlying Lf1 indicate another transgression leading to deepening environment which drowned the reef setting.



3.5. Discussion

3.5.1. *The timing of reef recovery on the Laibin-Heshan platform*

The controversy of defining a reef has been ongoing for decades, but most definitions have a consensus on recognizing that reefs are recognized as having a: i) lateral topographic relief, ii) biological control during the formation of the structure, and iii) an inferred rigidity of the structure (Wood, 1999; Flügel, 2002). The nature of a sponge-algae bioherm, that developed during the *C. orientalis* conodont zone at the Tieqiao section, has long been discussed (Sha et al., 1990; Yang, 1987). However, recent studies have concluded that this bioherm, in fact, is a reef (Qiu, 2010; Huang et al., 2019a). This bioherm corresponds to the 5th transgressive-regressive cycle in our measured section. However, in the 1st and 2nd transgressive-regressive cycles at the Tieqiao section, the lenticular shape of massive limestones indicates the existence of lateral topographic relief. The algal bindstone and algal-sponge boundstone of the 1st and 2nd transgressive-regressive cycles, respectively, suggests that these lenticular bodies were biologically controlled. In addition, the structures are inferred to have been a rigid structure because of the presence of syndepositional cements (Figures 3.6K, L, and 3.7P). Therefore, based on these features we infer that the development of reef bodies developed two conodont zones earlier in the Wuchiapingian on the Laibin-Heshan platform, within or after the *C. leveni* conodont zone (Figure 3.3). Furthermore, in the 2nd transgressive-regressive cycle both the size of the reef body and the abundance of sponges increased, which suggests that the reef community has stabilized in the environment and started to flourish much faster than previously thought. But although the size of the reef does increase within the rising abundance of sponges in the 2nd cycle, the abundance of metazoans is not a requirement for defining a reef.

As well as identifying that the recovery of reefs occurred much earlier on the Laibin-Heshan platform than previous studies, we also recognize six phases of reef growth associated with transgressive-regressive cycles (Figure 3.4). The 3rd and 4th cycles are interpreted as *Tubiphytes* and sponge-biostromes, respectively, owing to the lack of an observed topographic relief. This may, however, be because the reef bodies are much wider than the investigated exposure. We also recognize for the first time a reef body in the uppermost part of the Tieqiao

section (Figure 3.4). The development of these reefs at the Tieqiao section shows the importance of a shallower depositional environment and the impact of fluctuating sea-level during the initial development of the reef. Whereby, the development of the reef bodies is restricted to the shallower part of the cycles interpreted to reflect deposition on the upper slope of the platform. This restriction to shallower settings may be due to the importance of the encrusters in constructing the reef bodies (see discussion below) which appears to be affected by the amount of light availability, thus restricting the development of reefs on the Laibin-Heshan isolated platform to the euphotic zone.

3.5.2. *The Guadalupian-Lopingian evolution of sponge reef ecosystems*

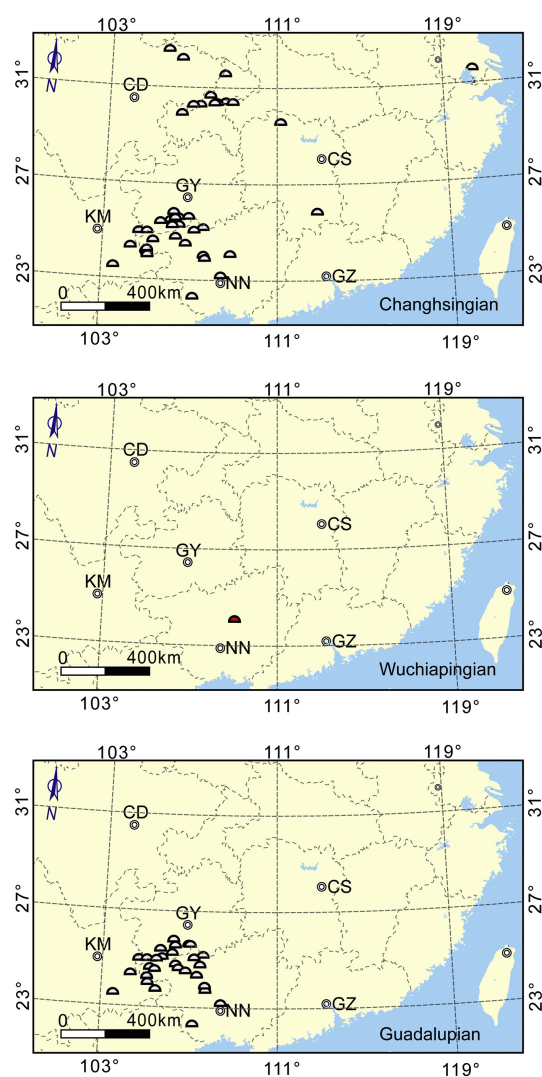


Figure 3.9: Distribution of reefs in South China (reef data of Guadalupian and Changhsingian from Zhang and Zhang (1992)). Lower: Guadalupian; Middle: Wuchiapingian, red semi-circle is the Tieqiao reef; Upper: Changhsingian.

The Capitanian and Changhsingian are the two most important reef-building intervals of the Permian in South China (Figure 3.9) (Fan et al., 1990; Rigby et al., 1989a, 1989b), and sponges are typically the primary reef builder. The sponge reef-building communities are dominated by different sponge groups between Capitanian and the Changhsingian. The large Sphinctozoan sponges, *Intrasporeocoella* and *Rhabdactinia*, dominated the Capitanian sponge reef communities, but these large sized Sphinctozoans lost their dominance in the Changhsingian sponge-reef communities to smaller Sphinctozoan sponges, *Amblysiphonella* and *Polycystocoelia*, and Inozoan sponges, especially *Peronidella* (Zhang and Zhang, 1992). How this transition happens is, however, unknown as the only reefs known from the Wuchiapingian in south China are restricted to the Tieqiao section (Figure 3.9).

The Tieqiao reef complex represents the transition between Capitanian and Changhsingian reef communities. Inozoans, including *Peronidella* and *Corynella*, and the Sphinctozoan sponges include *Amblysiphonella*, *Sollasia*, *Guadalupia*, *Cystothalamia*, *Cryptocoelia*, *Colospongia*, *Intrasporeocoelia*, and *Salzburgia* (Yang, 1987) are abundant in the Wuchiapingian Tieqiao reef complex as reef builders. Most of the Inozoans observed in Tieqiao reef are toppled and part of them encrusted by *Archaeolithoporella*, *Tubiphytes*, and microbial crusts. The predominant Sponge groups in Tieqiao Wuchiapingian reef are Inozoans and small Sphinctozoans, which is more similar to the late Permian Changhsingian reefs than the Capitanian reefs suggesting that the ecological turnover from Capitanian sponge reefs to Changhsingian sponge reefs occurred as a consequence of the ecological reorganization after the Middle Permian mass extinction event.

3.5.3. The role and importance of encrusters in Permian reef-building

The ecology of Permian reef communities has been studied worldwide, and most extensively from the Capitan reef in Texas and New Mexico (Kirkland et al., 1998; Wood et al., 1994, 1996). Guadalupian-Lopingian reefs are significantly contributed by small sized, low-growing organisms including *Archaeolithoporella*, *Tubiphytes*, bryozoans, small sponges and rugose corals and calcareous algae. Erect, large sized reef builders have not prevailed in the construction of buildups. The rigidity of Permian reefs substantially strengthened by a

significant proportion of encrusting organism, microbial carbonates and syndepositional cements (Guo and Riding, 1992; Kirkland et al., 1998; Nakazawa et al., 2015, 2012; Shen and Xu, 2005; Wood et al., 1996, 1994). In the Capitan reef, it has been demonstrated that post-mortem encrustation by *Archaeolithoporella*, *Tubiphytes*, and microbial micrites was an important factor for the Capitan reef to establish a rigid structure to support the reef community (Kirkland et al., 1998; Wood et al., 1996, 1994). Investigations of Capitanian and Changhsingian sponge reef communities from south China also highlighted the importance of the binding function of encrusting organisms such as *Archaeolithoporella*, *Tubiphytes*, and Tabulozoan to form rigid structures (Fan et al., 1990; Wang et al., 1994). It was hypothesized that these encrusting organisms had a close (but not symbiotic) relationship with sponges to develop reef bodies, where these encrusters developed on toppled sponges that died in a high energy environment, which in turn formed a stable substrate for growth of next generation of sponges, with these cycles of sponges and encrusting organisms forming a biologically-controlled rigid reef structure (Zhang and Zhang, 1992). The sponges were not strong enough to build rigid reef structure without the encrusting organisms and the higher the abundance of encrusting organisms the better stability and higher maturity of reef build-up.

In Tieqiao, the reef-building is done by sponges and encrusting organisms including *Archaeolithoporella*, *Tubiphytes*, Tabulozoans (Figure 3.6F, M) and Microbial micrite (crust). In the reef core facies of the 1st and 3rd cycles, where sponges are rare (Algae-*Tubiphytes*-sponge boundstone), the Inozoan sponges are normally toppled and not acting as frame builders. Whereas, in the reef core facies where sponges are common (Sponge-*Tubiphytes* bafflestone/boundstone), the density of Inozoan sponges are not suggesting a direct frame builder character, but the frame building process can be achieved by Inozoan sponges together with encrusting organisms such as *Tubiphytes*, *Archaeolithoporella*, and microbial crusts. Whilst, in the 5th and 6th phases of reef development the sponges are abundant in the reef core facies (Sponge-*Archaeolithoporella* bindstone, Sponge-Algae-microbial boundstone, and Sponge-Algae framestone), and some longer or wider Inozoan sponges acted as roof or walls of caves in the reef, which sheltered smaller Inozoan sponges and cryptic Sphinctozoan sponges. In those reef cavities, sponges assembled or bound together by encrusting organisms, some can be observed attaching to the roof of the cavities. The sponges, therefore, were not primary reef

builders in the onset of the bioherm/reef development at the Tieqiao section but did become increasingly important during the subsequent phases of reef development.

In the Tieqiao reef complex, *Tubiphytes* acts as an encrusting and frame building element in the reef core facies. It's abundant in the initial phase of bioherm/reef development, to form bafflestone/boundstone facies together with sponges. At least two Paleozoic (Permian) species has been observed in Tieqiao reef, *Tubiphytes obscurus* Maslov and *Tubiphytes carinthiacus* (Flügel). *T. carinthiacus* (Flügel) which is bigger than *T. obscurus* Maslov. *T. carinthiacus* differs from *T. obscurus* by the coarser internal network of the envelope (Senowbari-Daryan, 2013). *T. carinthiacus* act as reef builder or encruster, *T. obscurus* usually acts as encruster or attached on the lower surface of reef-building organisms. *T. carinthiacus* sometimes encrusted by other organisms like *Archaeolithoporella*.

Archaeolithoporella has been observed over the entire section. The thickness of *Archaeolithoporella* varied from 0.5 to 5mm in Tieqiao. *Archaeolithoporella* partly lived in a dimly-lit habitat in Tieqiao reefs, which is similar to examples from the Capitan reef (Kirkland et al., 1998). In some of the centimeter to decimeter sized cavities which were formed by toppled sponges, *Archaeolithoporella* encrusted the inner walls. In this case, *Archaeolithoporella* also encrusted/bound other smaller sponges to the toppled sponges. But in the really narrow place of the cavities or in really small cavities, *Archaeolithoporella* only grows on the upper surface of the sponges that build the roof/wall of these cavities (Figure 3.7N), which may suggest the Phototropic growth of *Archaeolithoporella*. In the reef core facies, *Archaeolithoporella*-sponge bindstone is normally abundant in the middle/upper part of shallowing up cycles, which may suggest the facilitation of shallower sunlit environment to the growth of *Archaeolithoporella* (Figure 3.4).

3.5.4. The recovery pattern for the reef during Wuchiapingian stages comparing with the recovery of reef system after end Permian extinction

The recovery of reef ecosystems following the end-Permian mass extinction has been described as occurring in 5 stages, 1st with microbialites reefs replacing the niche previously occupied by species-rich Changhsingian reefs in the Early Triassic, 2nd small metazoan reefs (built by bivalves and sponges) in the Olenekian, 3rd *Tubiphytes* reefs in the Anisian, 4th ‘Wetterstein’ reefs dominated by *Tubiphytes* and sponges in the upper Anisian, and finally the final recovery/restructuring of reefs with the evolution of ‘Dachstein’ reefs dominated by scleractinian corals that became significant reef builders after they developed a symbiotic relationship with zooxanthellae in the Late Triassic (Flügel, 2002; Martindale et al., 2019). Even though the Middle Permian extinction was not as catastrophic as the end-Permian, it caused a loss of 89% of reef carbonate production, together with a loss of 55% of reef diversity, and left a globally desolate reef record (Kiessling and Simpson, 2011; Weidlich et al., 2003). The recovery of reef ecosystems at the Tieqiao section shows a similar trend to the Triassic reef recovery patterns with distinct stages of reef and metazoan reef recovery.

The initial recovery of reefs at Tieqiao is represented by non-metazoan reefs with algal bioherms and small-sized algal-sponge reefal build-ups representing the initial recovery, which is followed by a *Tubiphytes* biostrome, and then the recovery of metazoan reefs with sponges being one of the main reef builders in the 4th, 5th, and 6th reef development cycles (Figure 3.4). In addition, to the delayed recovery of metazoan reefs, the importance (relative abundance) of sponges in the reef bodies increases with distance from the G/L boundary. This suggests that even after the recovery of metazoan reefs in the Tieqiao section that sponges are still recovering and becoming increasingly important (Figure 3.5B). The difference between the recovery of reefs after the Middle Permian and end-Permian is that subtidal microbialites were not observed at Tieqiao, and this may be because it is most likely that the microbialites were able to develop in the Early Triassic because of the absence of mat-inhibitors (Schubert and Bottjer, 1992), whereas the competition for space is much likely to have remained high after the Middle Permian extinction. New locations revealing the recovery of reefs following the Middle Permian extinction are required to test if the metazoan reef recovery at the Tieqiao section is a local or global phenomenon, but the similarity in the delayed recovery of metazoan reef ecosystems to mass extinction events demonstrates their sensitivity to rapid climate change.

3.6. Conclusion

Our sedimentological analysis of the Tieqiao reef on the Laibin-Heshan platform margin shows that: a) there are six transgressive-regressive cycles which correspond to six cycles of reef development, with the reefal buildups developing during the regressive phase on the outer platform above wave base and in the euphotic zone, b) that different reef types characterize these reef cycles with non-metazoan reefs built by algae and *Tubiphytes* with sponges as minor component during the initial four transgressive-regressive cycles, which is earlier than documented in previous studies. Whereas the recovery of metazoan reefs occurs later in the 5th and 6th cycles, suggesting a delayed recovery of metazoan reefs following the Middle Permian extinction event, c) the encrusting organisms are a key component in constructing a rigid reef structure with a topographic relief. In addition, the increasing thickness, towards the top of the succession, of the encruster *Archaeolithoporella* on toppled sponges is inferred to represent growth in the shallower part of the euphotic zone, and/or increased growth rates in shallower and warmer waters.

Acknowledgments

Wuqiang Xue, Fayao Chen, Qi Meng, Bo Li, Yajuan Yan, Qian Ding, Jianbin Wang are thanked for the help with the field work. We also thank Daizhao Chen, Xiting Liu, Fei Li, Sara Tomás, Matteo di Lucia, Gianluca Frijia, Nicolas Christ, Xiaoxia Huang, and Sven Maerz for constructive discussion about this work. An anonymous reviewer and GPC Editor Fabienne Marret-Davies are thanked for the constructive comments that improved the manuscript. This study is supported by National Natural Science Foundation of China (grant numbers: 41872117 and 41472087), and by a doctoral Scholarship of China Scholarship Council awarded to XW. WJF was supported by a Geo. X grant SO_087_GeoX.

Chapter 4

Quantifying ecosystem functioning in post-extinction reef communities: a test of ecological restructuring after the Middle Permian mass extinction

Submitted to *Palaeogeography, Palaeoclimatology, and Palaeoecology*

Abstract

The Middle Permian (Capitanian) mass extinction was devastating for metazoan reef ecosystems, but when reef ecosystems recovered, they were prevalent during the subsequent Wuchiapingian and Changhsingian. Due to the limited exposure of reefs during the Wuchiapingian, the magnitude, process and pattern of metazoan reef recovery during the Wuchiapingian remains poorly understood. Here, we carried out a quantitative investigation of the Tieqiao reef complex, which is the only known Wuchiapingian reef complex in South China. Based on the quantitative analysis of skeletal grains and whole rock components, eleven biocommunity clusters and eight rock composition clusters were recognized and were discussed within a sequence stratigraphic and depositional environmental framework. In addition, the ecological affiliation and functional significance of primary components were discussed. Sponges, *Tubiphytes* and *Archaeolithoporella* were ecologically important components of the Tieqiao reef: sponges are significant components through the six recognized reef development cycles, *Tubiphytes* are broadly distributed and played a key role in the initiation of reef communities within the reef growth cycles, meanwhile *Archaeolithoporella* is restricted to the shallow part of reef cores which indicates its light dependence, and *Archaeolithoporella* was functionally crucial for increasing reef volume. The reestablishment of post-extinction reefs was largely controlled by the changing of organism associations, habitat availability and stability of the physiochemical environment.

4.1. Introduction

Mass extinctions events are not only characterized by significant losses in taxonomic diversity but also major ecological changes including catastrophic declines in reef volume and diversity (Kiessling and Simpson, 2011). Furthermore, the late Devonian, end-Permian, and end-Triassic mass extinction events are characterized by reef eclipses and delayed recoveries of metazoan reef ecosystems (Leinfelder et al., 2002; Martindale et al., 2019; Yao et al., 2020). These demises in reef ecosystem health are associated with rapid climate warming that characterizes these events. The Middle Permian (Capitanian) extinction event has also been

likened to these mass extinction events in sharing a common trigger, i.e., volcanism associated with a large igneous province, specifically the Emeishan Traps (Zhou et al., 2002; Wignall et al., 2009a; Bond et al. 2010a, 2010b; Zhong et al., 2013; Chen and Xu, 2019; Yan et al., 2020) leading to a similar degree of ecological severity (McGhee et al., 2004), and considered a mass extinction event by many workers (e.g., Bond et al., 2010b; Wignall et al., 2012; Rampino and Shen, 2019).

Although the severity on overall biodiversity loss through this Middle Permian crisis is still under debate (McGhee et al., 2013; Fan et al., 2020), the impact on reef ecosystems is conspicuous. The Middle Permian (Capitanian) mass extinction caused a 55% decline in reef diversity and reduced the distribution of reefs to a narrow equatorial belt (Weidlich et al., 2003). The transition of reef ecosystems across the Guadalupian/Lopingian (Capitanian/Wuchiapingian) boundary is, however, poorly understood. This is because there are few locations or regions that record reef ecosystems on either side of the G/L boundary. Even though there has been a substantial amount of research investigating the reefs of the Zechstein Basin (central Europe), where spectacular Wuchiapingian reef complexes composed of bryozoans and microbialites occur, these reef complexes are not considered to have developed during the earliest Wuchiapingian (e.g., Peryt et al., 2012). The Tieqiao section, in South China, is currently the only known location that records the earliest evolution of reefs above the G/L boundary (Yang, 1987; Chen et al., 2009; Huang et al., 2019a; Wang et al., 2019), and a regional study of reefs across the South China block shows that this was the only reef locality during the Wuchiapingian (Wang et al., 2019). Furthermore, using two-dimensional semi-quantitative analyses on outcrop combined with detailed lithofacies analysis and their spatial and stratigraphic distribution, Wang et al. (2019) showed that metazoan reefs had a delayed, and stepwise recovery following the Middle Permian (Capitanian) extinction event. To further understand the reef recovery process and functional roles of the biogenic and non-biogenic reef-building elements, a quantitative components analysis is crucial for taxonomic and ecological interpretations (e.g., Weidlich et al., 1993; Fagerstrom and Weidlich, 2005). Here, we, therefore, present a quantitative investigation on the functioning and evolution of reef ecosystems following the Middle Permian (Capitanian) mass extinction at Tieqiao section.

4.2. Geological setting

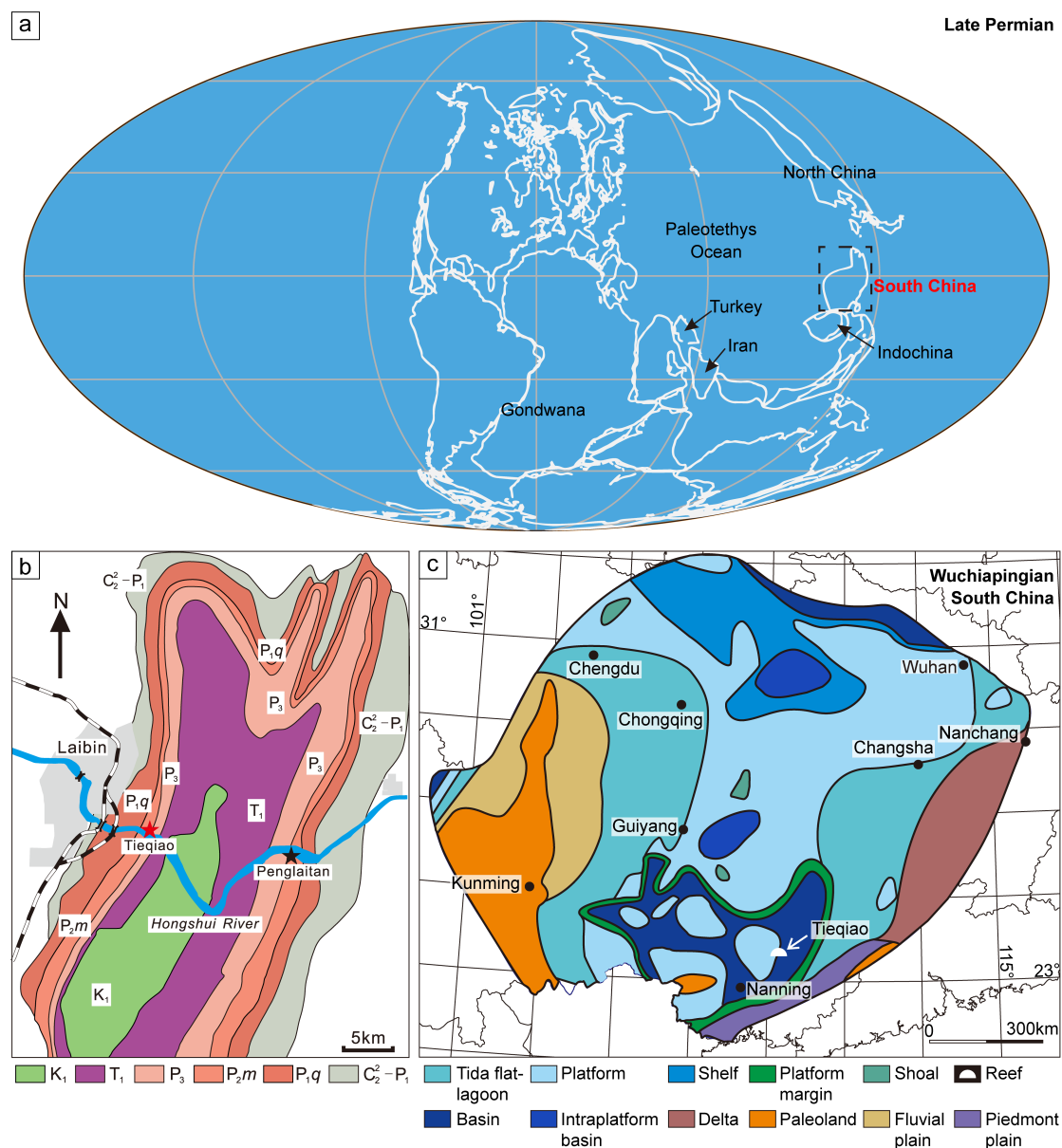


Figure 4.1: (a) Location of the South China block during the Late Permian, modified from Bagherpour et al.(2018), resources from PALEOMAP Project; www.scotese.com; (b) Location of the Tieqiao Section (red star) and the Penglaitan section (black star), spanning the Guadalupian/Lopingian (G/L) boundary GSSP, modified from Jin et al. (2006); (c) Paleogeographic map of the southern part of Yangtze Platform (South China block) during the Wuchiapingian Stage, modified from Liu et al. (2010), white semi-circle indicates the location of Tieqiao section.

During the Wuchiapingian, the Tieqiao section was deposited in the margin of Laibin-Heshan isolated platform (Figure 4.1c) (Yao et al., 2012; Qiu et al., 2014), and through sea-level changes transitioned between an isolated platform slope and basinal depositional environment. The Laibin-Heshan Platform was located within the Dian-Qian-Gui Basin, which

was located south of the Yangtze Platform (South China block) (Figure 4.1c), in the eastern Paleotethys near the equator (Figure 4.1a).

The Tieqiao section (109.251°E; 23.704°N) is a supplementary reference section of G/L boundary GSSP (Global Stratotype Section and Point). It is located at the northern bank of Hongshui river, next to the G72 highway. It is 5 km southeast from the center of Laibin City, Guangxi Zhuang Autonomous Region, China (Figure 4.1b). Researchers commonly use the bed number established by Sha et al., (1990) on the Tieqiao section, which allows a correlation between different studies. The high-resolution subdivided bedding around the G/L boundary is also available from Jin et al. (2006). The reef collapse associated with the Middle Permian (Capitanian) extinction, occurs in the upper part of the Guadalupian Maokou Formation (Laibin Limestone, within Bed 119) (Chen et al., 2009; Huang et al., 2019b). Overlying the Maokou Formation, the Heshan Formation begins at Bed 120, and beds 120-122 are alternations of thin-bedded limestones and thin-bedded cherts or cherty limestones, which represents deposition in the basin below the photic zone that was unfavorable for reef development (Wang et al., 2019). Reef development during the Wuchiapingian occurs from Bed 123 to Bed 134, in the upper part of Heshan Formation. The Wuchiapingian reef setting of Tieqiao section was divided to 6 reef growing cycles, representing transitions from the basin to outer platform setting (Wang et al., 2019). Metazoans, however, were not a dominant component of the reef facies until the 5th and 6th cycle in the Wuchiapingian *Clarkina orientalis* conodont zone (Wang et al., 2019).

4.3. Material and methods

4.3.1. Material and point-counting methods

A transect spanning the top part of Bed 122 to Bed 134 of the Heshan Formation at the Tieqiao section was studied to quantitatively investigate compositional changes in the reefs that developed following the Middle Permian (Capitanian) mass extinction (Figure S1). Hand samples were collected from each bed, or every ~1 m in beds thicker than 1 m for thin sectioning. Overall, this led to ninety thin sections for quantitative microscopic investigation. To calculate the relative abundance of the components, point counting was applied to each thin section. Thin

sections were scanned using an optical scanner and imported to photoQuad v1.4 (Trygonis and Sini, 2012). In photoQuad, a rectangle quadrat (28756575 pixels, ca. 2 cm x 3.5 cm) was randomly chosen on each sample, and 256 points were automatically chosen using the uniform spawn mode within this quadrat. Some of the thin sections were smaller than the chosen quadrat area. In this situation, the entire thin section was investigated, and the number of total points was reduced to get a similar point density for a fair comparison with the other thin sections. The scanning photo under photoQuad was combined with a Nikon transmitted light microscope to define each point. The point-counting methods we used are counting all the points falling on a particle (including the inner-particle voids filled with sediments or cements) as the particle itself. All the fossils were identified to class level, except the *Tubiphytes* and foraminifera which were identified to family level. Cements are additional important whole rock component and can be locally abundant. Radial fibrous cement is interpreted to be very early, syndepositional, and as such it is treated as a separate class in the quantitative analysis. Later generations of cements including pore filling blocky calcite, spar, dolomite, and calcite-filled veins, are post-depositional. Given that the focus of this work is on the primary, depositional features of the reef, all post-depositional cements have been grouped into one single class in the quantitative analysis (Table S1).

4.3.2. Statistical methods

The point-counting data was divided into two data sets (Table S1), which is similar with the methods used in Knoerich and Mutti (2003), in which cements were separated from the whole rock data to find out the respective variation of diagenetic components within the rock composition. The first data set is a subset of the skeletal grain data only, whereas the second data set included all the point-counting data, i.e., the whole rock components. One sample (T130-001) was excluded from the analysis because no fossils were counted in this sample. The skeletal grain data was analyzed at the class-level for all samples (Table S1). In addition, unidentified bioclasts from the skeletal grain data set were removed. The datasets were standardized into relative abundances and then square-root transformed to deemphasize the influence of the most dominant components (Clarke and Warwick, 2001).

A hierarchical cluster analysis following Foster et al., (2018) where an unweighted pair-group average cluster model (Clarke and Warwick 2001) and the Bray-Curtis similarity matrix were used, was applied to recognize those components that tend to co-occur in samples and to group together samples with a similar composition. To identify significant differences between the recognized clusters, the similarity profile test (SIMPROF) was applied (999 permutations, significance level of 0.05) (Clarke and Warwick 2001) following the cluster analysis. Then the samples of identified clusters were analyzed using a similarity percentages routine (SIMPER) to calculate the percent contribution of individual components to the similarity within each cluster. Non-metric multidimensional scaling (nMDS) was applied to visualize the level of similarity between samples, which determined the trends and groupings of the samples. The hierarchical cluster, SIMPROF, and SIMPER analysis were performed using PRIMER-e software (version 6).

Spearman's rank correlation was applied on the first data set (transformed point counting data to relative abundance) to reveal the link between different skeletal grains in the samples, and partial linear correlation was applied on the same data set to remove the "dummy" correlations in the results of Spearman's rank correlation (Rasser, 2000). The correlations between variables were determined to be significant when $p < 0.05$. In the Spearman's rank correlation, correlation coefficient (R_s value) indicates the strength of monotonic relationships between paired variables, when the R_s value equal to 0 or 1, indicates that the paired variables are not monotonically or monotonically increasing/decreasing. The positive or negative of R_s value revealed the direction of monotonic function between paired data. Low degree ($0.2 < |R_s| < 0.5$), medium degree ($0.5 < |R_s| < 0.7$), high degree ($0.7 < |R_s| < 0.9$) was used in this study to describe the strength of spearman's rank correlations (Rasser, 2000). The Spearman's rank correlation and partial linear correlation were calculated using PAST (Hammer et al., 2001).

4.4. Results

4.4.1. *Quantitative analysis of skeletal grains*

The cluster analysis divides the samples into 11 quantitative clusters (biocommunity

clusters (BCs)) (Figure 4.2). The SIMPER test shows the dominant skeletal grains for each cluster (Figure 4.3). There are 3 main groups (Figures 4.2 and 4.4a) in the clustering with different dominant skeletal grains: Sponges primarily dominate the first group, which includes

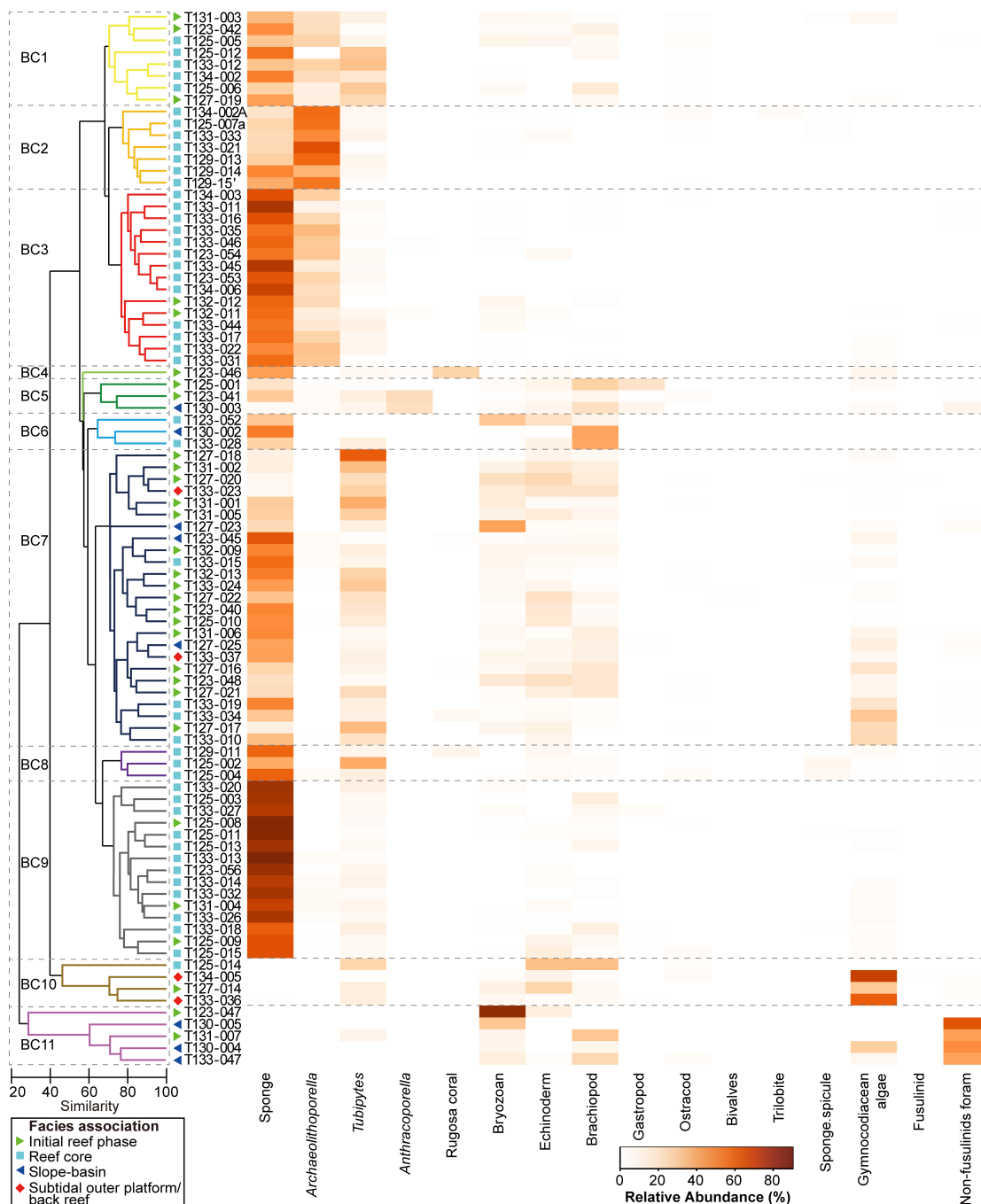


Figure 4.2: Cluster analysis with the similarity profile test (SIMPROF) on the skeletal grain data set from the Tieqiao section. The SIMPROF test identified 11 significantly distinct biocommunity clusters (BCs, colored and numbered 1 to 11). The relative abundances of each fossil group within each sample are shown using a heat map (see scale). Facies associations following Wang et al. (2019).

BC 1-9, but these clusters can also be subdivided into 4 characteristic groups. BC 1-3 (Figures 4.5a, 5d, and 5e) are dominated by sponges, *Archaeolithoporella*, and *Tubiphytes*. BC 4-6 (Figures 4.5b, 5c, 5i, and 5l) are characterized by a high evenness and high species richness (Figure 4.6a) with sponges as the common dominant component between samples. BC 7-8 (Figures 4.5f and 5h) record high a taxonomic richness (Figure 4.6a) and are dominated by sponges and *Tubiphytes*: BC 7 has a higher evenness and higher average proportion of Gymnociodiacean algae than BC 8. BC 9 (Figure 4.5g) is samples with a low evenness and dominated by sponges. The second group contains BC 10. BC 10 (Figures 4.5m and 5j) is dominated by Gymnociodiacean algae and has a high evenness, but unlike the first group, sponges are either absent or at very low abundances. The third group includes BC 11 (Figure 4.5k), which has a low species richness (Figure 4.6a) and is dominated by non-fusulinids foraminifera, bryozoans, and brachiopods.

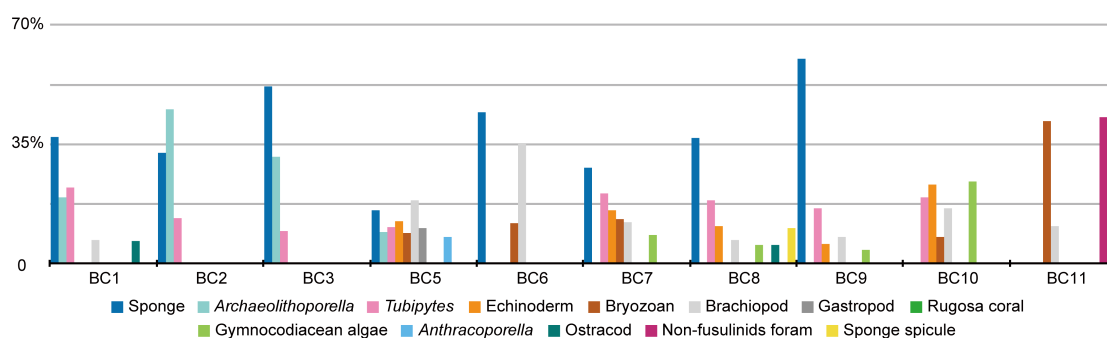


Figure 4.3: Similarity percentages (SIMPER) analysis for the different biocommunity clusters (BCs) identified from the cluster analysis. Only the taxa with contributions up to 80% for each BC are shown.

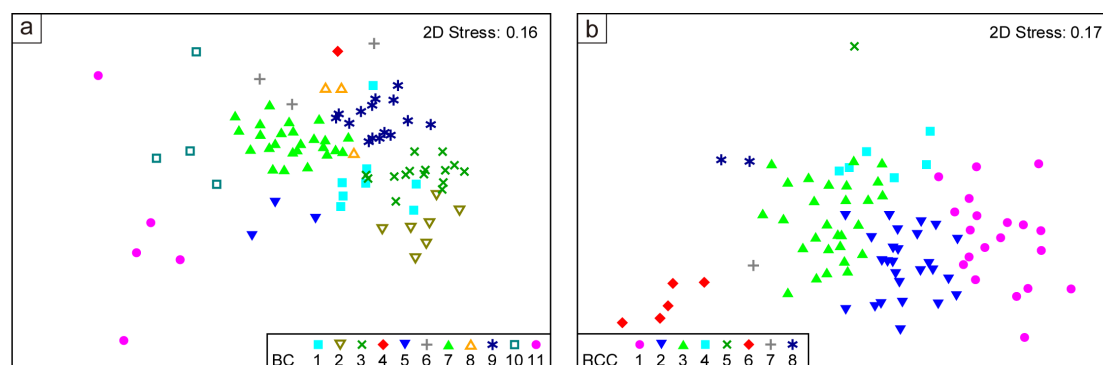


Figure 4.4: Non-metric multi-dimensional scaling (nMDS) ordination of samples, grouped according to (a) biocommunity cluster (BC), and (b) rock composition cluster (RCC).

The different BCs show a spatial trend (Table 4.1). The first group, where sponges are a dominant biological component, characterize the reef cores (except BC 4 and 5). This suggests,

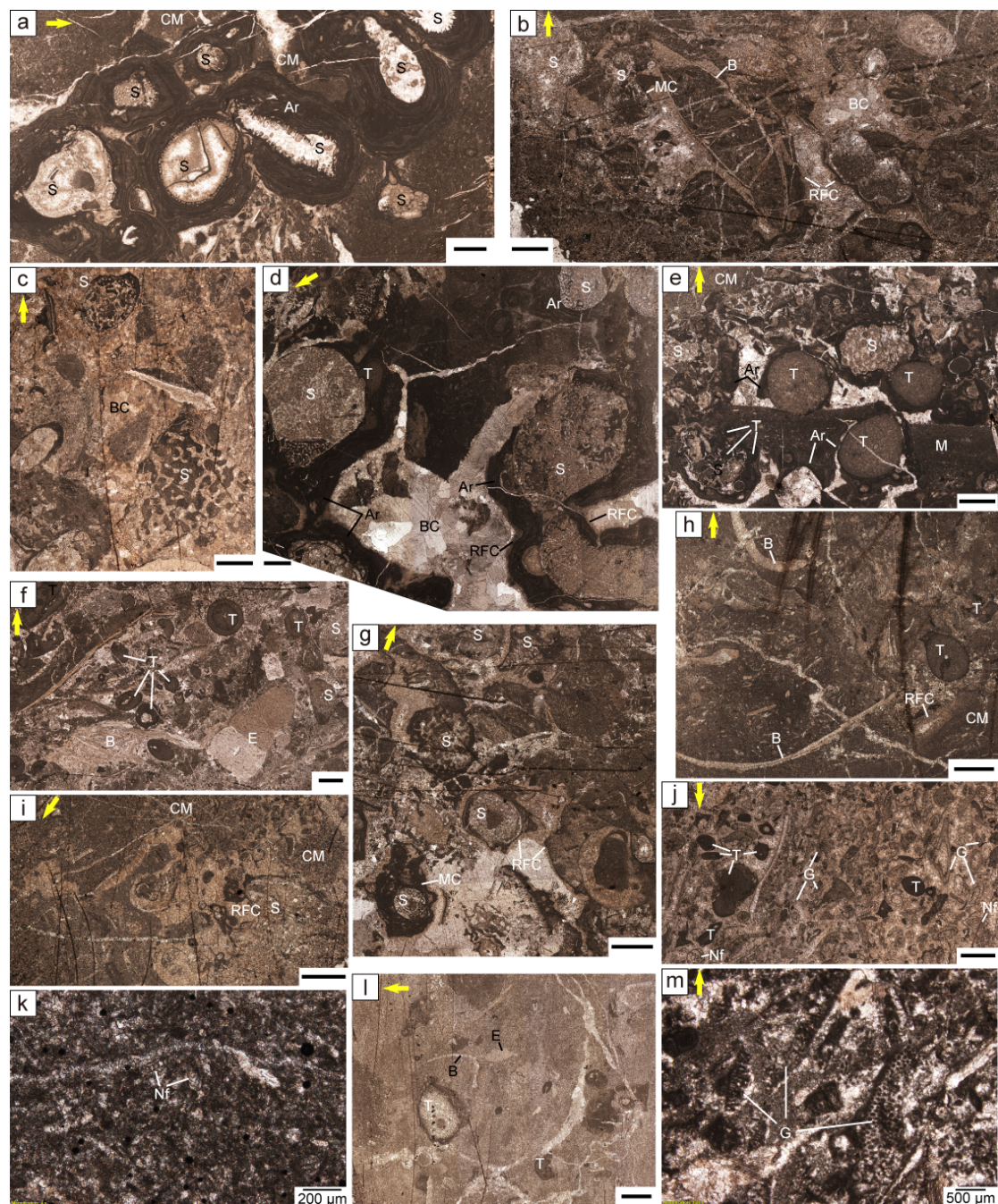


Figure 4.5: Thin-section photomicrographs with examples of different biocommunity clusters (BCs) and rock composition clusters (RCCs). (a) RCC 1, BC 2; (b) RCC 4, BC 5; (c) RCC 4, BC 4; (d) RCC 1, BC 3; (e) RCC 2, BC 1; (f) RCC 3, BC 7; (g) RCC 4, BC 9; (h) RCC 3, BC 8; (i) RCC 4, BC 6; (j) RCC 5, BC 10; (k) RCC 6, BC 11; (l) RCC 7, BC 5; (m) RCC 8, BC 10. Ar: *Archaeolithoporella*; B: Brachiopod; BC: Blocky calcite; CM: Clotted micrite; D: Dolomite; E: Echinoderm; G: (Gymnocodiacean algae); MC: Microbial crust; Nf: Non-fusulinids foram; RFC: Radial fibrous cement; S: Sponge; T: *Tubiphytes*. Scale bar is 2mm except k and m. Yellow arrows indicate stratigraphic top.

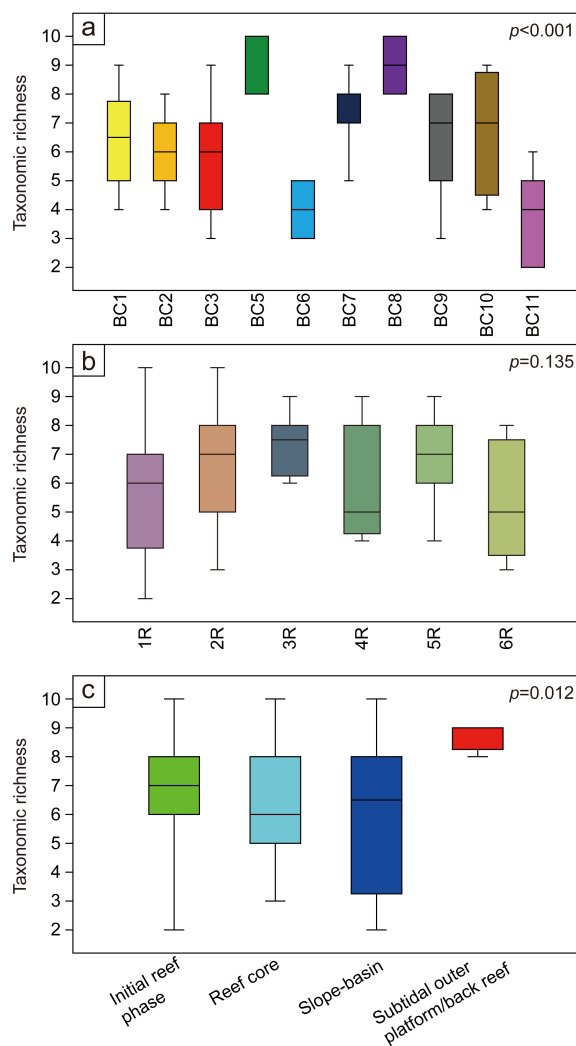


Figure 4.6: Differences in alpha diversity between (a) biocommunity clusters (BC), (b) regressive system tracts, and (c) depositional environments for the Heshan Formation in the Tieqiao section. BC – biocommunity cluster, R – regressive phase of transgressive-regressive cycles. Differences in taxonomic richness are shown as box plots: the horizontal black lines inside the boxes represent the medians, the top and bottom edges of the boxes correspond to the first and third quartiles, and whiskers represent the lowest and highest datum. Facies associations and cycles following Wang et al. (2019).

therefore, that metazoans (specifically sponges) were a key component of reefs recovering from the Middle Permian (Capitanian) extinction. Whereas, the role of *Archaeolithoporella* and *Tubiphytes* in reef-building was more variable between samples. Back-reef samples only occur in BC 7 and 10, those samples are typically characterized by lower abundances of sponges and a higher contribution of Gymnodiacean algae (Figures 4.2 and 4.3). All the BCs, except BC 2 and 6, occur in the transition between the reef core and the slope-basin. The slope-basin setting, on the other hand, is dominated by foraminifera, bryozoans and brachiopods with sponges as a minor component. Despite showing a spatial trend, the BCs do not appear to show

Table 4.1: Distribution of biocommunity clusters (BCs) and rock composition clusters (RCCs) within different facies associations and reef cycles. Facies associations and cycles following Wang et al. (2019).

	Slope-basin	Initial reef phase	Reef core	Subtidal outer platform/back reef	Reef cycle					
					1 st	2 nd	3 rd	4 th	5 th	6 th
BC1		3	5		1	3	1		2	1
BC2			7			1		3	2	1
BC3		2	13		2				11	2
BC4		1			1					
BC5	1	2			1	1			1	
BC6	1		2		1				2	
BC7	3	16	4	2	3	1	6	2	13	
BC8			3			2		1		
BC9		3	12		1	6			8	
BC10		1	1	2		1	1		1	1
BC11	3	2			1				3	1
RCC1			20		2	1		3	10	4
RCC2	1	11	14		2	5			19	
RCC3	2	15	9	2	4	7	8	2	7	
RCC4		2	4		2	2			2	
RCC5				1					1	
RCC6	3	2			1			1	3	
RCC7	1								1	
RCC8	1			1						2

a temporal trend. There are six reef growth cycles in Tieqiao Section (Wang et al., 2019). The sponge-*Archaeolithoporella* clusters (BC 1-3) occur in the reef core of each reef cycle. The sponge-*Tubiphytes* clusters (BC 7-8) occur in the reef cores of cycles 2, 4, and 5. The sponge-dominated BCs occur in the reef cores of cycles 1, 2, and 5. The distribution of the BCs within the reef cores, therefore, do not show a temporal aspect. Changes in the taxonomic richness of samples, however, do not show a significant temporal trend (Figure 4.6b).

Spatial, rather than temporal, factors, therefore, better explains the distribution of the different BCs (Figure 4.7). The BC 11 is distributed in the slope-basin environment below each reef growth. The BC 4-7 are mainly distributed in the lower part of the regressive phase, which including packstone/rudstone from the initial reef phase and packstone from the slope-basin environment. The BC 8 is mainly distributed in the lower part of the reef core, within the 2nd and 4th cycle. The BC 9 is mainly distributed in the upper part of the reef core, within the 1st, 2nd, and lower part of the 5th cycle. The BC 1 is distributed in the upper part of the initial reef phase or the lower part of the reef core. The BC 2 and 3 are mainly distributed in the upper part of the reef core, and most of the BC 3 appeared in the 5th and 6th reef growing cycles. Samples of BC 10 are mainly within the upper part of the reef core and the subtidal outer platform/back reef environment that covering the reef core facies.



Figure 4.7: Stratigraphic log with facies associations, transgressive-regressive cycles, biocommunity clusters (BCs), and relative abundance of skeletal grains. Facies associations and cycles following Wang et al. (2019).

4.4.2. Quantitative analysis of whole rock components

The cluster analysis divides the data into 8 clusters (rock composition clusters (RCCs)) (Figure 4.8). The SIMPER test shows the dominant components of each cluster (Figure 4.9).

There are 3 main groups (Figures 4.4b and 4.8) can be recognized from the clusters: The first group including RCC 1 to 4 but can be divided into 3 characteristic groups. Micrite is the primary contributor in this group except in RCC 1, as well as sponges, *Archaeolithoporella*, *Tubiphytes* and (early/late) cements are significantly contributed to this group. However, the

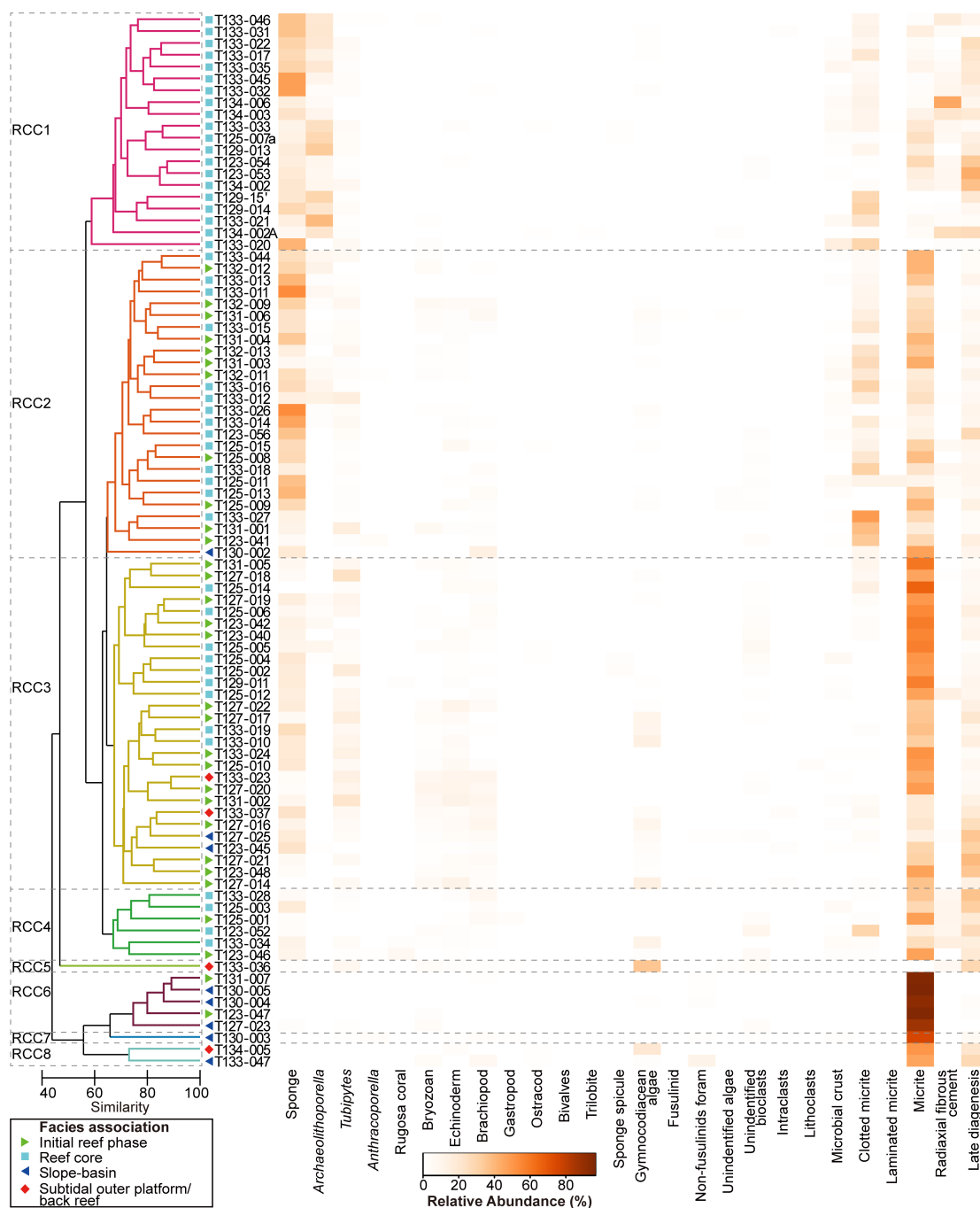


Figure 4.8: Cluster analysis with the similarity profile test (SIMPROF) of the whole rock components data set in the samples from the Tieqiao section. The SIMPROF test identified 8 significantly distinct rock composition clusters (RCCs, colored and numbered 1 to 8). The relative abundances of each component within each sample are shown using a heat map (see scale). Facies associations following Wang et al. (2019).

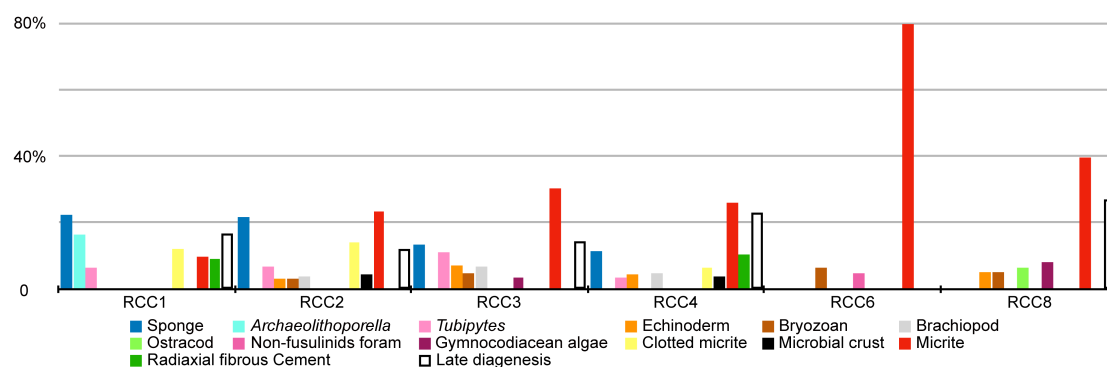


Figure 4.9: Similarity percentages (SIMPER) analysis for the different rock composition clusters (RCCs) identified from the cluster analysis. Only the components with contributions up to 80% for each RCC are shown.

contribution of micrite is significantly less compared to the group of RCC 6, 7 and 8 which will be described in the ensuing paragraphs. RCC 1 (Figures 4.5a and 5d) is primarily dominated by sponge, late diagenesis fabrics and *Archaeolithoporella*, but clotted micrite, micrite, radioaxial fibrous cement and *Tubiphytes* also contribute to this cluster, meanwhile, micrite has the lowest contribution to this cluster comparing to others. The RCC 1 is identified as sponge-*Archaeolithoporella* boundstone cluster. The RCC 2 and 3 are primarily dominated by micrite, but also with contributions from skeletal grains and additional components. RCC 2 (Figure 4.5e) is largely dominated by micrite, sponge, clotted micrite, and late diagenesis fabrics, and with contributions from *Tubiphytes*, microbial crust, brachiopod, echinoderm and bryozoan. RCC 2 is identified as sponge-*Tubiphytes* boundstone cluster. RCC 3 (Figure 4.5f) is primarily dominated by micrite but compared to RCC 2, RCC 3 has a higher evenness of skeletal grains, including sponges, *Tubiphytes*, echinoderms, bryozoans, brachiopods and Gymnocodiacean algae. Late diagenesis fabrics also make up significant components of RCC 3. RCC 3 is identified as sponge-*Tubiphytes*-bioclastic packstone-rudstone cluster. RCC 4 (Figures 4.5b, 5c, 5g, and 5i) is primarily dominated by micrite, but sponge, late diagenesis fabrics and radioaxial fibrous cement are also significant contributors between the samples. *Tubiphytes*, echinoderms, brachiopods, clotted micrite and microbial fabrics also contribute to RCC 4. RCC 4 is identified as sponge-bioclastic rudstone-boundstone cluster. Significant contributors of the first group such as sponges, *Archaeolithoporella* and *Tubiphytes* are absent as contributors in the second and third groups. The second group only contains RCC 5 which including a single sample that has low similarity with all other samples. This group is dominated by Gymnocodiacean algae

and late diagenesis fabric. RCC 5 (Figure 4.5j) is identified as Gymnodiacean algae grainstone cluster. The third group is composed of RCC 6, 7 and 8 is distinguished from other groups because of the absolute predominance of micrite in these samples. RCC 6 (Figure 4.5k) is primarily dominated by micrite. Echinoderm and non-fusulinids foram also contribute to this cluster. RCC 6 is identified as mudstone-wackestone cluster. RCC 7 (Figure 4.5l) contains a single sample that mainly composed by abundant micrite (75.83%) and bioclasts. RCC 7 is identified as wackestone cluster. RCC 8 (Figure 4.5m) is primarily dominated by micrite, and significantly contributed of late diagenesis fabrics. Gymnodiacean algae, ostracods, bryozoan and echinoderms also contribute to this cluster. RCC 8 is identified as bioclastic packstone cluster.

The distribution of the RCCs also has a spatial pattern (Figure 4.10, Table 4.1). The primary dominance of micrite in most of the RCCs (Figure 4.9) except RCC 1 and 5, indicates that the hydrodynamic level at Tieqiao section was generally not very high. RCC 1 is concentrated in the reef-core facies, while the low level of micrite and abundant radioaxial fibrous cement reflecting a high level of hydrodynamic energy. RCC 2 is distributed in a range from slope-basin to reef core facies, mainly in the reef core facies. The nMDS result shows that the RCC 2 is a transition between RCC 1 and 3 (Figure 4.4b), meanwhile RCC 2 contains less micrite comparing with RCC 3, but more micrite comparing with RCC 1, which indicate a medium level of hydrodynamic energy. RCC 3 is distributed in a broad range from slope-basin to subtidal outer platform/back reef facies, but mainly in the initial reef phase facies. The primary dominance of micrite and structure of packstone-rudstone in RCC 3 reflects the low to medium level of hydrodynamic energy. RCC 4 is distributed in a range from initial reef phase to reef core facies, mainly in the reef core facies. The primary dominance of micrite and the coexisting of radioaxial fibrous cement in RCC 4, reflects the medium level of hydrodynamic energy. RCC 5 is distributed in the subtidal outer platform/back reef facies, while the grainstone structure reflecting a high level of hydrodynamic energy. RCC 6 and 7 are mainly distributed in the slope-basin facies except 2 samples from the nearby deepest part of initial reef phase. RCC 8 contains two samples, from slope-basin and subtidal outer platform/back reef facies. The high abundance of micrite in RCC 6, 7 and 8 reflects a low level of hydrodynamic energy.

The stratigraphic distribution of RCCs (Figure 4.10, Table 4.1) is related with the spatial change of sedimentary environment but also characterized in different reef cycles. RCC 1 only occurs in reef core facies and mainly concentrates in cycle 4 to 6, but also occurs in the upper part of cycle 1 and 2. RCC 2 mainly occurs in the initial reef phase and reef core of cycle 1, 2,



Figure 4.10: Stratigraphic log with facies associations, transgressive-regressive cycles, rock composition clusters (RCCs), and relative abundance of whole rock components. Facies associations and cycles following Wang et al. (2019).

and 5. RCC 3 mainly occurs in the initial reef phase and reef core of cycle 1 to 5. RCC 4 occurs in the reef core facies of cycle 1, 2, and 5, with 2 samples separate in the initial reef phase of cycle 1 and 2. RCC 5 occurs in cycle 5 within the subtidal outer platform/back reef facies. RCC 6 occurs in transition from slope-basin to initial reef phase of cycle 1, 4, and 5. RCC 7 occurs in the slope-basin of cycle 5. RCC 8 occurs in the slope-basin and subtidal outer platform/back reef facies of cycle 6. For RCCs that related with reef core environment, RCC 4 is abundant in the early stage of reef development like cycle 1 and 2, RCC 3 occurs in cycle 2, 4 and 5 but mainly in cycle 2, RCC 2 occurs in the cycle 1, 2 and 5 but mainly in late stage of reef development like cycle 5, and RCC 1 occurs in cycle 1, 2, 4, 5 and 6 but mainly in in late stage of reef development like cycle 4 to 6.

4.4.3. Rank correlation of skeletal grains

The result of Spearman's rank correlation of skeletal grain data, between 15 variables, shows 29 pairs of statistically significant ($p < 0.05$) correlation sorted by correlation coefficient (R_s) (Table S2). Partial correlation was applied on these 29 pairs to exclude false correlations. There are 16 of the 29 correlations remained significance in the partial correlation test (Table 4.2, Figure 4.11).

Table 4.2: Positive (a) and Negative (b) correlations which are significant in both Spearman's rank correlation and Partial correlation, and their R_s value.

(a) Positive Correlations		R_s
a.1	Echinoderm – <i>Tubiphytes</i>	0.361
a.2	Echinoderm – Bryozoan	0.450
a.3	Brachiopod – Echinoderm	0.450
a.4	Fusulinid– Gymnociacean algae	0.238
a.5	Non-fusulinids foram – Bryozoan	0.334
(b) Negative Correlations		R_s
b.1	<i>Tubiphytes</i> – Sponge	-0.262
b.2	<i>Tubiphytes</i> – <i>Archaeolithoporella</i>	-0.260
b.3	Bryozoan – Sponge	-0.584
b.4	Bryozoan – <i>Archaeolithoporella</i>	-0.411
b.5	Echinoderm – Sponge	-0.410
b.6	Echinoderm – <i>Archaeolithoporella</i>	-0.492
b.7	Brachiopod – Sponge	-0.332
b.8	Brachiopod – <i>Archaeolithoporella</i>	-0.617
b.9	Ostracod – Sponge	-0.263
b.10	Gymnociacean algae – <i>Archaeolithoporella</i>	-0.403
b.11	Non-fusulinids foram – Sponge	-0.368

The results (Table 4.2) reveal that all positive correlations and 9 negative correlations fell into range of low degree correlation (R_s value between +/-0.2 and +/-0.5), and 2 negative correlations fell into range of medium degree correlation (R_s value between +/-0.5 and +/-0.7).

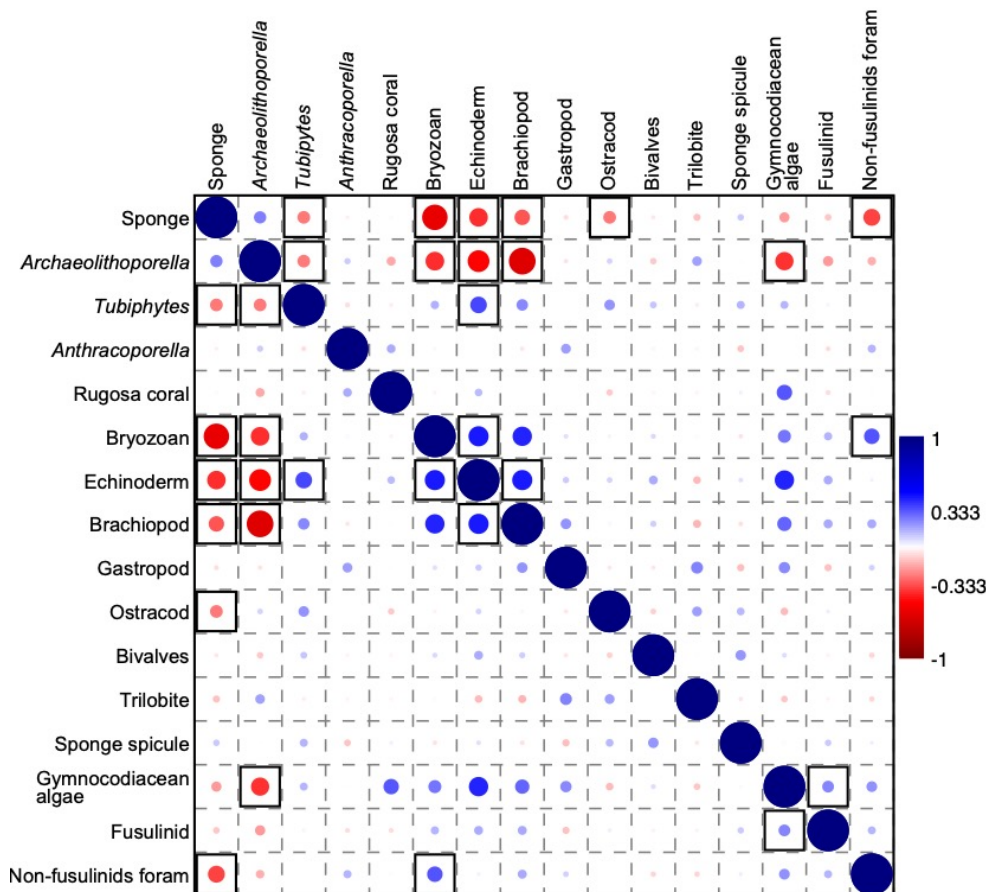


Figure 4.11: Plot of R_s value from Spearman's rank correlation. Correlations significant in both Spearman's rank correlation and the partial correlation are marked by black boxes.

Correlations a.1 to a.3 show that echinoderms have significant positive correlation with *Tubiphytes*, bryozoans, and brachiopods. Meanwhile, correlation b.1 to b.8 show that *Tubiphytes*, bryozoans, echinoderms and brachiopods individually has significant negative correlation with both sponge and *Archaeolithoporella*. Above mentioned positive/negative correlations can be interpreted by the abundance and cooccurrence of *Tubiphytes*, bryozoan, echinoderm and brachiopod in the non-reef core samples, and the abundance and cooccurrence of sponge and *Archaeolithoporella* in the reef core samples. But among the above-mentioned correlations, the pairs of correlations that involving *Tubiphytes* has relatively lower degree of R_s value, which can be explained by the extensive occurrence of *Tubiphytes* that can weaken the strength of pairwise monotonic relationship between *Tubiphytes* and other organisms. The

positive correlation a.5 between non-fusulinids foram and bryozoan can be interpreted by their cooccurrence in the samples of slope-basin facies, and the negative correlation between non-fusulinids foram and sponge is because the abundant non-fusulinids forams are observed in the slope-basin samples, and sponges are observed in samples from initial-reef phase and reef core. The negative correlation b.10 between Gymnocodiacean algae and *Archaeolithoporella* can be interpreted by the abundance of Gymnocodiacean algae in the samples from back reef, and the abundance of *Archaeolithoporella* in the reef core. The positive correlation a.4 between fusulinids and Gymnocodiacean algae could be the result of similar ecology, and the negative correlation b.9 between ostracod and sponge could be the result of dissimilarity of ecology, but the R_s value is low in a.4 and b.9.

4.5. Discussion

4.5.1. Reef-building elements in the Tieqiao reefs

The six reef episodes occurring within each cycle of Wuchiapingian Tieqiao section were composed by biogenic associations dominated by different organisms. The lateral and vertical development of each reef are highly correlated with the dominant fossil associations (Wang et al., 2019; this study). Analysis of skeletal grains suggests that sponges, *Archaeolithoporella*, and *Tubiphytes* were ecologically important reef builders (Figure 4.12). In addition, the analysis of whole rock components, indicates that additional components such as clotted micrite and syndepositional cements (Figure 4.12, Figure 4.13) are also significant in the reef development.

4.5.1.1. *Microproblematica* and sponges

The role of algae and problematic algae in the construction of Permian reefs were noticed since early investigations of the Capitan reef complex in west Texas and southeastern New Mexico (e.g., Babcock, 1974, 1977). In addition, crustose coralline algae, which appear to be functionally similar to *Archaeolithoporella*, have a key role in reef formation during the Cenozoic and today (Weiss and Martindale, 2017). Within the Capitan reef complex, due to the

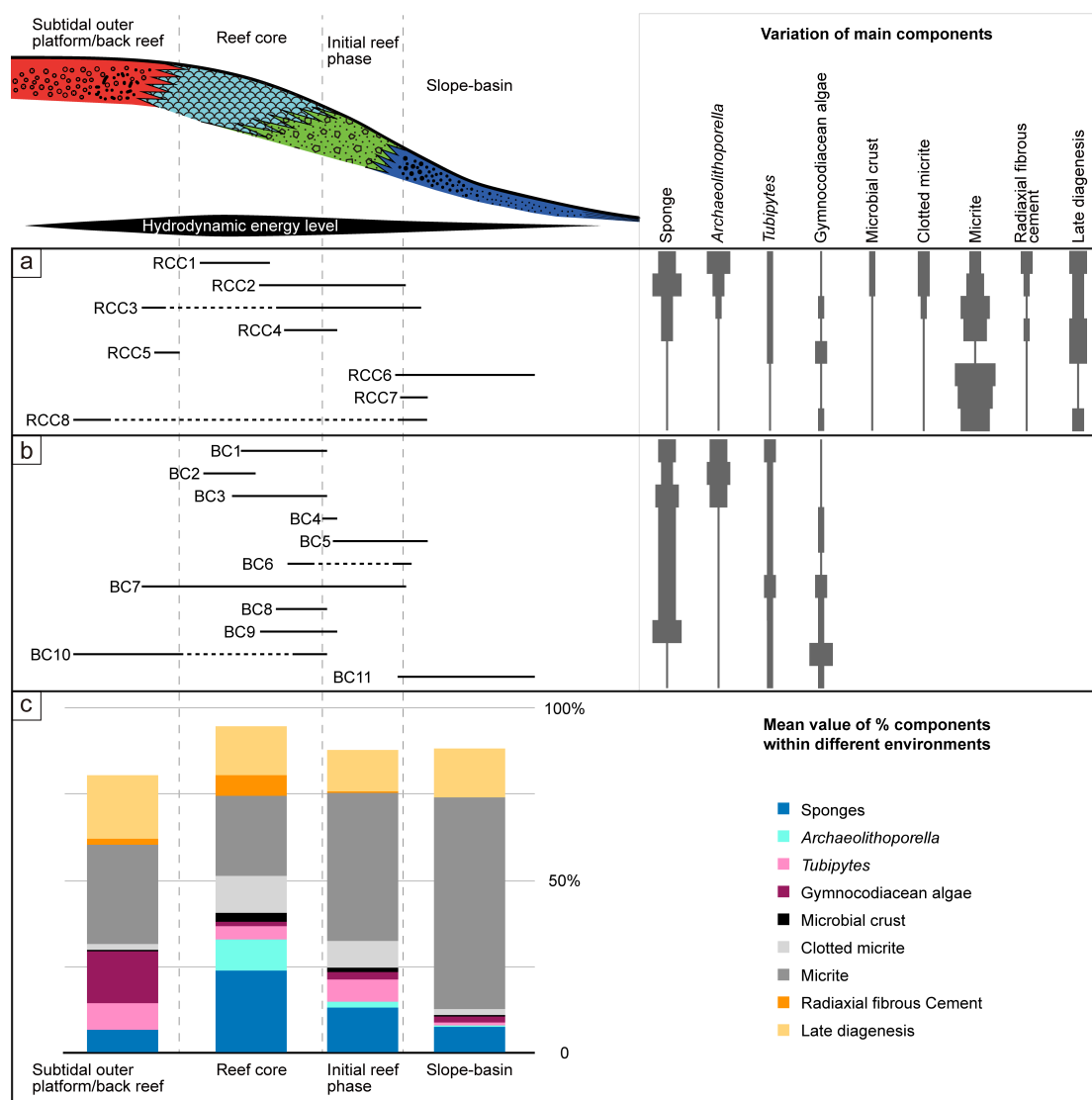


Figure 4.12: Summary of the spatial distribution and variation in the main components of (a) rock composition clusters (RCCs) and (b) biocommunity clusters (BCs, b); and (c) mean value of components within different environments (facies associations). Facies associations following Wang et al. (2019).

relatively less skeletonization of primary components such as sphinctozoans and inozoans, the building process was interpreted as largely controlled by the dense packing of bafflers (e.g., sponges), binders (e.g., *Archaeolithoporella* and *Tubiphytes*) and early cementation (Fagerstrom, 1987). The important constructional role of the “micro-framework”, which described the consortium of syndepositional marine-phreatic cements and “low-growing organisms” such as small sponges, *Archaeolithoporella*, *Tubiphytes*, and bryozoans, was highlighted in the building process of upper Capitan massive (e.g., Weidlich and Fagerstrom, 1999). The formation of rigid structure of the Capitan reef was suggested to be supported by *Archaeolithoporella*, *Tubiphytes* and microbial micrites through post-mortem encrustation on

the primary components (Wood et al., 1994, 1996; Kirkland et al., 1998). The importance of the encrusting organisms such as *Archaeolithoporella* and *Tubiphytes*, and microbial carbonates were also described in the Middle and Late Permian sponge reefs of from South China (Fan et al., 1990; Guo and Riding, 1992; Zhang and Zhang, 1992; Wang et al., 1994; Shen and Xu, 2005) and other locations (Toomey, 1991; Nakazawa et al., 2012, 2015; Wahlman et al., 2013).

Understanding the ecology of reef-building organisms is essential for revealing their function in the reef-building process. The affinity of *Tubiphytes* and *Archaeolithoporella* are still controversial. *Tubiphytes* was interpreted as a cyanobacterium (Maslov, 1956), porifera (Riding and Guo, 1992), or a foraminifera (or other organisms) enveloped in microbial structures (Senowbari-Daryan and Flügel, 1993; Senowbari-Daryan, 2013). *Archaeolithoporella*, which is characterized by homogeneous laminations composed by parallel-subparallel micritic and sparite layers, has been interpreted as red algae (e.g., Babcock 1977; Wu, 1991; Wang et al., 1994; Kirkland et al., 1998) or microbial crust (e.g., Grotzinger and Knoll, 1995; Shen and Xu, 2005). In the biocommunity analysis of the Tieqiao reefs, *Tubiphytes* is a significant component within 8 of the 11 biocommunity clusters (BCs), while *Archaeolithoporella* is only significant within 4 of the 11 biocommunity clusters (BCs) (Figure 4.3). In the rock composition analysis (Figures 4.8 and 4.9), *Archaeolithoporella* only significantly contributes to rock composition cluster 1 (RCC 1), which only contains samples from reef core facies, whereas *Tubiphytes* significantly contributes to RCC 1 to 4, which contain samples from the transition between slope-basin to subtidal outer platform/back reef. Obviously, *Tubiphytes* has a broader occurrence and distribution in different environments compared to *Archaeolithoporella* (Figure 4.12). The strong environmental tolerance of *Tubiphytes* is also discussed in other geological records, such as the Anisian high relief Great Bank of Guizhou, where *Tubiphytes* build-ups occur in the initial stage of platform margin reef recovery after the end-Permian mass extinction, and *Tubiphytes* performed there as the only framework builder and shows a wide distribution in different environments (Payne et al., 2006a; Kelley et al., 2020). In the Tieqiao section, *Tubiphytes* significantly contributes to BC 7 which characterizes the initial reef phase (Figures 4.2 and 4.12a). So, in Tieqiao, *Tubiphytes* may be an important component for the initial establishment of the reef community. For the *Tubiphytes*,

the wide facies distribution and important role within the initial reef community may be seen to reflect a high level of environmental tolerance in their ecology. Unlike *Tubiphytes*, *Archaeolithoporella* mainly occurs in the upper part of the reef core in the Tieqiao reefs, which indicates a relatively narrow adaptability to environmental variables such as the water depth and light penetration. Furthermore, *Archaeolithoporella* may have a strong competitive edge in environments with high hydrodynamic energy such as shallower reef core or reef crest, as suggested by its dominance in the rock composition cluster (RCC) with less micrite such as RCC 1 (Figures 4.8 and 4.12b). Furthermore, data show significant negative correlations between the occurrence of *Archaeolithoporella* and organisms such as brachiopods, echinoderms and bryozoans (Figure 4.11, Table 4.2), that are rare or absent in samples of RCC 1. The preferences of shallow water and high hydrodynamic energy could also suggest a possible light dependence and algae affinity of *Archaeolithoporella*, because the highest light intensity is only available in such environments.

The functional roles of sponges in the Middle and Upper Permian reefs in different reef environments are varied, depending on their size or growth position, from constructor to baffler (e.g., Babcock, 1977; Weidlich, 2002b). Within the Capitan reef, some of the calcareous sponges are even suggested to be part of the cryptic community that inhabit in the primary reef cavities, rather than direct constructor of the reef framework or baffler (Wood, et al., 1994, 1996). At the Tieqiao section, the dominant sponges in the Wuchiapingian are inozoan and small sphinctozoan sponges, with abundant toppled fragments of inozoan sponges (Yang, 1987). The biocommunity analysis (Figure 4.2) indicates that sponges are significant in 46 of 47 samples from reef core facies, with the relative abundance of sponges being up to 90.4%. There are 24 of 47 reef core samples belong to the BC 1 and 7-9, where *Tubiphytes* is the second most significant component besides the sponges, the relative abundance of *Tubiphytes* is up to 40.7%. There are 20 of 47 reef core samples belong to the BC 2-3, where *Archaeolithoporella* is the most significant or second most significant component besides the sponges, the relative abundance of *Archaeolithoporella* is up to 67.6%. Stratigraphically, the relative abundance of sponges is not significantly changed, except that within each reef cycle the sponges have an increasing trend from the lower part to the upper part (Figure 4.7). Previous observations on the outcrop, had indicated a temporal change in the abundance of sponges following the

recovery process of reefs (Wang et al., 2019), but the quantitative biocommunity clusters (BCs) or rock composition clusters (RCCs) do not reveal the same trend. On the other hand, the frequency and proportion of *Archaeolithoporella* dominated BCs and RCCs rise up following the volumetric enlargement of the reef cores (Figure 4.7 and Figure 4.10). The high amount of sponges and the issues around its temporal trend could be a result from the bias of limited area of thin sections. However, the function of *Archaeolithoporella*, is still proven significant in the reef enlargement process.

4.5.1.2. Additional components

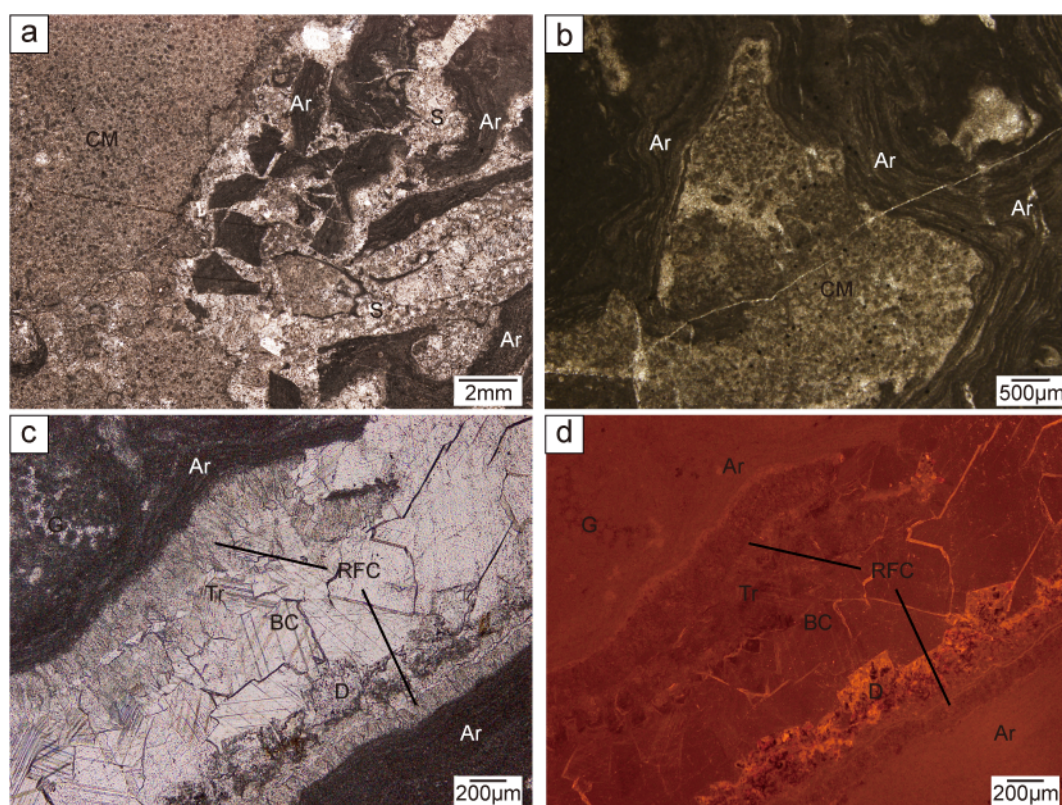


Figure 4.13: Thin-section photomicrographs of clotted micrite (a, b) and cements (c, d). d is Cathodoluminescence image of c. Ar: *Archaeolithoporella*; BC: Blocky calcite; CM: Clotted micrite; D: Dolomite; G: (Gymnocodiacean algae); RFC: Radial fibrous cement; S: Sponge; Tr: Transition zone between RFC and BC.

Micrite is generally abundant in the Tieqiao section. The origin of micrite is multi-genesis (e. g. Kazmierczak et al., 1996; Munnecke et al., 1996; Guido et al., 2016), and in some cases, it is difficult to separate detrital from microbial micrite. In the building process of Tieqiao reefs, the uncertainty of contribution from micrites, especially micrites of microbial origin, still exists.

However, the result of rock composition analyses shows that the boundstone RCCs such as RCC 1 and 2 distribute sparsely in the 1st to 2nd reef cycle but dominate in the 5th and 6th reef cycle (Figure 4.10), in other words, their appearing frequencies and proportions in the 5th and 6th cycle is higher than the cycles below. If the *in situ* boundstone structure reflects the existence of solid reef core, then the upwards increased proportion of boundstone RCCs at Tieqiao section can indicate the enlargement of solid reef cores that further reflects the stabilization of reef growth, which is also correlated with the field observation (Wang et al., 2019). Furthermore, the amount of micrites decrease with the increase of the boundstone RCCs in the 5th and 6th reef cycle, along with the increase of clotted micrites and cements (Figure 4.10). Therefore, the high amount of clotted micrites (Fig.13a-b) and syndepositional cements (Figure 4.13c-d) were significant for the reef-building process, besides the *in situ* biological framework build by the primary components and encrusters (Figure 4.13c).

4.5.2. Comparison of shallow-water build-ups across the G/L transition at the Laibin-Heshan isolated platform

The latest Guadalupian reefal build-ups from Laibin-Heshan isolated platform were described in the Tieqiao section (Chen et al., 2009) and Penglaitan section (Huang et al., 2019b). A part of the so called “Laibin limestone” were described as reefal build-ups (skeletal mound in Tieqiao section, and skeletal reef in Penglaitan section) in these studies. The term “Laibin limestone” described a unit of massive limestone that crossed the G/L boundary, observed in the area of Laibin-Heshan, which was explained to be deposited in an upper slope environment (Wignall et al., 2009b; Qiu et al., 2010; Qiu and Wang, 2014) or deep slope environment (Sha et al., 1990). Both of the Tieqiao and Penglaitan pre-crisis build-ups are overlain by crinoidal grainstones which indicate a shallow water environment that would prior to the crisis had been suitable for reefal build-ups (Chen et al., 2009; Huang et al., 2019b), i.e., it signals the start of a reef collapse. If we consider the reefal build-ups within “Laibin limestone” as the youngest shallow water reefal build-ups before the Middle Permian mass extinction, to compare them with Wuchiapingian reef will be important to understand the evolution of reef ecosystems across the Guadalupian/Lopingian boundary.

In the Penglaitan section, facies dominated by in-situ bryozoan colonies, which act as bafflers/binders, are a major part of pre-crisis reefs; in addition, facies with Alatoconchid shells (a group of large, specialized bivalves restricted to the Permian; Yancey and Boyd, 1983) are also significant in the end-Guadalupian reefs (Huang et al., 2019b). Following the Guadalupian/Lopingian boundary in Penglaitan, only 2-3 m of limestone that contains silicified reef-building sponges were reported from late Wuchiapingian strata, which was considered as contemporaneous deposition of Wuchiapingian Tieqiao reef (Shen et al., 2007). In the Tieqiao section, facies dominated by sponge, *Tubiphytes* and coral are the major composition of the end-Guadalupian skeletal mound, while sponges are the principal frame constructors that encrusted by *Archaeolithoporella* and *Tubiphytes* in the sponge boundstone facies; the mound building sponges including *Peronidella*, *Parauvanella*, and *Sollasia*, and the inozoan sponge *Peronidella* was the most abundant of them (Chen et al., 2009). Chen et al. (2009) also indicated that the major reef builders of this skeletal mound are absent from the early Wuchiapingian, they are Lazarus taxa-organisms that rebound after the crisis through late Wuchiapingian and Changhsingian in South China. During the Wuchiapingian, sponges, *Archaeolithoporella*, *Tubiphytes* were the major composition of the reef core facies in Tieqiao section (Wang et al., 2019, this study). In the Tieqiao section, the sponges include inozoan sponges such as *Peronidella* and *Corynella*, sphinctozoan sponges such as *Amblysiphonella*, *Cystothalamia*, *Cryptocoelia*, *Colospongia*, *Guadalupia*, *Intrasporeocoelia*, *Sollasia*, and *Salzburgia*, and Tabulozoan (Yang, 1987). Sponges in the Wuchiapingian Tieqiao reefs show higher diversity and abundance comparing with the older Guadalupian skeletal mounds below. But at the class-level, the main group of primary components and encrusters are similar, suggesting that the Middle Permian (Capitanian) mass extinction did not significantly alter the fundamental elements of reef construction on the Laibin-Heshan isolated platform. Just like in the process of building a wall, it is different between using bricks and stones, but for the building process it is not significantly different between cementing bricks together to build a wall and cementing stones together to build a wall. In the Middle-Late Permian reefs, sponges are the “bricks and stones”; encrusters such as *Archaeolithoporella* and *Tubiphytes*, and syndepositional cements are the “cements”. Nevertheless, at the higher taxonomic levels, the alternation of reef communities should exist after the Middle Permian (Capitanian) mass extinction, such as the

differences of sponges between Middle Permian and Late Permian, which still requires further quantitative investigation, especially in the Wuchiapingian.

4.5.3. Controlling factors of reef evolution during the G/L transition

Reef growth is a composite process that combined multiple controlling factors such as the development of biota that able to construct reef, the availability of habitat (Wood, 1999), and the ocean physiochemical condition that conducive for carbonate productions (Webb, 1996). All of these factors affected the reappearance and development of reefal build-ups after the mass extinction.

In the Tieqiao section, Wuchiapingian reef recovery has six cycles, each cycle corelated with a transgressive-regressive cycle (Wang et al., 2019). Within each cycle, the lowest taxonomic richness is with the transgressive phase in the slope-basin environment (Figure 4.4c), then slowly rise up following the regressive process. The taxonomic richness can reach a high-level during the initial reef phase (Figure 4.6c), which is an unstable phase for the colonization of reef community. Once the colonization stabilized, in the reef core facies, taxonomic richness is likely more related with the dominating organisms. The *Archaeolithoporella* dominated communities has lower taxonomic richness compared with the communities dominated by *Tubiphytes* (Figure 4.6a). As the *Archaeolithoporella* always encrusted the *Tubiphytes* when they cooccurred (Figure 4.5d-e), the decrease of taxonomic richness in *Archaeolithoporella* dominated communities can be a result of the biological competition. The sponge and *Archaeolithoporella* community significantly contributed to the largest part of reef core in the 5th cycle of reef growth within Wuchiapingian Tieqiao reef complex, which is consistent with the field observation (Wang et al., 2019). Thus, in the small scale, the growth of reef is also controlled by the organism besides the changes of sea-level.

The prolonged Middle Permian (Capitanian) mass extinction had a different effect on the pace of disappearance within different fossil groups (Bond et al., 2010a). Chen et al. (2009) recorded that the majority of skeletal mound builders in Tieqiao section (sponge, algae, and *Tubiphytes*) disappeared at or shortly before the horizon of end-Guadalupian crisis (*sensu* Wang et al. 2004), but the growth of the mound was terminated earlier when the relative sea level

reached the lowest point in end-Guadalupian at upper *J. granti* Zone. After the crisis, the pace of recovery varied within different communities, for example, brachiopods started to recover in the early Wuchiapingian (Chen et al., 2005; Shen et al., 2008), which was earlier than the recovery of reefs; but for terrestrial vertebrate such as tetrapods, their global and ecological diversities did not recover to Artinskian levels until the Changhsingian (Sahney and Benton, 2008). The reoccurrence of reef-building biota after the Middle Permian (Capitanian) mass extinction was not simultaneously accompanied with a reemergence of reefal build-ups in Tieqiao section. The fragments of sponges were observed within thin- to medium-bedded packstone/rudstone at the topmost part of Bed 122 (e.g., see Figures 4.7 and 4.10) at Tieqiao section, below the first occurrence of Wuchiapingian reef. The reef-building biotas have wider environment tolerances than the reef itself, because the proper habitat (carbonate platform or ramp) for reef construction has higher sensitivity to the environmental perturbation (Wood, 1999). The shrinking of Laibin-Heshan Platform in the upper Maokouwan (Guadalupian) was reflected by the succession of shallow water lenticular carbonate caps (Bed 114, and Bed 119 - Laibin limestone - at Tieqiao section) deposited in between the deep-water siliceous deposits (Yao et al., 2012). The shrinking of carbonate platforms in Guadalupian and the succeed paleogeographic pattern in early Wuchiapingian may lead to a restriction of habitat for reef community that cause the eclipse of reef development in the Wuchiapingian. Conversely, the evolution of the middle to late Wuchiapingian Tieqiao reefs can also indicate the reestablishment and enlargement of habitat - the carbonate platform at that time. But further detailed study of the development of carbonate platforms in the Wuchiapingian is necessary to refine the causal relationship between reef recovery and carbonate platform evolution.

The faunal turnover across the G/L transition was considered to be related with the Emeishan Large Igneous Province (ELIP) (e.g., Bond et al., 2010a, Chen and Xu, 2019). Zhong et al. (2020) constrained the range of waning stage of ELIP until upper part of conodont zone *C. transcaucasica* or the lower *C. orientalis* Zone, ca. 257.4 Ma, which provided an evidence of possible environmental perturbation related with the ELIP that continued through early Wuchiapingian after the Middle Permian mass extinction. Qiu and Wang (2011) suggested a submarine hydrothermal origin of the Middle-Upper Permian chert in the Tieqiao section, and the submarine hydrothermal activity was related with the eruption of the Emeishan basalts.

Nevertheless, in the Upper Permian, the alternations of chert and cherty limestones with mudstone-wackestone which reflect the basin-slope environment were deposited between the reef growth cycles within Wuchiapingian Tieqiao reef. The fluctuation of sulfate isotope at Tieqiao section suggested the ocean is strongly stratified around the G/L transition (Yan et al., 2013). Zhang et al. (2015) proposed repeated shoaling of sulfidic waters that widely spread across the G/L transition from the anomalies of sulfur isotope at Penglitan and Tieqiao section from South China, and west Texas. The sea-level of the earliest Wuchiapingian went through a rapid transgressive phase (Haq and Schutter, 2008, Qiu et al., 2014) combined with climate cooling which probably link to the post eruptive weathering of ELIP (Yang et al., 2018). This cooling event is consistent with the loss of benthic foraminifera diversity in North America shelves (Davydov, 2014). The loss of diversity of benthic foraminifera and calcareous algae during the G/L transition was also detected in South China (e.g., Lai et al., 2008). Those environmental perturbations and records of biodiversity losses during early Wuchiapingian cooccurred with the global absence of shallow water metazoan reef community (Weidlich et al., 2003). Huang et al. (2019a) proposed that the metazoan reef recovered in the Tieqiao section along with the stabilization of $\delta^{13}\text{C}$ in *C. orientalis* zone, they also mentioned that the similar stabilization of $\delta^{13}\text{C}$ also occurred during Middle Triassic recovery of metazoan reef (Payne et al., 2004, 2006b), and they suggested this indicated the restoration of reef ecosystems to a favorable condition, i.e., with less environmental perturbations.

4.6. Conclusions

Quantitative analyses reveal the composition and the spatial distribution of skeletal grains and whole rock components within the Wuchiapingian Tieqiao reef and suggest that the reef growth within each growth cycle was largely controlled by the different associations of organisms. Sponges, *Archaeolithoporella* and *Tubiphytes* were the most significant contributors to the Tieqiao reef-building process and reef recovery, but still ecologically and functionally differentiated. Sponges played a key role from the beginning of reef recovery. *Tubiphytes* has the widest environmental distribution and was important for the initiation of reef community. *Archaeolithoporella* was mostly constrained in the upper part of the reef core

and important for the enlargement of the reef core, which suggests a light dependence of *Archaeolithoporella*. The observed spatial distribution and stratigraphic variation of biocommunity clusters and rock composition clusters are related with the spatial change of depositional environments, which indicate that the environmental factors still played a critical role on the post-extinction reef evolution in modulating the availability of environments for reef establishment and growth. The recovery of Wuchiapingian Tieqiao reef after the Middle Permian (Capitanian) mass extinction is a multiparameter-controlled process that combined factors including recovery of biota, evolution of biocommunities, availability of habitat and suitable stable environments.

Acknowledgments

Wuqiang Xue, Fayao Chen, Aozhu Li, Bo Li, Yajuan Yan, Qian Ding, and Jingbin Wang are thanked for the help with the field work. We also thank Sara Tomás, Fei Li, Xiting Liu for constructive discussion about this work. This study is supported by National Natural Science Foundation of China (grant number: 41872117), Programm Projektbezogener Personenaustausch of German Academic Exchange service (DAAD) (grant number: 57318506), and a doctoral Scholarship of China Scholarship Council awarded to XW.

Chapter 5

Synthesis and conclusions

The reef recovery following the Middle Permian (Capitanian) mass extinction is much less investigated comparing to other post-extinction reef evolution, due to the limited records of reefs in Wuchiapingian. This thesis contributes to extend the understanding of the post-extinction reef recovery in Wuchiapingian, based on a study on the only known reef complex in South China. Starting with the revision of biostratigraphic conodont zonations, the detailed semi-quantitatively/quantitatively sedimentological and palaeoecological studies were implemented on the outcrop and microscopic scales to depict the scenario of reef recovery. The findings of this thesis 1) constrained the age of the Tieqiao reef, 2) updated the timing of reef recovery after the Middle Permian (Capitanian) mass extinction, 3) divided the cycles of post-extinction reef evolution, 4) and quantitatively described the reef ecosystem and the functioning of reef-building organisms.

5.1. Revision of conodont stratigraphic zonation of Tieqiao section and constraining the age of the Tieqiao reefs

The studies of conodont stratigraphy on Tieqiao section were initially focused on the transition from Capitanian to Wuchiapingian (Guadalupian to Lopingian) (Mei et al., 1994c; Mei et al., 1998; Henderson et al., 2002; Wang, 2002). Based on the high-resolution study of the conodonts, a revised stratigraphic zonation including twenty main and seven subordinate conodont zones are recognized at the Tieqiao section in this study. It is generally difficult to find conodonts from the shallow water depositional realms, for example reefs. However, two conodont zone were recognized in the earliest Wuchiapingian (*C. postbitteri* Zone) below the reefs and within bed 134 (*C. transcaucasica* Zone), which constrained the age of Tieqiao reefs into early-middle Wuchiapingian.

5.2. Timing of reef recovery following the Middle Permian (Capitanian) mass extinction

To define the time of reef recovery, the first step is to correctly identify the first occurrence of post-extinction reef. The term “reef” was originally derived from the nautical term “rif”, which indicate a topographic high close to the sea surface that beaches the boats. However, the geological definition of (biological) reef and its synonyms (ecological reef, bioherm, biostromes, etc.) have been proposed and revised by many researchers (e.g., Cuming, 1932; Scoffin, 1987; James, 1979; Wood, 1999; Flügel, 2002; Riding, 2002). The widespread classic definition of reef includes the “wave resistant” character and “large sized reef building organism” which persevered *in situ* in the upward growth position. But the broad definition of reef, which emphasized the lateral topographic relief, the organic original (i.e., biological controlled) reef formation, and the inferred rigid reef structure, are accepted and applied by more and more researchers. Here in this study, this broad definition of reef was applied to identify the reefs in Wuchiapingian Tieqiao section.

At Tieqiao section, the massive limestone (Bed 133) in the upper part of the Heshan (Wuchiaping) Formation were not identified as a reef by the early workers (Yang, 1987; Sha et al., 1990). One of the reasons that they didn’t recognize it as a reef is the absence of *in situ* large size sponges, such as large sphinctozoans, and another reason is the missing of a reef geometry. Several recent studies have discussed the massive limestone of upper Heshan (Wuchiaping) Formation at the Tieqiao section was a reef in substance (Qiu and Wang, 2010; Qiu et al., 2014; Huang et al., 2019a). But the discussion is still restricted to the massive limestone at Bed 133, which aged *C. orientalis* conodont zone by Shen et al., (2007), and the time of reef recovery was therefore also determined at *C. orientalis* zone (e.g., Huang et al., 2019a).

Although the large sphinctozoans such as *Intrasporoecoella* and *Rhabdactinia* have been considered as the primary reef-builders in the Middle Permian of the South China, they are not dominant in the Late Permian (Zhang and Zhang, 1992). From the investigation of this study, the large sphinctozoans only sparsely occurred at the upper part of the Heshan Formation, and do not represent a dominant component in the reef core structure (Figure 3.5B). However, the observed bafflestone/bindstone/boundstone structures built by sponges, encrusting organisms, and microbial carbonate indicate the existence of *in situ* structures built by a biological controlled process (Figure 3.4B). The extensive syndepositional cementation suggests the

structures built by above mentioned organisms were rigid. Therefore, in the upper part of bed 123, the bindstone/boundstone structure suggests a biological controlled formation mechanism of the massive limestones, and abundant syndepositional cementation indicate a structural rigidity of these bioconstructions. In addition, the lenticular geometry of these massive limestones from bed 123 suggests such build-ups were laterally restricted (Figure 3.8N), i.e., the existence of topographic relief. Thus, the coexistence of a rigid, biological controlled structure and a laterally restricted geometry suggests these massive limestones in the upper part of the bed 123 were reefs (this study). In addition, Mei et al., (1998) identified *C. leveni* conodont zone within upper part of bed 121 on Tieqiao section. Therefore, the recovery of the reefs following the Middle Permian (Capitanian) mass extinction is revised to be started within or after *C. leveni* conodont zone (Figure 3.3), which is earlier than previous understanding.

5.3. Cycles of the post-extinction reef evolution and the delayed recovery of metazoan reefs at Tieqiao section

Previous works on the Wuchiapingian Tieqiao section (Shen et al., 2007; Qiu and Wang, 2010; Qiu et al., 2014, Huang et al., 2019a) suggested that: deposition above the G/L boundary occurred during a transgressive phase, represented in early Wuchiapingian by chert and cherty limestone from bed 120 to 122; this transgressive phase followed by a regressive phase interrupted by frequently occurred small-scale transgressive phases which represented by the deposition of massive limestone and alternated bedded chert from bed 123 to 133; a transgressive phase started from bed 134 until the end of Wuchiapingian. However, based on the new recognition of the initial reefal build-ups within bed 123, 125, 127 and 129, and a newly identified reef body within bed 134, detailed six reef growth cycles were determined within six transgressive-regressive cycles from the Wuchiapingian Tieqiao section (Figure 3.3). The reefs developed in each of the regressive phases, and the reef core were dominated by different lithofacies and biocommunities (Figures 3.4B and 4.7, Table 4.1). The first reefal build-up appeared at upper part of bed 123, indicating the initial recovery of reef ecosystem started at the first cycle. However, the metazoan such as sponges were only the minor components in the reef and not the primary reef builders. Stepwise, the sponges become more and more abundant

following the reef recovery. The recovery of metazoan reefs was determined to be started from the 4th cycle, and sponges become dominant in the 5th and 6th cycles. So, the recovery of metazoan (sponge) reefs was delayed compare with the reefs composed of non-metazoans. Additionally, although the starting point of reef recovery was brought forward by this study, the reef ecosystem still recovered much later in comparison to other level-bottom communities (e.g., brachiopods, Chen et al., 2005; Shen et al., 2008) and distanced from the G/L boundary or the level of Middle Permian (Guadalupian) mass extinction. This is generally corresponded with the previous understanding (Huang et al., 2019a), but substantially with different contents because of the updated timing of reef recovery following the mass extinction from this study.

5.4. Wuchiapingian reef ecosystem and functioning of reef-building organisms

The shallow water photosynthetic taxa such as large fusulinids and calcareous algae were the most affected organisms by the Middle Permian (Capitanian) mass extinction (Wignall et al., 2009a, 2009b; Bond et al., 2010b). In the reef ecosystem, while the corals were selectively affected and cool-water reef communities were disrupted by the Middle Permian mass extinction, sponges were thought to be less affected (Weidlich 2002a, 2002b; Weidlich et al., 2003). Nevertheless, sphinctozoan sponges were the dominated reef-building sponges in the Middle Permian of South China (Fan et al., 1990; Zhang and Zhang, 1992), and Inozoan sponges were the most sustained group within the radiation and evolution of sponge reefs in Late Permian Changhsingian (Fan et al., 1990), which indicate the changes within sponges in a higher taxonomic level existed within the transition of Middle-Late Permian. How the changes of sponges have happened from the Middle Permian to Late Permian remains a mystery due to the reef eclipse of Wuchiapingian. Based on the previous studies (Yang, 1987; Huang et al., 2019a) and investigation of this study, the dominance of Inozoan sponges and small sized sphinctozoan sponges, combined with the flourishing of encrusters such as *Archaeolithoporella* and *Tubiphytes*, suggest that the reef community of Wuchiapingian Tieqiao reefs are similar with the Changhsingian rather than Guadalupian. The transition of reef communities from Middle Permian to Late Permian can correspond to what Flügel and

Kiessling (2002) has suggested, that the constructor guild generally turns to be the most affected one by the mass extinction, and the binder (encruster) guild turns to flourish in the following recovery phase.

Both of the semi-quantitative and quantitative analyses suggest the encrusting organisms played a significant role in the reef building process of the Wuchiapingian Tieqiao reefs. *Archaeolithoporella* and *Tubiphytes* were the two most significant encrusting organisms within the Tieqiao reefs. *Archaeolithoporella* is abundant in the upper part of reef core (Figures 4.7, 4.10 and 4.12), combined with the negative correlation between *Archaeolithoporella* and other organisms (Table 4.2; Figure 4.11), suggest a competitive edge of *Archaeolithoporella* in the upper part of reef core as well as a possible light dependence of it. *Archaeolithoporella* is also more abundant in the upper part of the entire reef complex, along with the expanding of reef bodies in 4th to 6th reef cycles (Figures 3.5A and 4.7), which suggests that it was significant for the enlargement of reef volume. *Tubiphytes* acted as both baffler and encruster. Unlike *Archaeolithoporella*, *Tubiphytes* is widely distributed in different environments but more often in the initial reef phase (Figures 4.7, 4.10 and 4.12), suggesting that it played a significant role in the initiation and stabilization of reef community.

The function of sponge is varied between different types. Generally, the sponges at Tieqiao section were not strong reef constructors. At most of the cases, encrusting organisms connected sparsely distributed sponges (normally inozoan) together to form the reef structure. But, locally, some of the bigger sponges can also build cavities. Some of the small sphinctozoans attach to the wall of such cavities (Figure 3.6G), showing a cryptic ecology, which is similar to the examples described from the Capitan reef in New Mexico (Wood et al., 1994, 1996). Sponges were not a dominant component in the lower part of the reef complex but became more important in the upper part of the reef complex, along with the metazoan reef recovery and the enlargement of reef bodies both vertically and laterally (Figure 3.5B). Nevertheless, such trend is not significantly shown in the result of quantitative analysis of the thin sections (Figures 4.7 and 4.10), possibly because of the size of the thin section is too small to capture the changing of sponges.

5.5. Conclusions

This thesis investigated the recovery of reef ecosystem on outcrop and microscopic scale, through biostratigraphic, sedimentologic, and palaeoecological perspectives, applied semi-quantitative/quantitative analyses, and concluded the following findings:

- 1) The reef complex within the Heshan/Wuchiaping Formation at Tieqiao section was developed within the early to middle Wuchiapingian.
- 2) The conodonts were not significantly impacted by the Middle Permian (Capitanian) mass extinction.
- 3) The Wuchiapingian Tieqiao reef complex including six reef cycles correlated to six transgressive-regressive cycles. The reefal build-ups developed within each regressive phase, on the outer platform above the wave base and in the euphotic zone.
- 4) The recovery of reef following the Middle Permian (Capitanian) mass extinction started from the first reef cycle, in the upper part of bed 123 at Tieqiao section, within or after the *C. leveni* conodont zone, which is two conodont zones earlier than previous understanding.
- 5) The metazoans such as sponges were not the dominant components until the 5th and 6th reef cycles, but the abundance of sponges did increase along with the recovery of reef and become more and more important starting from the 4th cycle. This finding is significantly observed from the semi-quantitative analysis of the outcrop scale studies and indicate a delayed recovery of metazoan reefs after the Middle Permian (Capitanian) mass extinction. Nevertheless, it still has to be noticed that such trend of sponges was not significantly shown in the quantitative analyses of the thin sections.
- 6) However, the dominant types of sponges are not the high relief and big sized one in Wuchiapingian Tieqiao reefs, i.e., they cannot be frame builders. So, the functions of the encrusting organisms, especially *Tubiphytes* and *Archaeolithoporella* were significant. Their functions are varied and relevant to their ecological characters. *Tubiphytes* were widely adopted to different environments and acted as bafflers and encrusters, they were important in the initiation of reef community. *Archaeolithoporella* were showing a competitive edge and concentrated in the shallower part of reef (i.e., upper part of reef core) and played a significant role for the enlargement of reef volume.

5.6 Perspective of future researches

After the Middle Permian (Capitanian) mass extinction, the reef recovery in Wuchiapingian is one of the most critical questions about the Permian-Triassic transition. Because of the limited reef preservation within the Wuchiapingian, the Tieqiao section is irreplaceable on this topic. But whether the recovery process at Tieqiao is a local or global phenomenon still needs further tests from other new reef localities.

Meanwhile, the semi-quantitative/quantitative analyses on a higher taxonomic level are also necessary to reveal the detail of the recovery process on different reef organisms. For large-sized organisms such as sponges, quantitative analyses on a bigger scale than a thin section are also recommended.

Furthermore, the current forward modeling methods are continuously digging the interaction of biological controlled sedimentary process and the geometry of carbonate settings. How the evolution of reef community controls the formation of reefs could be further investigated through the correlation between backward sedimentary process interpretation and the forward simulation.

In addition, the further comparison of time, pattern, and controlling factors between the reef recovery processes following different mass extinctions is worth discussing.

References

- Aljinović, D., Isozaki, Y., Sremac, J., 2008. The occurrence of giant bivalve Alatoconchidae from the Yabeina zone (Upper Guadalupian, Permian) in European Tethys. *Gondwana Res.*, **13**, 275–287.
- Babcock, J.A., 1974. *The role of algae in the formation of the Capitan Limestone (Permian, Guadalupian), Guadalupe Mountains, West Texas—New Mexico*. University of Wisconsin, Madison, Ph.D. dissertation, 241 pp.
- Babcock, J.A., 1977. Calcareous algae, organic boundstones, and the genesis of the upper Capitan Limestone (Permian, Guadalupian), Guadalupe Mountains, west Texas and New Mexico. In: Hileman, M.E., Mazzullo, S.J. (Eds.), *Upper Guadalupian Facies, Permian Reef Complex, Guadalupe Mountains, New Mexico and West Texas. Permian Basin Sect. SEPM Publ.*, **77**, Midland TX, pp. 3–44.
- Bagherpour, B., Bucher, H., Schneebeli-Hermann, E., Vennemann, T., Chiaradia, M., Shen, S.Z., 2018. Early Late Permian coupled carbon and strontium isotope chemostratigraphy from South China: Extended Emeishan volcanism? *Gondwana Res.*, **58**, 58–70.
- Baker, A.C., Glynn, P.W., Riegl, B., 2008. Climate change and coral reef bleaching: An ecological assessment of long-term impacts, recovery trends and future outlook. *Estuar. Coast. Shelf Sci.*, **80**, 435–471.
- Bambach, R.K., Knoll, A.H., Wang, S.C., 2004. Origination, extinction, and mass depletions of marine diversity. *Paleobiology*, **30**, 522–542.
- Barnosky, A.D., Matzke, N., Tomiya, S., Wogan, G.O.U., Swartz, B., Quental, T.B., Marshall, C., McGuire, J.L., Lindsey, E.L., Maguire, K.C., Mersey, B., Ferrer, E.A., 2011. Has the Earth's sixth mass extinction already arrived? *Nature*, **471**, 51–57.
- Beauchamp, B., Henderson, C.M., 1994. The Lower Permian Raanes, Great Bear Cape and Trappers Cove Formations, Sverdrup Basin, Canadian Arctic - stratigraphy and conodont zonations. *Bull. Can. Petrol. Geol.*, **42**, 562–597.
- Behnken, F.H., 1975. Leonardian and Guadalupian (Permian) conodont biostratigraphy in Western and Southwestern United States. *J. Paleontol.*, **49**, 284–315.
- Bell, J.J., Davy, S.K., Jones, T., Taylor, M.W., Webster, N.S., 2013. Could some coral reefs become sponge reefs as our climate changes? *Glob. Chang. Biol.*, **19**, 2613–2624.
- Bellwood, D.R., Hughes, T.P., Folke, C., Nyström, M., 2004. Confronting the coral reef crisis. *Nature*, **429**, 827–833.
- Bender, H., Stoppel, D., 1965. Perm-Conodonten. *Geol. Jahrb.*, **82**, 331–364.
- Boardman, D.R., Wardlaw, B.R., Nestell, M.K., 2009. Stratigraphy and conodont biostratigraphy of the Uppermost Carboniferous and Lower Permian from the North American Midcontinent. *Kans. Geol. Surv. Bull.*, **255**, 1–130.
- Bond, D.P.G., Hilton, J., Wignall, P.B., Ali, J.R., Stevens, L.G., Sun, Y.D., Lai, X.L., 2010a. The Middle Permian (Capitanian) mass extinction on land and in the oceans. *Earth-Sci. Rev.*, **102**, 100–116.

- Bond, D.P.G., Wignall, P.B., Wang, W., Izon, G., Jiang, H.S., Lai, X.L., Sun, Y.D., Newton, R.J., Shao, L.Y., Védérine, S., Cope, H., 2010b. The mid-Capitanian (Middle Permian) mass extinction and carbon isotope record of South China. *Palaeogeogr. Palaeoclimatol. Palaeoecol.*, **292**, 282–294.
- Bond, D.P.G., Wignall, P.B., Joachimski, M.M., Sun, Y.D., Savov, I., Grasby, S.E., Beauchamp, B., Blomeier, D.P.G., 2015. An abrupt extinction in the Middle Permian (Capitanian) of the Boreal Realm (Spitsbergen) and its link to anoxia and acidification. *Geol. Soc. Am. Bull.*, **127**, 1411–1421.
- Bucur, I.I., Munnecke, A., Granier, B., Yan, J., 2009. Remarks on the Permian dasycladalean alga *Sinoporella leei* Yabe, 1949. *Geobios*, **42**, 221–231.
- Burrett, C., Udchachon, M., Thassanapak, H., Chitnarin, A., 2015. Conodonts, radiolarians and ostracodes in the Permian E-Lert Formation, Loei Fold Belt, Indochina Terrane, Thailand. *Geol. Mag.*, **152**, 106–142.
- Catalano, R., Di Stefano, P., Kozur, H., 1991. Permian circumpacific deep-water faunas from the western Tethys (Sicily, Italy)—new evidences for the position of the Permian Tethys. *Palaeogeogr. Palaeoclimatol. Palaeoecol.*, **87**, 75–108.
- Ceballos, G., Ehrlich, P.R., Barnosky, A.D., García, A., Pringle, R.M., Palmer, T.M., 2015. Accelerated modern human-induced species losses: Entering the sixth mass extinction. *Sci. Adv.*, **1**, e1400253.
- Chen, B., Joachimski, M.M., Sun, Y.D., Shen, S.Z., Lai, X.L., 2011. Carbon and conodont apatite oxygen isotope records of Guadalupian-Lopingian boundary sections: climatic or sea-level signal? *Palaeogeogr. Palaeoclimatol. Palaeoecol.*, **311**, 145–153.
- Chen, F., Xue, W., Yan, J., Wignall, P.B., Meng, Q., Luo, J., Feng, Q., 2018. Alatoconchids: Giant Permian bivalves from South China. *Earth Sci. Rev.*, **179**, 147–167.
- Chen, J., Xu, Y.G., 2019. Establishing the link between Permian volcanism and biodiversity changes: Insights from geochemical proxies. *Gondwana Res.*, **75**, 68–96.
- Chen, Z.Q., Campi, M.J., Shi, G.R., Kaiho, K., 2005. Post-extinction brachiopod faunas from the Late Permian Wuchiapingian coal series of South China. *Acta Palaeontol. Pol.*, **50**, 343–363.
- Chen, Z.Q., George, A.D., Yang, W.R., 2009. Effects of Middle–Late Permian sea-level changes and mass extinction on the formation of the Tieqiao skeletal mound in the Laibin area, South China. *Austr. J. of Earth Sci.*, **56**, 745–763.
- Chernykh, V.V., 2005. *Zonal Method in Biostratigraphy, Zonal Conodont Scale of the Lower Permian in the Urals*. Institute of Geology and Geochemistry of RAN, Ekaterinburg, 217 pp.
- Chernykh, V.V., 2006. *Lower Permian Conodonts of the Urals*. Russian Academy of Science, Uralian Branch, Ekaterinburg, 130 pp.
- Chuvashov, B.I., Dyupina, G.V., Mizens, G.A., Chernykh, V.V., 1990. *Basic Sections of Carboniferous and Lower Permian of Western Slope of Urals*. Ural Branch Academic Science of Russia, Sverdlovsk, 369 pp.
- Chuvashov, B.I., Chernykh, V.V., Leven, E.Ya., Davydov, V.I., Bowring, S., Ramezani, J., Glenister, B.F., Henderson, C., Schiappa, T.A., Northrup, C.J., Snyder, W.S., Spinosa, C.,

- Wardlaw, B.R., 2002. Progress report on the base of the Artinskian and base of the Kungurian by the Cisuralian Working Group. *Permophiles*, **41**, 13–16.
- Clapham, M.E., 2015. Ecological consequences of the Guadalupian extinction and its role in the brachiopod-mollusk transition. *Paleobiology*, **41**, 266–279.
- Clapham, M.E., Shen, S., Bottjer, D.J., 2009. The double mass extinction revisited: reassessing the severity, selectivity, and causes of the end-Guadalupian biotic crisis (Late Permian). *Paleobiology*, **35**, 32–50.
- Clark, D.L., Behnken, F.H., 1971. Conodonts and biostratigraphy of the Permian. *Geol. Soc. Am. Mem.*, **127**, 415–439.
- Clark, D.L., Carr, T.R., Behnken, F.H., Wardlaw, B.R., Collinson, J.W., 1979. Permian conodont biostratigraphy in the Great Basin. In: Sandberg, C.A., Clark, D.L. (Eds.), *Conodont Biostratigraphy of the Great Basin and Rocky Mountains*. Brigham Young University, Geology Studies, pp. 143–150.
- Clarke, K.R., Warwick, R.M., 2001. *Change in Marine Communities: An approach to statistical analysis and interpretation, 2nd ed.* PRIMER-E: Plymouth.
- Copper, P., 1994. Ancient reef ecosystem expansion and collapse. *Coral Reefs*, **13**, 3–11.
- Cuming, E.R., 1932. Reefs or Bioherms? *Geol. Soc. Am. Bull.*, **43**, 331–352.
- Davydov, V., 2014. Warm water benthic foraminifera document the Pennsylvanian–Permian warming and cooling events — The record from the Western Pangea tropical shelves. *Palaeogeogr. Palaeoclimatol. Palaeoecol.*, **414**, 284–295.
- Ding, H., Wan, S., 1990. The Carboniferous-Permian conodont event-stratigraphy in the South of the North China Platform. *Cour. Forschungsinst. Senck.*, **118**, 131–155.
- Dunham, R.J., 1962. Classification of carbonate rocks according to depositional texture. In: Ham, W.E. (Ed.), *Classification of Rock Texture—a Symposium*. Edwards Brothers, Inc, Norman, pp. 108–121.
- Embry III, A.F., Klovan, J.E., 1971. A late Devonian reef tract on northeastern Banks Island, NWT. *Bull. Can. Pet. Geol.*, **19**, 730–781.
- Fagerstrom, J.A., 1987. *The evolution of reef communities*. John Wiley and Sons Inc., New York, 600 pp.
- Fagerstrom, J.A., Weidlich, O., 2005. Biologic response to environmental stress in tropical reefs: Lessons from modern Polynesian coralgal atolls and Middle Permian sponge and *Shamovella*-microbe reefs (Capitan Limestone USA). *Facies*, **51**, 501–515.
- Fan, J.S., Rigby, J.K., Qi, J., 1990. The Permian reefs of South China and comparisons with the Permian reef complex of the Guadalupe Mountains, West Texas and New Mexico. *Brigham Young Univ. Geol. Stud.*, **36**, 15–55.
- Fan, J.S., Qi, J.W., Zhou, T.M., Zhang, W., Zhang, X.L., 1990. *Permian Reefs of Longlin, Guangxi*. Geological Publishing House, Beijing, 128 pp.
- Fan, J.X., Shen, S.Z., Erwin, D.H., Sadler, P.M., MacLeod, N., Cheng, Q.M., Hou, X.D., Yang, J., Wang, X.D., Wang, Y., Zhang, H., Chen, X., Li, G.X., Zhang, Y.C., Shi, Y.K., Yuan, D.X., Chen, Q., Zhang, L.N., Li, C., Zhao, Y.Y., 2020. A high-resolution summary of Cambrian to Early Triassic marine invertebrate biodiversity. *Science*, **367**, 272–277.

- Fheed, A., Świerczewska, A., Krzyżak, A., 2015. The isolated Wuchiapingian (Zechstein) Wielichowo Reef and its sedimentary and diagenetic evolution, SW Poland. *Geol. Q.*, **59**, 1–19.
- Flügel, E., 2002. Triassic reef patterns. In: Kiessling, W., Flügel, E., Golonka, J. (Eds.), *Phanerozoic Reef Patterns*. SEPM Society for Sedimentary Geology, pp. 391–463.
- Flügel, E., 2010. Depositional models, facies zones and standard microfacies. In: *Microfacies of Carbonate Rocks*. Springer Berlin Heidelberg, Berlin, Heidelberg, pp. 657–724.
- Flügel, E., Kiessling, W., 2002. Patterns of Phanerozoic reef crises. In: Kiessling, W., Flügel, E., Golonka, J. (Eds.), *Phanerozoic Reef Patterns*. SEPM Society for Sedimentary Geology, pp. 691–733.
- Flügel, E., Reinhardt, J., 1989. Uppermost Permian reefs in Skyros (Greece) and Sichuan (China): implications for the Late Permian extinction event. *PALAIOS*, **4**, 502–518.
- Flügel, E., Kochansky-Devidé, V., Ramovš, A., 1984. A Middle Permian calcisponge/algal/cement reef: Straža near bled, Slovenia. *Facies*, **10**, 179–255.
- Foster, W.J., Danise, S., Price, G.D., Twitchett, R.J., 2018. Paleoecological analysis of benthic recovery after the late Permian mass extinction event in eastern Lombardy, Italy. *PALAIOS*, **33**, 266–281.
- Gong, Y.M., Shi, G.R., Zhang, L.J., Weldon, E.A., 2010. *Zoophycos* composite ichnofabrics and tiers from the Permian neritic facies in South China and south-eastern Australia. *Lethaia*, **43**, 182–196.
- Grotzinger, J.P., Knoll, A.H., 1995. Anomalous Carbonate Precipitates: Is the Precambrian the Key to the Permian? *PALAIOS*, **10**, 578–596.
- Guido, A., Mastandrea, A., Stefani, M., Russo, F., 2016. Role of autochthonous versus detrital micrite in depositional geometries of Middle Triassic carbonate platform systems. *Geol. Soc. Am. Bull.*, **128**, 989–999.
- Gullo, M., Kozur, H., 1992. Conodonts from the pelagic deep-water Permian of central Western-Sicily (Italy). *Neues Jb. Geol. Paläontol. Abh.*, **184**, 203–234.
- Guo, L., Riding, R., 1992. Microbial micritic carbonates in uppermost Permian reefs, Sichuan Basin, southern China: some similarities with recent travertines. *Sedimentology*, **39**, 37–53.
- Hammer, Ø., Harper, D.A., Ryan, P.D., 2001. PAST: Paleontological statistics software package for education and data analysis. *Palaeontol. Electron.*, **4**, 9.
- Haq, B.U., Schutter, S.R., 2008. A Chronology of Paleozoic Sea-Level Changes. *Science*, **322**, 64–68.
- Heindel, K., Foster, W.J., Richoz, S., Birgel, D., Roden, V.J., Baud, A., Brandner, R., Krystyn, L., Mohtat, T., Koşun, E., Twitchett, R.J., Reitner, J., Peckmann, J., 2018. The formation of microbial-metazoan bioherms and biostromes following the latest Permian mass extinction. *Gondwana Res.*, **61**, 1–17.
- Henderson, C.M., Mei, S., Wardlaw, B.R., 2002. New conodont definitions at the Guadalupian-Lopingian boundary. In: Hills, L.V., Henderson, C.M., Bamber, E.W. (Eds.),

Carboniferous and Permian of the World. Memoir - Canadian Society of Petroleum Geologists, pp. 725–735.

- Henderson, C.M., Mei, S., 2003. Stratigraphic versus environmental significance of Permian serrated conodonts around the Cisuralian-Guadalupian boundary: new evidence from Oman. *Palaeogeogr. Palaeoclimatol. Palaeoecol.*, **191**, 301–328.
- Henderson, C.M., Davydov, D.I., Wardlaw, B.R., 2012. The Permian period. In: Gradstein, F.M., Ogg, J.G., Schmitz, M.D., Ogg, G.M. (Eds.), *The Geologic Time Scale 2012*. Elsevier, pp. 653–679.
- Hoegh-Guldberg, O., 1999. Climate change, coral bleaching and the future of the world's coral reefs. *Mar. Freshwater Res.*, **50**, 839–866.
- Hoegh-Guldberg, O., Mumby, P.J., Hooten, A.J., Steneck, R.S., Greenfield, P., Gomez, E., Harvell, C.D., Sale, P.F., Edwards, A.J., Caldeira, K., Knowlton, N., Eakin, C.M., Iglesias-Prieto, R., Muthiga, N., Bradbury, R.H., Dubi, A., Hatziolos, M.E., 2007. Coral Reefs Under Rapid Climate Change and Ocean Acidification. *Science*, **318**, 1737.
- Hollingworth, N.T.J., Tucker, M.E., 1987. The upper Permian (Zechstein) tunstall reef of North East England: Palaeoecology and early diagenesis. In: *The Zechstein Facies in Europe, Lecture Notes in Earth Sciences*. Springer Berlin Heidelberg, Berlin, Heidelberg, pp. 23–50.
- Hou, Z.S., Fan, J.X., Henderson, C.M., Yuan, D.X., Shen, B.-H., Wu, J., Wang, Y., Zheng, Q.F., Zhang, Y., Wu, Q., Shen, S., 2020. Dynamic palaeogeographic reconstructions of the Wuchiapingian Stage (Lopingian, Late Permian) for the South China Block. *Palaeogeogr. Palaeoclimatol. Palaeoecol.*, **546**, 109667.
- Huang, Y.G., Chen, Z.Q., Zhao, L.S., Stanley, G.D., Yan, J.X., Pei, Y., Yang, W.R., Huang, J.H., 2019a. Restoration of reef ecosystems following the Guadalupian–Lopingian boundary mass extinction: Evidence from the Laibin area, South China. *Palaeogeogr. Palaeoclimatol. Palaeoecol.*, **519**, 8–22.
- Huang, Y.G., Chen, Z.Q., Wignall, P.B., Grasby, S.E., Zhao, L.S., Wang, X.D., Kaiho, K., 2019b. Biotic responses to volatile volcanism and environmental stresses over the Guadalupian-Lopingian (Permian) transition. *Geology*, **47**, 175–178.
- Igo, H., 1981. *Permian conodont biostratigraphy of Japan*. *Palaeontological Society of Japan Special Papers vol. 24*. Palaeontological Society of Japan, Tokyo, 51 pp.
- Isozaki, Y., Aljinović, D., 2009. End-Guadalupian extinction of the Permian gigantic bivalve Alatoconchidae: end of gigantism in tropical seas by cooling. *Palaeogeogr. Palaeoclimatol. Palaeoecol.*, **284**, 11–21.
- Jackson, J.B.C., Kirby, M.X., Berger, W.H., Bjorndal, K.A., Botsford, L.W., Bourque, B.J., Bradbury, R.H., Cooke, R., Erlandson, J., Estes, J.A., Hughes, T.P., Kidwell, S., Lange, C.B., Lenihan, H.S., Pandolfi, J.M., Peterson, C.H., Steneck, R.S., Tegner, M.J., Warner, R.R., 2001. Historical Overfishing and the Recent Collapse of Coastal Ecosystems. *Science*, **293**, 629.
- James, N.P., 1979. Reefs. In: Walker, R.B. (Eds.), *Facies models. Geosci. Repr. Ser.*, **1**. Geological Association of Canada, Toronto, pp. 121–132.

- Ji, Z.S., Yao, J.X., Jin, X.C., Yang, X.N., Wang, Y.Z., Yang, H.L., Wu, G.C., 2004. Early Permian conodonts from the Baoshan Block, Western Yunnan, China. *Acta Geol. Sin.*, **78**, 1179–1184.
- Jiang, H.S., Lai, X.L., Luo, G.M., Aldridge, R., Zhang, K.X., Wignall, P.B., 2007. Restudy of conodont zonation and evolution across the P/T boundary at Meishan section, Changxing, Zhejiang, China. *Glob. Planet. Chang.*, **55**, 39–55.
- Jin, Y.G., Shang, Q.H., 2000. The Permian of China and its interregional correlation. In: Yin, H.F., Dickins, J.M., Shi, G.R., Tong, J.N. (Eds.), *Permo-Triassic Evolution of Tethys and Western Circum-Pacific*. Elsevier, pp. 71–98.
- Jin, Y.G., Zhang, J., Shang, Q.H., 1994. Two phases of the end-Permian mass extinction. In: Embry, A.F., Beauchamp, B., Glass, D.J. (Eds.), *Pangea: Global Environments and Resources*. Canadian Society of Petroleum Geologists, pp. 813–822.
- Jin, Y.G., Wardlaw, B.R., Glenister, B.F., Kotlyar, G.V., 1997. Permian chronostratigraphic subdivisions. *Episodes*, **20**, 10–15.
- Jin, Y.G., Shen, S.Z., Henderson, C.M., Wang, X.D., Wang, W., Wang, Y., Cao, C.Q., Shang, Q.H., 2006. The Global Stratotype Section and Point (GSSP) for the boundary between the Capitanian and Wuchiapingian stage (Permian). *Episodes*, **29**, 253–262.
- Kaiho, K., Chen, Z.Q., Ohashi, T., Arinobu, T., Sawada, K., Cramer, B.S., 2005. A negative carbon isotope anomaly associated with the earliest Lopingian (Late Permian) mass extinction. *Palaeogeogr. Palaeoclimatol. Palaeoecol.*, **223**, 172–180.
- Kazmierczak, J., Coleman, M.L., Gruszczynski, M., Kempe, S., 1996. Cyanobacterial key to the genesis of micritic and peloidal limestones in ancient seas. *Acta Palaeontol. Pol.*, **41**, 319–338.
- Kelley, B.M., Daniel, L.J., YU, M.Y., Jost, A.B., Meyer, K.M., Lau, K.V., Altiner, D., LI, X.W., Minzoni, M., Schaal, E.K., Payne, J.L., 2020. Controls on carbonate platform architecture and reef recovery across the Palaeozoic to Mesozoic transition: A high-resolution analysis of the Great Bank of Guizhou. *Sedimentology*. doi:10.1111/sed.12741
- Kerans, C., Tinker, S.W., 1999. Extrinsic Stratigraphic Controls on Development of the Capitan Reef Complex. In: Saller, A.H., Harris, P.M.M., Kirkland, B.L., Mazzullo, S.J. (Eds.), *Geologic Framework of the Capitan Reef*. SEPM Society for Sedimentary Geology, pp. 15–36.
- Kiessling, W., 2005. Long-term relationships between ecological stability and biodiversity in Phanerozoic reefs. *Nature*, **433**, 410–413.
- Kiessling, W., Simpson, C., 2011. On the potential for ocean acidification to be a general cause of ancient reef crises. *Glob. Chang. Biol.*, **17**, 56–67.
- Kirkland, B.L., Dickson, J.A.D., Wood, R.A., Land, L.S., 1998. Microbialite and microstratigraphy: the origin of encrustations in the middle and upper Capitan Formation, Guadalupe Mountains, Texas and New Mexico, USA. *J. Sediment. Res.*, **68**, 956–969.
- Knoerich, A.C., Mutti, M., 2003. Controls of facies and sediment composition on the diagenetic pathway of shallow-water Heterozoan carbonates: the Oligocene of the Maltese Islands. *Int. J. Earth Sci. (Geol Rundsch)*, **92**, 494–510.
- Knowlton, N., 2001. The future of coral reefs. *Proc. Natl. Acad. Sci. USA*, **98**, 5419.

- Kozur, H., 1987. Beiträge zur Stratigraphie des Perms Teil II: Die Conodontenchronologie des Perms. *Freib. Forsch.*, **334**, 85–161.
- Kozur, H., 1993. *Gullodus* n. gen.—a new conodont genus and remarks to the pelagic Permian and Triassic of Western Sicily. *Jahrb. Geol. Bundesanst.*, **136**, 77–87.
- Kozur, H.W., 1994. Preliminary report on the Permian conodont fauna of Darvas and SE Pamir and its importance for the Permian time scale. *Permophiles*, **24**, 13–15.
- Kozur, H., 1995. Permian conodont zonation and its importance for the Permian stratigraphic standard scale. *Mitt. Geol. Paläontol. Innsbruck*, **20**, 165–205.
- Kozur, H., Mostler, H., 1995. Guadalupian (Middle Permian) conodonts of sponge-bearing limestones from the margins of the Delaware Basin, West Texas. *Geol. Croat.*, **48**, 107–128.
- Lai, X.L., Wang, W., Wignall, P.B., Bond, D.P.G., Jiang, H.S., Ali, J.R., John, E.H., Sun, Y.D., 2008. Palaeoenvironmental change during the end-Guadalupian (Permian) mass extinction in Sichuan, China. *Palaeogeogr. Palaeoclimatol. Palaeoecol.*, **269**, 78–93.
- Lambert, L.L., Bell Jr., G.L., Fronimos, J.A., Wardlaw, B.R., O. Yisa, M., 2010. Conodont biostratigraphy of a more complete Reef Trail Member section near the type section, latest Guadalupian Series type region. *Micropaleontology*, **56**, 233–253.
- Lambert, L.L., Wardlaw, B.R., Nestell, M.K., Nestell, G.P., 2002. Latest Guadalupian (Middle Permian) conodonts and foraminifers from West Texas. *Micropaleontology*, **48**, 343–364.
- Leinfelder, R.R., Schmid, D.U., Nose, M., Werner, W., 2002. Jurassic Reef Patterns—The Expression of a Changing Globe. In: Kiessling, W., Flügel, E., Golonka, J. (Eds.), *Phanerozoic Reef Patterns*. SEPM Society for Sedimentary Geology, pp. 465–520.
- Li, Z.S., Zhan, L.P., Dai, J.Y., Jin, G.G., Zhu, X.F., Zhang, J.H., Huang, H.Q., Xu, D.Y., Yan, Z., Li, H.M., 1989. Study on the Permian-Triassic biostratigraphy and event stratigraphy of northern Sichuan and southern Shaanxi. *Geological Memoirs Vol. 9*. Geological Publishing House, Beijing, 435 pp.
- Liu, X.T., Ma, Z.X., Yan, J.X., 2010. Sedimentary environments and controlling factors of hydrocarbon source rocks of the late Permian Wujiaping Age in Yangtze area. *J. Palaeogeogr.*, **12**, 244–252.
- Martindale, R.C., Foster, W.J., Velledits, F., 2019. The survival, recovery, and diversification of metazoan reef ecosystems following the end-Permian mass extinction event. *Palaeogeogr. Palaeoclimatol. Palaeoecol.*, **513**, 100–115.
- Maslov, V.P., 1956. *Fossil calcareous algae of the USSR*. Acad. Sci. USSR, Geol. Inst, Moscow.
- McGhee, G.R., Sheehan, P.M., Bottjer, D.J., Droser, M.L., 2004. Ecological ranking of Phanerozoic biodiversity crises: ecological and taxonomic severities are decoupled. *Palaeogeogr. Palaeoclimatol. Palaeoecol.*, **211**, 289–297.
- McGhee, G.R., Jr, Clapham, M.E., Sheehan, P.M., Bottjer, D.J., Droser, M.L., 2013. A new ecological-severity ranking of major Phanerozoic biodiversity crises. *Palaeogeogr. Palaeoclimatol. Palaeoecol.*, **370**, 260–270.

- Mei, S.L., Jin, Y.G., Wardlaw, B.R., 1994a. Succession of Wuchiapingian conodonts from northeast Sichuan Province and its worldwide correlation. *Acta Micropalaeontol. Sin.*, **11**, 121–139.
- Mei, S.L., Jin, Y.G., Wardlaw, B.R., 1994b. Succession of conodont zones from the Permian ‘Kuhfeng’ Formation, Xuanhan, Sichuan and its implication in global correlation. *Acta Palaeontol. Sin.*, **33**, 1–23.
- Mei, S.L., Jin, Y.G., Wardlaw, B.R., 1994c. Zonation of conodonts from the Maokouan-Wuchiapingian boundary strata, South China. *Palaeoworld* **4**, 225–233.
- Mei, S.L., Jin, Y.G., Wardlaw, B.R., 1998. Conodont succession of the Guadalupian-Lopingian Boundary Strata in Laibin of Guangxi, China and West Texas, USA. *Palaeoworld*, **9**, 53–76.
- Mei, S.L., Henderson, C.M., Wardlaw, B.R., 2002. Evolution and distribution of the conodonts *Sweetognathus* and *Iranognathus* and related genera during the Permian, and their implications for climate change. *Palaeogeogr. Palaeoclimatol. Palaeoecol.*, **180**, 57–91.
- Menning, M., Alekseev, A.S., Chuvashov, B.I., Davydov, V.I., Devuyst, F.X., Forke, H.C., Grunt, T.A., Hance, L., Heckel, P.H., Izokh, N.G., Jin, Y., Jones, P.J., Kotlyar, G.V., Kozur, H.W., Nemyrovska, T.I., Schneider, J.W., Wang, X.D., Weddige, K., Weyer, D., Work, D.M., 2006. Global time scale and regional stratigraphic reference scales of Central and West Europe, East Europe, Tethys, South China, and North America as used in the Devonian–Carboniferous–Permian Correlation Chart 2003 (DCP 2003). *Palaeogeogr. Palaeoclimatol. Palaeoecol.*, **240**, 318–372.
- Metcalf, I., Sone, M., 2008. Biostratigraphy and palaeobiogeography of Lower Permian (lower Kungurian) conodonts from the Tak Fa Formation (Saraburi Limestone), Thailand. *Palaeogeogr. Palaeoclimatol. Palaeoecol.*, **257**, 139–151.
- Munnecke, A., Samtleben, C., 1996. The formation of micritic limestones and the development of limestone-marl alternations in the Silurian of Gotland, Sweden. *Facies*, **34**, 159.
- Nakazawa, T., Ueno, K., Fujikawa, M., 2012. Middle Permian sponge-microencruster bioherms in the Akiyoshi Limestone, SW Japan: implications for late Palaeozoic reef evolution on mid-Panthalassan atolls. *Geol. J.*, **47**, 495–508.
- Nakazawa, T., Igawa, T., Ueno, K., Fujikawa, M., 2015. Middle Permian sponge-microencruster reefal facies in the mid-Panthalassan Akiyoshi atoll carbonates: observations on a limestone slab. *Facies*, **61**, 1–14.
- Nestell, M.K., Nestell, G.P., Wardlaw, B.R., Sweatt, M.J., 2006. Integrated biostratigraphy of foraminifers, radiolarians and conodonts in shallow and deep water Middle Permian (Capitanian) deposits of the “Rader slide”, Guadalupe Mountain, West Texas. *Stratigraphy*, **3**, 161–194.
- Nestell, M.K., Wardlaw, B.R., 2010a. *Jinogondolella palmata*, a new Gondolellid conodont species from the Bell Canyon Formation, Middle Permian, West Texas. *Micropaleontology*, **56**, 185–194.
- Nestell, M.K., Wardlaw, B.R., 2010b. Radiolarians and conodonts of the Guadalupian (Middle Permian) of West Texas: advances in taxonomy and biostratigraphy. *Micropaleontology*, **56**, 1–6.

- Newell, N.D., 1972. The Evolution of Reefs. *Scientific American*, **226**, 54–69.
- Novacek, M.J., Cleland, E.E., 2001. The current biodiversity extinction event: Scenarios for mitigation and recovery. *Proc. Natl. Acad. Sci. USA*, **98**, 5466.
- Orchard, M.J., 1984. Early Permian conodonts from the Harper Ranch beds, Kamloops area, southern British Columbia. *Paper - Geological Survey of Canada*, **84**, pp. 207–215.
- Orchard, M.J., Forster, P.J.L., 1988. Permian Conodont Biostratigraphy of the Harper Ranch Beds, Near Kamloops, South-central British Columbia. *Energy, Mines and Resources Canada*, pp. 1–27.
- Pandolfi, J.M., Bradbury, R.H., Sala, E., Hughes, T.P., Bjorndal, K.A., Cooke, R.G., McArdle, D., McClenahan, L., Newman, M.J.H., Paredes, G., Warner, R.R., Jackson, J.B.C., 2003. Global Trajectories of the Long-Term Decline of Coral Reef Ecosystems. *Science*, **301**, 955.
- Pandolfi, J.M., Connolly, S.R., Marshall, D.J., Cohen, A.L., 2011. Projecting Coral Reef Futures Under Global Warming and Ocean Acidification. *Science*, **333**, 418.
- Paul, J., 1980. Upper Permian algal stromatolite reefs, Harz Mountains (F. R. Germany). *Contributions to Sedimentology*, **9**, 253–268.
- Paul, J., 1995. Stromatolite reefs of the upper Permian Zechstein basin (Central Europe). *Facies*, **32**, 28–31.
- Payne, J.L., Lehrmann, D.J., Wei, J.Y., Orchard, M.J., Schrag, D.P., Knoll, A.H., 2004. Large Perturbations of the Carbon Cycle During Recovery from the End-Permian Extinction. *Science*, **305**, 506–509.
- Payne, J.L., Lehrmann, D.J., Christensen, S., Wei, J., Knoll, A.H., 2006a. Environmental and biological controls on the initiation and growth of a Middle Triassic (Anisian) reef complex on the Great Bank of Guizhou, Guizhou province, China. *PALAIOS*, **21**, 325–343.
- Payne, J.L., Lehrmann, D.J., Wei, J.Y., Knoll, A.H., 2006b. The Pattern and Timing of Biotic Recovery from the End-Permian Extinction on the Great Bank of Guizhou, Guizhou Province, China. *PALAIOS*, **21**, 63–85.
- Peryt, T.M., Durakiewicz, T., Kotarba, M.J., Oszczepalski, S., Peryt, D., 2012. Carbon isotope stratigraphy of the basal Zechstein (Lopingian) strata in Northern Poland and its global correlation. *Geol. Quart.*, **56**, 285–298.
- Peryt, T.M., Raczyński, P., Peryt, D., Chłódek, K., 2012. Upper Permian reef complex in the basinal facies of the Zechstein Limestone (Ca1), western Poland. *Geol. J.*, **47**, 537–552.
- Peryt, T.M., Jasionowski, M., Raczyński, P., Chłódek, K., 2020. Demise of the Jabłonna Reef (Zechstein Limestone) and the onset of gypsum deposition (Wuchiapingian, west Poland): carbonate-to-evaporite transition in a saline giant. *J. Palaeogeogr.*, **9**, 18.
- Qiu, Z., Wang, Q.C., 2010. Upper Permian Sedimentary Microfacies in the Tieqiao Section in Laibin, Guangxi, China. *Acta Sediment. Sin.*, **28**, 1020–1036.
- Qiu, Z., Wang, Q.C., 2011. Geochemical evidence for submarine hydrothermal origin of the Middle-Upper Permian chert in Laibin of Guangxi, China. *Sci. China Earth Sci.*, **54**, 1011–1023.

- Qiu, Z., Wang, Q.C., Zou, C.N., Yan, D.T., Wei, H.Y., 2014. Transgressive–regressive sequences on the slope of an isolated carbonate platform (Middle–Late Permian, Laibin, South China). *Facies*, **60**, 327–345.
- Raczyński, P., Peryt, T.M., Strobel, W., 2017. Sedimentary and environmental history of the Late Permian Bonikowo Reef (Zechstein Limestone, Wuchiapingian), western Poland. *J. Palaeogeogr.*, **6**, 183–205.
- Rampino, M.R., Shen, S.Z., 2019. The end-Guadalupian (259.8 Ma) biodiversity crisis: the sixth major mass extinction? *Hist. Biol.* doi:10.1080/08912963.2019.1658096
- Rasser, M.W., 2000. Coralline red algal limestones of the late Eocene alpine Foreland Basin in Upper Austria: Component analysis, facies and paleoecology. *Facies*, **42**, 59–92.
- Raup, D.M., Sepkoski, J.J., 1982. Mass Extinctions in the Marine Fossil Record. *Science New Series*, **215**, 1501–1503.
- Rhodes, F.H., 1963. Conodont from the topmost Tensleep Sandstone of the eastern Big Horn Mountains, Wyoming. *J. Paleontol.*, **37**, 401–408.
- Riding, R., 2002. Structure and composition of organic reefs and carbonate mud mounds: concepts and categories. *Earth-Sci. Rev.*, **58**, 163–231.
- Riding, R., Guo, L., 1992. Affinity of *Tubiphytes*. *Palaeontology*, **35**, 37–49.
- Rigby, J.K., Fan, J., Wei, Z., 1989a. Inozoan calcareous Porifera from the Permian reefs in South China. *J. Paleontol.*, **63**, 778–800.
- Rigby, J.K., Fan, J., Wei, Z., 1989b. Sphinctozoan sponges from the Permian reefs of South China. *J. Paleontol.*, **63**, 404–439.
- Ritter, S.M., 1986. Taxonomic revision and phylogeny of post-Early Permian crisis *bisselli-whitei* Zone conodonts with comments on late Paleozoic diversity. *Geol. Palaeontol.*, **20**, 139–165.
- Sahney, S., Benton, M.J., 2008. Recovery from the most profound mass extinction of all time. *P. Roy. Soc. B-Biol. Sci.*, **275**, 759–765.
- Schubert, J.K., Bottjer, D.J., 1992. Early Triassic stromatolites as post-mass extinction disaster forms. *Geology*, **20**, 883–886.
- Scoffin, T. P., 1987, *An introduction to carbonate sediments and rocks*. Glasgow, London, Blackie, 274 p.
- Scotese, C.R., Langford, R.P., 1995. Pangea and the Paleogeography of the Permian. In: Scholle, P.A., Peryt, T.M., Ulmer-Scholle, D.S. (Eds.), *The Permian of Northern Pangea: Volume 1: Paleogeography, Paleoclimates, Stratigraphy, The Permian of Northern Pangea: Volume 1: Paleogeography, Paleoclimates, Stratigraphy*. Springer Berlin Heidelberg, Berlin, Heidelberg, pp. 3–19.
- Senowbari-Daryan, B., 2013. *Tubiphytes* Maslov, 1956 and description of similar organisms from Triassic reefs of the Tethys. *Facies*, **59**, 75–112.
- Senowbari-Daryan, B., Flügel, E., 1993. *Tubiphytes* Maslov, an enigmatic fossil: classification, fossil record and significance through time: Part I. Discussion of Late Paleozoic material. *B. Soc. Paleontol., Ita. Special Volume 1*, 353–382.

- Sepkoski, J.J., 1996. Patterns of Phanerozoic Extinction: A Perspective from Global Data Bases. In: Walliser, O.H. (Ed.), *Global Events and Event Stratigraphy in the Phanerozoic: Results of the International Interdisciplinary Cooperation in the IGCP-Project 216 "Global Biological Events in Earth History."* Springer Berlin Heidelberg, Berlin, Heidelberg, pp. 35–51.
- Sha, Q.A., Wu, W.S., Fu, J.M., 1990. *An integrated investigation on the Permian System of Qian-Gui areas, with discussion on the hydrocarbon potential.* Science Press, Beijing, 215 pp.
- Shen, J.W., Xu, H.L., 2005. Microbial carbonates as contributors to Upper Permian (Guadalupian–Lopingian) biostromes and reefs in carbonate platform margin setting, Ziyun County, South China. *Palaeogeogr. Palaeoclimatol. Palaeoecol.*, **218**, 217–238.
- Shen, S.Z., Shi, G.R., 2002. Paleobiogeographical extinction patterns of Permian brachiopods in the Asian–western Pacific region. *Paleobiology*, **28**, 449–463.
- Shen, S.Z., Shi, G.R., 2009. Latest Guadalupian brachiopods from the Guadalupian/Lopingian boundary GSSP section at Penglaitan in Laibin, Guangxi, South China and implications for the timing of the pre-Lopingian crisis. *Palaeoworld*, **18**, 152–161.
- Shen, S.Z., Zhang, Y.C., 2008. Earliest Wuchiapingian (Lopingian, Late Permian) brachiopods in southern Hunan, South China: implications for the pre-Lopingian crisis and onset of Lopingian recovery/radiation. *J. Paleontol.*, **82**, 924–937.
- Shen, S.Z., Wang, Y., Henderson, C.M., Cao, C.Q., Wang, W., 2007. Biostratigraphy and lithofacies of the Permian System in the Laibin–Heshan area of Guangxi, South China. *Palaeoworld*, **16**, 120–139.
- Shen, S.Z., Yuan, D.X., Henderson, C.M., Tazawa, J., Zhang, Y.C., 2012. Implications of Kungurian (Early Permian) conodonts from Hatahoko, Japan, for correlation between the Tethyan and international timescales. *Micropaleontology*, **58**, 505–522.
- Shen, S., Zhang, H., Zhang, Y., Yuan, D., Chen, B., He, W., Mu, L., Lin, W., Wang, W., Chen, J., Wu, Q., Cao, C., Wang, Y., Wang, X., 2018. Permian integrative stratigraphy and timescale of China. *Sci. China Earth Sci.* **62**, 154–188.
- Sheng, J.Z., Jin, Y.G., 1994. Correlation of Permian deposits of China. *Palaeoworld*, **4**, 14–113.
- Stanley Jr., G.D., 1988. The History of Early Mesozoic Reef Communities: a Three-Step Process. *PALAIOS*, **3**, 170–183.
- Stanley Jr., G.D., 2006. Photosymbiosis and the evolution of modern coral reefs. *Science*, **312**, 857–858.
- Stanley, S.M., 2016. Estimates of the magnitudes of major marine mass extinctions in earth history. *Proc. Natl. Acad. Sci. USA*, **113**, E6325.
- Stanley, S.M., Yang, X., 1994. A double mass extinction at the end of the Paleozoic Era. *Science*, **266**, 1340–1344.
- Sun, Y.D., Lai, X.L., Wignall, P.B., Widdowson, M., Ali, J.R., Jiang, H.S., Wang, W., Yan, C.B., Bond, D.P.G., Védérine, S., 2010. Dating the onset and nature of the Middle Permian Emeishan large igneous province eruptions in SW China using conodont biostratigraphy and its bearing on mantle plume uplift models. *Lithos*, **119**, 20–33.

- Sun, Y.D., Liu, X.T., Yan, J.X., Li, B., Chen, B., Bond, D.P.G., Joachimski, M.M., Wignall, P.B., Wang, X., Lai, X.L., 2017. Permian (Artinskian to Wuchiapingian) conodont biostratigraphy in the Tieqiao section, Laibin area, South China. *Palaeogeogr. Palaeoclimatol. Palaeoecol.*, **465**, 42–63.
- Toomey, D.F., 1991. Late Permian reefs of southern Tunisia: Facies patterns and comparison with the Capitan reef, southwestern United States. *Facies*, **25**, 119–145.
- Trygonis, V., Sini, M., 2012. photoQuad: A dedicated seabed image processing software, and a comparative error analysis of four photoquadrat methods. *J. Exp. Mar. Biol. Ecol.*, **424–425**, 99–108.
- Wahlman, G.P., Orchard, D.M., Buijs, G.J., 2013. Calcisponge-microbialite reef facies, middle Permian (lower Guadalupian), northwest shelf margin of Permian Basin, New Mexico. *AAPG Bull.*, **97**, 1895–1919.
- Wake, D.B., Vredenburg, V.T., 2008. Are we in the midst of the sixth mass extinction? A view from the world of amphibians. *Proc. Natl. Acad. Sci. USA*, **105**, 11466.
- Wang, C.Y., 1995. A conodont fauna from the lowermost Kufeng Formation (Permian). *Acta Micropalaeontol. Sin.*, **12**, 293–297.
- Wang, C.Y., 2002. Permian conodonts from Laibin and Heshan, Guangxi. *Bull. Nanjing Inst. Geol. Palaeontol. Acad. Sin.*, **15**, 180–190.
- Wang, C.Y., Ritter, S.M., Clark, D.L., 1987. The *Sweetognathus* complex in the Permian of China: implications for evolution and homeomorphy. *J. Paleontol.*, **61**, 1047–1057.
- Wang, D., Jiang, H., Gu, S., Yan, J., 2016. Cisuralian–Guadalupian conodont sequence from the Shaiwa section, Ziyun, Guizhou, South China. *Palaeogeogr. Palaeoclimatol. Palaeoecol.*, **457**, 1–22.
- Wang, S.H., Fan, J.S., Rigby, J.K., 1994. *Archaeolithoporella* and *Tubiphytes*: Affinities and paleoecology in Permian reefs of South China. *Sci. China Ser. B*, **37**, 723–743.
- Wang, W., Cao, C.Q., Wang, Y., 2004. The carbon isotope excursion on GSSP candidate section of Lopingian–Guadalupian boundary. *Earth and Planet. Sci. Lett.*, **220**, 57–67.
- Wang, X., Foster, W.J., Yan, J.X., Li, A.Z., Mutti, M., 2019. Delayed recovery of metazoan reefs on the Laibin-Heshan platform margin following the Middle Permian (Capitanian) mass extinction. *Glob. Planet. Chang.*, **180**, 1–15.
- Wang, X.D., Sugiyama, T., 2000. Diversity and extinction patterns of Permian coral faunas of China. *Lethaia*, **33**, 285–294.
- Wang, Y., Wang, J., Chen, J., Wang, W.J., Shen, S.Z., Henderson, C.M., 2011. Progress, problems and prospects on the stratigraphy and correlation of the Kungurian stage, Early Permian (Cisuralian) series. *Acta Geol. Sin.*, **85**, 387–398.
- Wang, Y., Jin, Y.G., 2000. Permian palaeogeographic evolution of the Jiangnan Basin, South China. *Palaeogeogr. Palaeoclimatol. Palaeoecol.*, **160**, 35–44.
- Wang, Z.H., 1978. Permian-Lower Triassic conodonts of the Liangshan area, southern Shanxi. *Acta Palaeontol. Sin.*, **17**, 213–227.
- Wang, Z.H., 1994. Early Permian Conodonts from the Nashui Section, Luodian of Guizhou. *Palaeoworld*, **4**, 203–224.

- Wang, W., Cao, C.Q., Wang, Y., 2004. The carbon isotope excursion on GSSP candidate section of Lopingian-Guadalupian boundary. *Earth Planet. Sci. Lett.*, **220**, 57–67.
- Wardlaw, B.R., 2000. Guadalupian conodont biostratigraphy of the Glass and Del Norte Mountains. In: Wardlaw, B.R., Grant, R.E., Rohr, D.M. (Eds.), *The Guadalupian Symposium-Smithsonian Contributions to the Earth Sciences*, Smithsonian Institution Press, pp. 37–87.
- Wardlaw, B.R., Grant, R.E., 1990. Conodont biostratigraphy of the Permian Road Canyon Formation, Glass Mountains, Texas. *U.S. Geol. Surv. Bull.*, **1895**, 63–66.
- Wardlaw, B.R., Nestell, M.K., 2010. Latest Middle Permian conodonts from the Apache Mountains, West Texas. *Micropaleontology*, **56**, 149–183.
- Wardlaw, B.R., Gallegos, D.M., Chernykh, V.V., Snyder, W.S., 2015. Early Permian conodont fauna and stratigraphy of the Garden Valley formation, Eureka County, Nevada. *Micropaleontology*, **61**, 369–387.
- Webb, G.E., 1996. Was Phanerozoic reef history controlled by the distribution of non-enzymatically secreted reef carbonates (microbial carbonate and biologically induced cement)? *Sedimentology*, **43**, 947–971.
- Weidlich, O., 2002a. Permian reefs re-examined: extrinsic control mechanisms of gradual and abrupt changes during 40 my of reef evolution. *Geobios*, **35**, 287–294.
- Weidlich, O., 2002b. Middle and Late Permian Reefs—Distributional Patterns and Reservoir Potential. In: Kiessling, W., Flügel, E., Golonka, J. (Eds.), *Phanerozoic Reef Patterns*. SEPM Society for Sedimentary Geology, pp. 339–390.
- Weidlich, O., Fagerstrom, J.A., 1999. Influence of Sea-Level Changes on Development, Community Structure, and Quantitative Composition of the Upper Capitan Massive (Permian), Guadalupe Mountains, Texas and New Mexico. In: Saller, A.H., Harris, P.M.M., Kirkland, B.L., Mazzullo, S.J. (Eds.), *Geologic Framework of the Capitan Reef*. SEPM Society for Sedimentary Geology, pp. 139–160.
- Weidlich, O., Bernecker, M., Flügel, E., 1993. Combined quantitative analysis and microfacies studies of ancient reefs: An integrated approach to Upper Permian and Upper Triassic reef carbonates (Sultanate of Oman). *Facies*, **28**, 115–144.
- Weidlich, O., Kiessling, W., Flügel, E., 2003. Permian-Triassic boundary interval as a model for forcing marine ecosystem collapse by long-term atmospheric oxygen drop. *Geology*, **31**, 961–964.
- Weiss, A., Martindale, R.C., 2017. Crustose coralline algae increased framework and diversity on ancient coral reefs. *PLoS ONE*, **12**, e0181637.
- Wignall, P.B., Bond, D.P.G., Haas, J., Wang, W., Jiang, H.S., Lai, X.L., Altiner, D., Védérine, S., Hips, K., Zajzon, N., Sun, Y.D., Newton, R.J., 2012. Capitanian (Middle Permian) mass extinction and recovery in western Tethys: A fossil, facies, and $\delta^{13}\text{C}$ study from Hungary and Hydra Island (Greece). *PALAIOS*, **27**, 78–89.
- Wignall, P.B., Sun, Y.D., Bond, D.P.G., Izon, G., Newton, R.J., Védérine, S., Widdowson, M., Ali, J.R., Lai, X.L., Jiang, H.S., Cope, H., Bottrell, S.H., 2009a. Volcanism, mass extinction, and carbon isotope fluctuations in the Middle Permian of China. *Science*, **324**, 1179–1182.

- Wignall, P.B., Védérine, S., Bond, D.P.G., Wang, W., Lai, X.L., Ali, J.R., Jiang, H.S., 2009b. Facies analysis and sea-level change at the Guadalupian–Lopingian Global Stratotype (Laibin, South China), and its bearing on the end-Guadalupian mass extinction. *J. Geol. Soc.*, **166**, 655–666.
- Wood, R.A., 1999. *Reef evolution*. Oxford University Press, New York, 414 pp.
- Wood, R.A., Dickson, J.A.D., Kirkland, B.L., 1994. Turning the Capitan Reef Upside down: A New Appraisal of the Ecology of the Permian Capitan Reef, Guadalupe Mountains, Texas and New Mexico. *PALAIOS*, **9**, 422–427.
- Wood, R.A., Dixon, J., Kirkland, B.L., 1996. New observations on the ecology of the Permian Capitan Reef, Texas and New Mexico. *Palaeontology*, **39**, 733–762.
- Wu, Y.S., 1991. *Organisms and communities of the Permian reef of Xiangbo, China - calcisponges, hydrozoans, algae, microproblematica*. International Academic Publisher, Beijing, 192 pp.
- Yan, D.T., Zhang, L.Q., Qiu, Z., 2013. Carbon and sulfur isotopic fluctuations associated with the end-Guadalupian mass extinction in South China. *Gondwana Res.*, **24**, 1276–1282.
- Yan, H., Pi, D.H., Jiang, S.Y., Hao, W.D., Mänd, K., Robbins, L.J., Li, L., Konhauser, K.O., 2020. New constraints on the onset age of the Emeishan LIP volcanism and implications for the Guadalupian mass extinction. *LITHOS*, 105441.
- Yancey, T.E., Boyd, D.W., 1983. Revision of the Alatoconchidae: a remarkable family of Permian bivalves. *Palaeontology*, **26**, 497–520.
- Yang, J.H., Cawood, P.A., Du, Y.S., Condon, D.J., Yan, J.X., Liu, J.Z., Huang, Y., Yuan, D.X., 2018. Early Wuchiapingian cooling linked to Emeishan basaltic weathering? *Earth and Planet. Sci. Lett.*, **492**, 102–111.
- Yang, W.R., 1987. Bioherm of Wujiaping Formation in Laibin, Guangxi. *Oil Gas Geol.*, **8**, 424–430.
- Yao, L., Aretz, M., Wignall, P.B., Chen, J.T., Vachard, D., Qi, Y.P., Shen, S.Z., Wang, X.D., 2020. The longest delay: Re-emergence of coral reef ecosystems after the Late Devonian extinctions. *Earth-Sci. Rev.*, **203**, 103060.
- Yao, Y., Yan, J.X., Li, A.Z., 2012. Sedimentary Features and Evolution of Mid-Permian Carbonates from Laibin of Guangxi. *Eart. Scie.*, **37**, 184–194.
- Youngquist, W.L., Hawley, R.W., Miller, A.K., 1951. Phosphoria conodonts from southeastern Idaho. *J. Paleontol.*, **25**, 356–364.
- Zatoń, M., Niedźwiedzki, G., Rakociński, M., Blom, H., Kear, B.P., 2018. Earliest Triassic metazoan bioconstructions in East Greenland reveal a pioneering benthic community from immediately after the end-Permian mass extinction. *Glob. Planet. Change.*, **167**, 87–98.
- Zhang, G.J., Zhang, X.L., Li, D.D., Farquhar, J., Shen, S.Z., Chen, X.Y., Shen, Y.N., 2015. Widespread shoaling of sulfidic waters linked to the end-Guadalupian (Permian) mass extinction. *Geology*, **43**, 1091–1094.
- Zhang, K.X., Lai, X.L., Ding, M.H., Liu, J., 1995. Conodont sequence and its global correlation of Permian-Triassic boundary in Meishan section, Changxing, Zhejiang Province. *Earth Sci. J. China Univ. Geosci.*, **20**, 669–676.

- Zhang, M., 2015. *Late Permian Deep Water Foraminiferal Fauna from South China*. PhD thesis. China University of Geosciences.
- Zhang, W., Zhang, X.L., 1992. *Permian reefs and paleoecology in South China*. Geological Publishing House, Beijing, 157 pp.
- Zhang, Z., Wang, Y., Zheng, Q.F., 2015. Middle Permian smaller foraminifers from the Maokou formation at the Tieqiao section, Guangxi, South China. *Palaeoworld*, **24**, 263–276.
- Zhong, Y.T., He, B., Xu, Y.G., 2013. Mineralogy and geochemistry of claystones from the Guadalupian–Lopingian boundary at Penglaitan, South China: Insights into the pre-Lopingian geological events. *J. Asian Earth Sci.*, **62**, 438–462.
- Zhong, Y.T., Mundil, R., Chen, J., Yuan, D.X., Denyszyn, S.W., Jost, A.B., Payne, J.L., He, B., Shen, S.Z., Xu, Y.G., 2020. Geochemical, biostratigraphic, and high-resolution geochronological constraints on the waning stage of Emeishan Large Igneous Province. *Geol. Soc. Am. Bull.*, 1–19.
- Zhou, M.F., Malpas, J., Song, X.Y., Robinson, P.T., Sun, M., Kennedy, A.K., Leshner, C.M., Keays, R.R., 2002. A temporal link between the Emeishan large igneous province (SW China) and the end-Guadalupian mass extinction. *Earth and Planet. Sci. Lett.*, **196**, 113–122.

Appendix

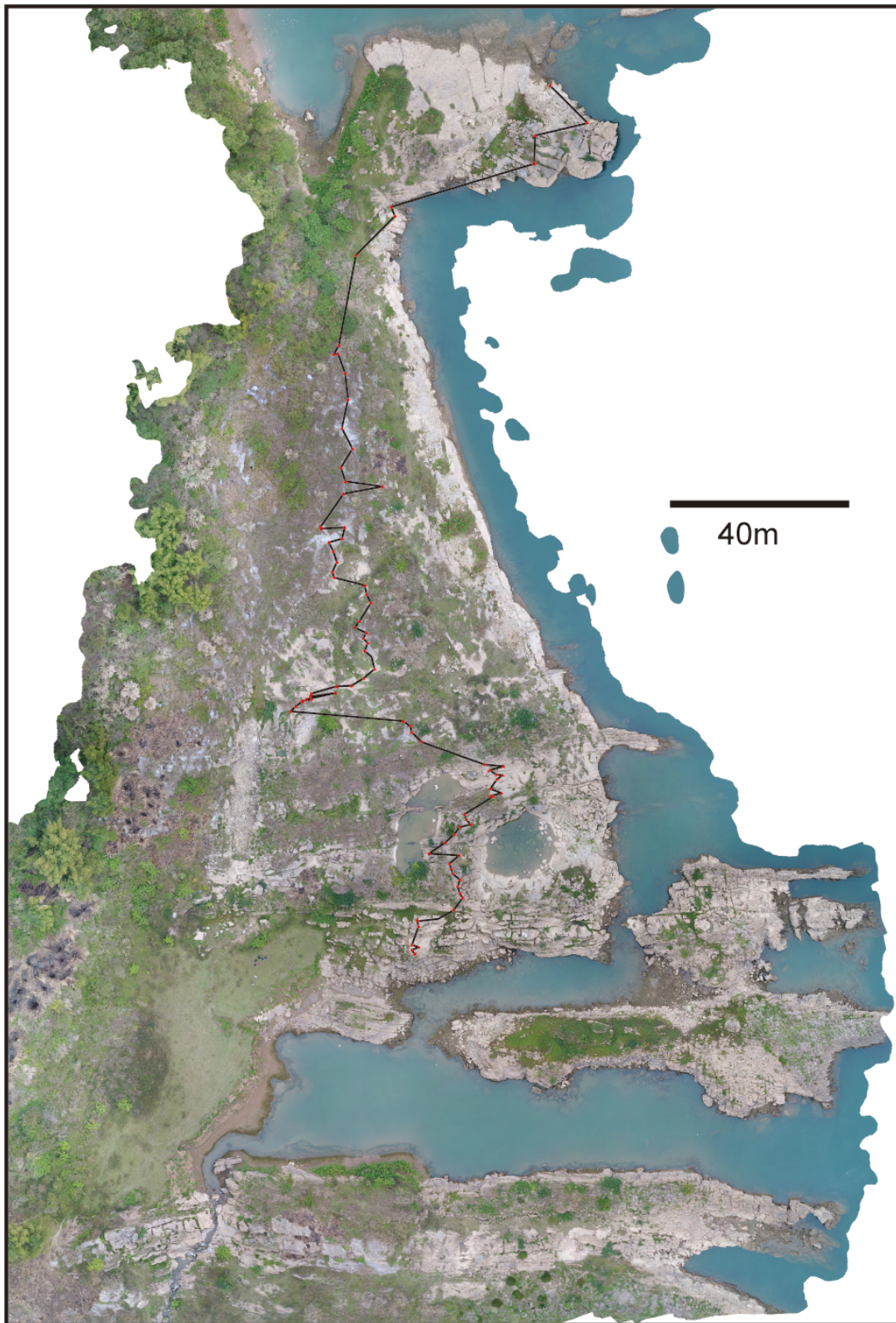


Figure S1: Trace of the section (dark grey line) and position of samples (red triangle) used for point counting on the Tieqiao section (Chapter 4).

